CHEMICAL REVIEWS
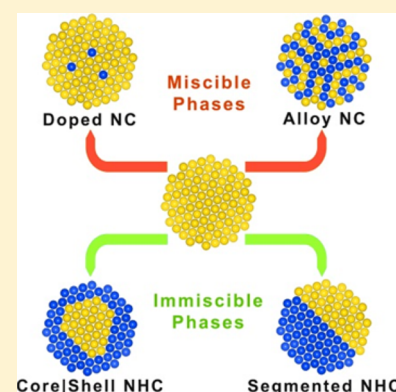
Forging Colloidal Nanostructures via Cation Exchange Reactions

Luca De Trizio*,† and Liberato Manna*,†

†Department of Nanochemistry, Istituto Italiano di Tecnologia (IIT), via Morego, 30, 16163 Genova, Italy

ABSTRACT: Among the various postsynthesis treatments of colloidal nanocrystals that have been developed to date, transformations by cation exchange have recently emerged as an extremely versatile tool that has given access to a wide variety of materials and nanostructures. One notable example in this direction is represented by partial cation exchange, by which preformed nanocrystals can be either transformed to alloy nanocrystals or to various types of nanoheterostructures possessing core/shell, segmented, or striped architectures. In this review, we provide an up to date overview of the complex colloidal nanostructures that could be prepared so far by cation exchange. At the same time, the review gives an account of the fundamental thermodynamic and kinetic parameters governing these types of reactions, as they are currently understood, and outlines the main open issues and possible future developments in the field.

CONTENTS

1. INTRODUCTION

Colloidal nanocrystals (NCs) have played a pivotal role in both fundamental research and in technological applications over the last 30 years.[1−14] Today, a rational synthetic approach to NC is of utmost importance due to the growing demand for nanomaterials having compositional diversity and that need to be engineered in shape, morphology, and surface functionality, such that they will possess well-defined optical, electronic, magnetic, and catalytic features, for use in the most disparate fields of science and technology. Over the years, the synthesis of colloidal NCs has evolved to a point that a fine level of control over size, shape, structural, and compositional parameters has finally become possible for many materials systems.[10,15−18] As an example, a huge variety of nanocrystal heterostructures, that is, NCs combining different domains of various chemical compositions, have been reported over the last two decades.[19−27] Among these types of nanoheterostructures (NHCs), perhaps semiconductor–semiconductor NHCs are those that have been exploited the most. Here, the fine-tuning of the size, shape, spatial orientation, composition, and crystalline structure of the component materials enables a careful adjustment of the relative band alignments of both

semiconductors and, thus, allows for a tight control over the physical and optical properties of the hybrid nanostructures. In type I core|shell NHCs, for instance, the band alignment of the semiconductors results in the confinement of the charges in the core material. By choosing a fluorescent semiconductor as core material, core|shell NHCs of this type can display enhanced photoluminescence, which is required for lighting, lasing, and sensing applications. On the other hand, in NHCs with a type II band alignment the charges can be spatially separated after photoexcitation, which makes these systems interesting for photovoltaic and photocatalytic applications. Even alloy NCs have gained increasing attention in recent years as their band gap, and in some cases their magnetic properties, can be tweaked by controlling the NCs composition, which makes them suitable for applications in displays, biomedical imaging and sensing, lab-on-a-chip, solid-state lighting, and photovoltaic devices.

While on the one hand a consolidated body of knowledge has been established around the colloidal synthesis of NCs, many materials or combinations of them remain poorly accessible in nanocrystalline form. Therefore, new postsynthetic strategies are emerging that compensate for the current limits imposed by direct reaction routes and that expand the library of possible structures that can be fabricated. It still remains a challenge, for example, to directly synthesize NHCs with simultaneous control over the size, shape, spatial orientation, composition, and crystalline structure of the component materials. Even the direct synthesis of alloyed semiconductor NCs, with regulation of the composition as well as the size and shape, is often not straightforward as the control over the reaction kinetics of multiple species in a single reaction step is hardly achievable. In part with the aim to overcome the yet unsolved issues related to direct colloidal synthesis and in part driven by the fundamental interest in chemical and structural transformations of materials at the nanoscale, a new area of research has emerged in the past decade in the field of colloidal NCs. This area encompasses the transformations of nanomaterials driven by cation exchange (CE).[28−35] At the nanoscale, CE has been applied and studied on a variety of materials, above all those belonging to the II−VI, I−III−VI, and IV−VI classes of semiconductors. This simple process consists, basically, in the replacement of cations of a starting NC with new cations, with preservation of the original anion sublattice, which in some cases undergoes a certain degree of structural reorganization. CE takes place instead of anion exchange because the diffusion rate of the cations is generally much higher than that of the anions. This can be explained by the fact that, in a crystal, cations are generally smaller than anions, and therefore, one can visualize the cations as diffusing within a comparatively rigid lattice of anions. In most cases, a CE reaction is a topotactic transformation in which the anion framework remains virtually intact and thus the morphology of the overall structure is typically retained.

Reports on CE in NCs have been growing steadily since the first landmark works in the 1990s and especially after important breakthroughs from 2004 on.[28,36,37] However, despite CE at the nanoscale having being studied for more than one decade, there is a fundamental knowledge gap for what concerns the detailed mechanisms and forces governing CE at this size regime, and the main reason is that CE had been used primarily as a means of synthesizing nanomaterials. Such a knowledge gap is slowly closing over the years, as recent works are finally addressing in detail the various issues. Examples are the studies that explore

the role of the most effective complexing agents in stabilizing the entering/exiting cations in the solution phase, the relevance of various structural parameters in promoting exchange reactions, as well as the importance of the size and valency of cations, which dictates the type of coordination that they can adopt in the lattice and ultimately their diffusivity and whether this occurs primarily via vacancies or via interstitials. All these studies used advanced analysis tools, including many electron microscopy and spectroscopy techniques, and time-resolved X-ray experiments.[38−43] A few recent papers have also attempted to model many aspects of CE, at least for the simplest cases. Also, many seminal review articles have been published in recent years by various leading groups on CE.[28,32−35]

In the present article, while giving ample credit to all those previous review articles on CE, we will present an updated snapshot of the field. To this aim, we will first provide an overview of the well-established thermodynamic concepts that are necessary for predicting the feasibility and the outcome of a CE reaction. This will be followed by a section dedicated to the progress that has been made so far in understanding the various possible mechanisms involved in CE, with particular emphasis on the aspects related to cation diffusion and replacement in NCs. At the same time, we will give an up-to-date overview of the astonishing complex nanostructures that are now accessible via CE (see Scheme 1). These systems, ranging from core|shell,

Scheme 1. Schematic Representation of Nanostructures Accessible via Cation Exchange Transformations of a Preformed Colloidal NC[a]
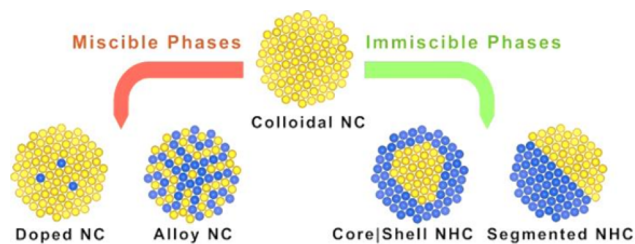
[a]The original cations (yellow spheres) are replaced with new guest cations (blue spheres) with minimal distortion (or no distortion at all) of the anion framework.

to segmented, and to alloyed NCs, nanorods (NRs), nanoplatelets (NPLs), nanowires (NWs), etc., can be now prepared by extracting just a fraction of the original cations from the starting nanomaterials and replacing them with new types of cations (also called partial CE). Without downplaying the importance of total CE transformations that have started the field and have first aroused the interest of the community in this technique, our review will focus mainly on heterostructured types of nanomaterials, as they represent one of the most fascinating and intriguing developments of CE. It is our conviction that a deeper comprehension of the mechanisms underlying ions interdiffusion and replacement in CE reactions, coupled with a rational choice of semiconductor materials, will generate, in the future, a wide range of sophisticated nanostructures that can be exploited in many disparate applications.

Before proceeding further, the question arises on why anion exchange has received much less attention to date.[44−52] One important reason, as mentioned earlier, is that at least in binary compounds the comparatively larger anions are generally much

Table 1. Lattice Energies (ΔH_{latt}) and Bond Dissociation Energies (BDE) of Some Metal Chalcogenides (M-Y) Expressed in kJ/mol (from refs 60−62)

| sulfides	ΔH_{latt}	BDE (M-S)	selenides	ΔH_{latt}	BDE (M-Se)	tellurides	ΔH_{latt}	BDE (M-Te)
Ag_2S	2677	216.7 ± 14.6	Ag_2Se	2686	210.0 ± 14.6	Ag_2Te	2600	195.8 ± 14.6
CdS	3460	208.5 ± 20.9	CdSe	3310	127.6 ± 25.1	CdTe		100.0 ± 15.1
Cu_2S	2865	274.5 ± 14.6	Cu_2Se	2936	255.2 ± 14.6	Cu_2Te	2683	230.5 ± 14.6
HgS	3573	217.3 ± 22.2	HgSe		144.3 ± 30.1	HgTe		<142
PbS	3161	398	PbSe	3144	302.9 ± 4.2	PbTe	3039	249.8 ± 10.5
ZnS	3674	224.8 ± 12.6	ZnSe		170.7 ± 25.9	ZnTe		117.6 ± 18.0

less mobile than the cations. Therefore, harsh conditions would be required to trigger transformations that involve the exchange of anions. However, the concept of cation sublattice preservation, and with that the integrity of the overall NCs, is seriously questionable, and one would wonder whether such transformations should be indeed categorized as occurring via ion exchange or if they should rather be seen as recrystallization processes: here, the initial NC seems to act as some sort of "precursor" for the nucleation/recrystallization of a new material on it, with often poor size/morphology retention or no retention at all. Obviously, when the degree of structural complexity and diversity in a crystal lattice increases, this statement shakes considerably. Indeed, in analogy with the well-known high-temperature diffusivity of oxygen ions in various oxide materials, many works (some recent, some dating back to the 1980s) on ternary halide perovskites have demonstrated that the halide ions have a remarkably high diffusivity in such materials.[53−55] This was immediately translated in the possibility to exchange, at least in lead halide perovskites, the halide ions (Cl-, Br-, and I-), while the two types of cations involved in the structure remain in place, which enabled tuning of the band gap by means of a simple (and fast) postsynthesis anion exchange at room temperature.[56−59] Such materials are receiving impressive attention nowadays due to their many fascinating physical properties and their great promise in photovoltaics, lighting, and lasing applications. Triggered by such surge, we are now witnessing a general revival in the study of materials involving halides in their composition, again both in their bulk form and as nanocrystalline domains. It is therefore plausible to expect that much more knowledge will be generated in the coming years in exchange reactions involving anions. For the time being, our focus here will be on exchange reactions involving cations.

We start this review with a series of basics considerations on the thermodynamic and kinetic of CE in colloidal nanostructures and on how their understanding has evolved over the past years. This section is then followed by an extensive section on selected examples from the literature, with emphasis on those cases in which the degree of structural and compositional complexity arises as a peculiar feature of CE.

2. THERMODYNAMICS OF CE

A CE reaction, in which the A^+ cations of an AX ionic NC are exposed to a solution of B^+ cations to give the BX structure, can be written as

$$AX(s) + B^+(sol) \rightarrow BX(s) + A^+(sol) \tag{1}$$
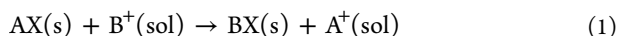
For the sake of simplicity we will consider, in the following discussion, only monovalent exchanging cations, even if typical CE reactions can occur between heterovalent ions. In a first approximation, we will assume that the specific crystallographic phases of the initial and final NC do not play any major role in

the overall energy balance. Following the same treatment proposed by Rivest et al., the process can be divided in four ideal steps: A-X dissociation, B-X association, B^+ desolvation, and A^+ solvation.[33] In order to predict a priori the spontaneity of a CE reaction it is necessary to know the energies involved in these four steps. The association and dissociation processes can be defined in terms of lattice and surface energy of the AX and BX crystals, while the determination of the energies involved in the solvation and desolvation requires a precise knowledge of the affinity of the exchanging cations for both the solvent and the possible ligands used in the CE process. No entropic variation is associated with the process as for each A^+ ion extracted from the host crystal a B^+ cation is desolvated. Furthermore, as will be discussed in more detail in section 2.2, even when working with heterovalent cations, the entropic contribution to the overall free energy can be neglected, as it plays a minor role.

2.1. Association and Dissociation Energies

The lattice energy (ΔH_{latt}) of a ionic crystal, also called lattice enthalpy, is commonly defined as the energy required to break the crystal apart into isolated ions at absolute zero temperature. This energy gives a measure of the strength of the chemical bonding among ions constituting the ionic solid and, thus, the higher is the lattice energy, the more stable is the crystal. The lattice energy takes into account the Coulomb attraction and repulsion among the ions in the lattice, and it is influenced not only by the charge and the radius of the cations and anions but also by their ordering, i.e. the crystal structure of the solid, as follows:

$$\Delta H_{latt} = -\frac{NMz_i z_j e^2}{r^+ + r^-}(1 - 1/n) \tag{2}$$

In the expression above, N is Avogadro's number, z_i and z_j are the integral charges on the ions (in units of e), e is the electron charge, r^+ and r^- are the ionic radii of the cations and anions, respectively, n is the Born exponent (that takes into account the ionic repulsion), and M is the Madelung constant. The latter term is intimately related to the spatial position of the ions, and it is, therefore, dependent on the crystal structure of the material under analysis. It follows that, when working with a given material, its allotropes can have significantly different lattice energies. The lattice energies of a wide range of materials are available in the literature as they have been experimentally calculated through the so-called "Born−Haber cycle".

Most of the CE reactions performed on NCs deal with metal chalcogenides and, unfortunately, it is not always easy to find the tabulated ΔH_{latt} values of many of those (see Table 1), especially when they have allotropes. This is particularly true when considering that, in some cases, these reactions can lead to the formation of metastable crystal structures that obviously

cannot be predicted a priori (see also Section 4). If the structure of the materials under study is known, then following eq 2 it is possible to make some qualitative conclusions about lattice energies. As ΔH_{latt} strongly depends on the distance between cations and anions (r), then given a certain cation M^+ and by increasing the size of the A^- anion (keeping the ionic charges and the crystal structure fixed) a decrease in ΔH_{latt} is expected. Therefore, in general, the ΔH_{latt} of metal chalcogenides decreases in absolute value as the ionic radius of the chalcogen increases: $\Delta H_{latt}(M_xS_y) > \Delta H_{latt}(M_xSe_y) > \Delta H_{latt}(M_xTe_y)$. As shown in Table 1, ΔH_{latt} values of M_xTe_y are lower than the corresponding M_xSe_y, and the same trend is seen by comparing M_xSe_y with M_xS_y.

When values of ΔH_{latt} are not known, then an alternative qualitative approach to estimate the relative stabilities of reactants and products, and thus to evaluate the thermodynamics of the CE reaction, is to consider the bond dissociation energies (BDEs).[42,63−65] The BDE of a generic AX compound is defined as the standard enthalpy of the following process: A−X → A + X. This energy, being calculated for diatomic molecules, does not take into account any ion ordering and it is independent from the crystal structure of the compound under analysis. As it possible to see in Table 1, using tabulated values of BDE the predicted relative stabilities of many compounds are in agreement with the trend in ΔH_{latt}. On the other hand, even if the lattice and the solvation/desolvation energies of the species involved in the CE reaction are known, the calculation of the overall energy of the process is still not trivial. The association and dissociation terms in eq 1 require, indeed, a precise knowledge of the surface energy of the NCs under analysis. One of the most common properties of nanomaterials is their large surface-to-volume ratio and thus a large fraction of the atoms are localized on their surface. Therefore, if compared to bulk materials, the high surface-to-volume ratio of NCs is thermodynamically mirrored by a large surface energy. Unfortunately, it is extremely challenging to calculate or even to give a rough estimate of the surface energy contribution in a CE reaction, as this depends on many variables, such as the types of stabilizing molecules bound at the surface of NCs and the chemical and structural nature of the facets by which the NCs are terminated (each of the facets being passivated by the various ligand molecules with different binding strengths).

2.2. Solvation and Desolvation Energies

Let us consider a CE reaction in which monovalent A^+ ions from a preformed A_2X NC are replaced with divalent B^{2+} ions to form a BX NC. Such transformation is entropically favored, since for each B^{2+} cation desolvated and incorporated into the host NC two A^+ ions are solvated, with the consequent increase of the overall entropy. If the product BX NC is more stable than the parent A_2X NC (that is $|\Delta H_{latt}BX| > |\Delta H_{latt}A_2X|$), then such CE reaction should be favored by both lattice enthalpy and entropy. The experimental evidence shows that, in many cases, such reaction does not take place if no proper solvents or ligands are used. A typical example is the CE transformation from Cu_2X or Ag_2X to CdX NCs. The reaction should be promoted by both the increase of entropy, as it proceeds with the solvation of two Cu^+ or Ag^+ ions for each Cd^{2+} incorporated in the host NC, and by lattice enthalpy, as the product CdX material is more stable than the starting Cu_2X or Ag_2X (see Table 1). Nevertheless, unless soft Lewis bases (such as alkyl phospines) are used, no exchange is observed (see next sections for further details). The solvation (and the desolva-

tion) energy, in this example, as in vast majority of CE reactions involving NCs, represents indeed the main driving force of the transformation. Often this energy term can be easily predicted and controlled. To this purpose, a careful choice of solvents and/or ligands can generally increase the solubility (and thus the efficiency of extraction) of the outgoing cations and to promote the entry of the desired host cations.[31,66]

2.2.1. Hardness. Pearson's hard and soft acids and bases (HSAB) theory is a qualitative concept that is of utmost importance in CE, as it helps to predict the affinity of metal ions to ligands/solvents and, thus, to finely tune the solubility of cations involved in a given CE reaction. This theory relies on the concept of chemical hardness and softness of Lewis acids (A) and bases (B).[67] Using specific reference bases, and depending on the stability of the resulting AB complexes, the Lewis acids are divided in two categories. Similarly, Lewis bases are divided in two categories according to the characteristics of their donor atom. These two types are called hard and soft, where the meaning of the word "hardness" is, in simple terms, the resistance to deformation or change. Soft bases are characterized by a donor atom of high polarizability and low electronegativity and that is easily oxidized; hard bases have a donor atom of low polarizability and high electronegativity that is hard to oxidize. On the other hand, in soft acids the acceptor atom is of low positive charge and large size, while in hard acids the acceptor atom is of high positive charge and small size. According to HSAB theory, hard acids prefer to bind to hard bases forming ionic complexes, whereas soft acids prefer to bind to soft bases yielding covalent complexes.

In order to compare acids and bases in terms of hardness, in 1983 Parr and Pearson introduced the concept of absolute hardness (η). Table 2 reports the absolute hardness of many cations, ligands and solvents typically employed in CE reactions. These values are a guideline for comparing the acidity of cations (Lewis acids) and the basicity of ligands or solvents (Lewis bases) in order to optimize a desired CE

Table 2. Experimental Absolute Hardness, η, of Typical Cations and Ligands or Bases That Can Be Used in CE Reactions (from ref 68)

acid	η	base	η
Cu^+	6.28	$C_6H_5NH_2$	4.4
Pd^{2+}	6.75	C_6H_5SH	4.6
Ag^+	6.96	C_6H_5OH	4.8
Fe^{2+}	7.24	C_5H_5N	5
Hg^{2+}	7.7	CH_3COCH_3	5.6
Sn^{2+}	7.94	CH_3CHO	5.7
Pt^{2+}	8	DMF	5.8
Co^{2+}	8.22	$(CH_3)_3P$	5.9
Cu^{2+}	8.27	PH_3	6
Au^{3+}	8.4	$(CH_3)_2S$	6
Pb^{2+}	8.46	CH_2O	6.2
Co^{3+}	8.9	$HCONH_2$	6.2
Mn^{2+}	9.02	$(CH_3)_3N$	6.3
Ge^{2+}	9.15	HCO_2CH_3	6.4
Cd^{2+}	10.29	CH_3CN	7.5
Zn^{2+}	10.88	CH_3Cl	7.5
Fe^{3+}	12.08	$(CH_3)_2O$	8
In^{3+}	13	NH_3	8.2
Ga^{3+}	17	CH_3F	9.4
Al^{3+}	45.77	H_2O	9.5

reaction. Among the bases, the most significant feature that can be extrapolated from the listed η values is that molecules in which the donor atom is F, O, or N have a strong hardness as a result of the negative values of their electron affinity. For similar molecules in which the donor atom is Cl, S, or P, there is always a large drop in hardness. Following this theory, as it will be discussed in the next sessions, it is easy to understand how many CE reactions are promoted by specific solvents/ligands: NCs in which the cations are hard Lewis acids (e.g., Zn^{2+} and Cd^{2+} cations) can be easily cation exchanged with cations acting as weaker acids (e.g., Cu^+, Pb^{2+}, and Ag^+ ions) when a hard base is used (such has water or alcohols); cations acting as weak acids, instead, are spontaneously exchanged with cations behaving as harder acids, if soft bases are employed (such as alkyl phosphines).

2.2.2. Solubility Product Constants. When working with water as a solvent, the solubility product constants of the starting NCs and the expected products can be used to predict the thermodynamic feasibility of a CE process.[31] The solubility product constant (K_{SP}) is a useful parameter for calculating the aqueous solubility of soluble ionic crystals under various conditions. It may be determined by direct measurements or it can be calculated from the standard Gibbs energies of formation $\Delta_f G°$ of the species involved at their standard states. Let us define $K_{SP} = [M^+][A^-]$ as the equilibrium constant for the reaction:

$$MA(s) \leftrightarrow M^+(aq) + A^-(aq) \tag{3}$$
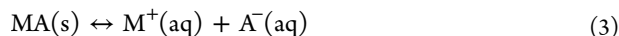
where MA is the soluble ionic crystal and M^+ and A^- are the ions produced in solution by the dissociation of MA. The Gibbs energy change can be written as

$$\Delta G° = \Delta_f G°(M^+, aq) + \Delta_f G°(A^-, aq) - \Delta_f G°(MA, s) \tag{2}$$

The solubility product constant is calculated from the equation:

$$\ln K_{SP} = -\Delta G°/RT \tag{3}$$

It follows that an ionic solid with a relatively high K_{SP} spontaneously transforms trough CE to another ionic solid with a comparatively lower K_{SP}. The solubility product constants of some metal chalcogenides of interest are reported in Table 3.

Even if the solubility of ionic crystals in many common polar solvents (such as methanol or ethanol) is not available, a rough

estimate of the thermodynamic feasibility of a specific CE reaction in these solvents can be made by a glance at the K_{SP} of that material in water.[32] With these considerations in mind, it is possible to explain why many CE reactions spontaneously take place in water or in polar solvents. For example, CE reactions involving CdS or CdSe NCs and Pb^{2+}, Ag^+, Cu^+, Cu^{2+}, or Hg^{2+} ions are thermodynamically favored as the solubilities of cadmium chalcogenides are higher than those of the expected metal chalcogenides.[36,37,70−81] Similarly, the spontaneous exchange of Zn^{2+} ions in ZnS NCs with softer Lewis acids (such as Ag^+, Pb^{2+}, Cu^{2+}, Cd^{2+}, Hg^{2+}, and Bi^{3+} ions) in water (or polar solvents) can be explained by considering the solubility product constants of these compounds.[49,82−86] The same argument applies to many other transformations taking place rapidly at room temperature in water (or in polar solvents): $CuS \rightarrow Ag_2S$, $CdSe \rightarrow Ag_2Se$ or HgSe, $PbS \rightarrow Cu_2S$, and $ZnSe \rightarrow CdSe$ or Ag_2Se.[28,63,76,79,87−90] Interestingly, when, in a polar solvent, two materials are exposed to an amount of guest cations that enables competition between the two, the solubility product constants can help to predict the outcome of the CE. In a recent work of ours, we demonstrated, for example, that the exposure of $Cu_{2-x}Se/Cu_{2-x}S$ core/shell NCs to a low amount of Hg^{2+} or Ag^+ ions led to a selective exchange of the selenide core, a transformation that can be explained by considering that metal selenides have lower K_{SP} than the corresponding sulfides.[65]

As it is possible to notice from Table 3, the solubility data of many ionic crystals, such as metal selenides, most of the metal tellurides, ternary chalcogenides (i.e., $CuInS_2$ and $CuInSe_2$) and their possible allotropes are hard to find in literature or simply they are not known.[91] In these cases, as pointed out by Moon et al., a qualitative estimate of K_{SP} for a generic MA compound can be made from its molar enthalpy of solvation (ΔH_{solv}), according to the following reaction:[31]

$$MA(s) \leftrightarrow M^+(aq) + A^-(aq)$$
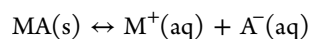
$\Delta H_{latt}[MA(s)]$ the lattice energy (or enthalpy) (see also the above discussion in section 2.1), is instead given by

$$M^+(g) + A^-(g) \rightarrow MA(s)$$
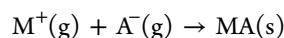
$\Delta H_{hyd}[M^+(g)]$ and $\Delta H_{hyd}[A^-(g)]$ are the hydration enthalpies of the M^+ cations and A^- anions, respectively:

$$M^+(g) \rightarrow M^+(aq)$$

$$A^-(g) \rightarrow A^-(aq)$$
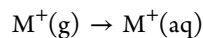
Then, the overall reaction solvation process can be written as

$$\Delta H_{solv} = \Delta H_{hyd} - \Delta H_{latt} \tag{4}$$

By defining r^+ as the radius of the M^+ cation and r^- as that of the A^- anion, ΔH_{latt} and ΔH_{hyd} are both negative values and are proportional to $(1/(r^+ + r^-))$ (see eq 2) and $(1/r^+ + 1/r^-)$, respectively. If the radius r^+ of the metal cation is held fixed and the radius r^- of the anion is increased, then the ΔH_{hyd} term decreases more than ΔH_{latt} term. Considering that $r_{S^{2-}} < r_{Se^{2-}} < r_{Te^{2-}}$, and that $\Delta H_{latt}(M_xS_y) > \Delta H_{latt}(M_xSe_y) > \Delta H_{latt}(M_xTe_y)$, it is possible to conclude that metal sulfides are more soluble than the corresponding selenides, as confirmed by the experimental values reported in Table 3.

Following the same line of reasoning, one can infer that metal tellurides have lower solubility product constants than the corresponding selenides (and sulfides). These consider-

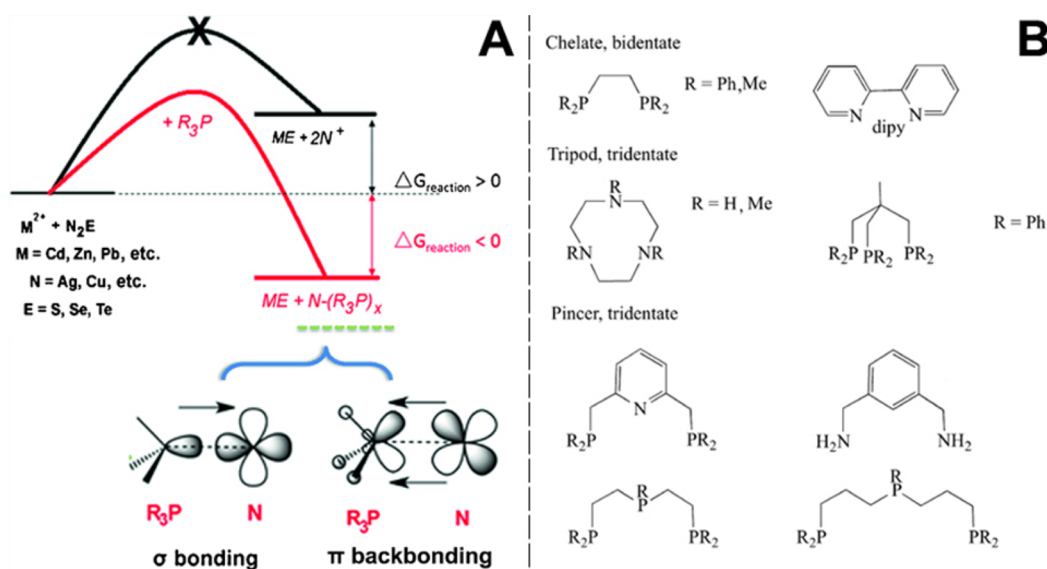**Table 3. Solubility Product Constants (K_{SP}) at 25°C of Different Metal Chalcogenides (from refs 31 and 69)**

compound	E≡S	E≡Se	E≡Te
Ag_2E	6.3×10^{-50}	3×10^{-54}	N.A.
Bi_2E_3	1×10^{-97}	1×10^{-130}	N.A.
CdE	8×10^{-27}	4×10^{-35}	1×10^{-42}
CuE	6.3×10^{-36}	2×10^{-40}	N.A.
Cu_2E	2.5×10^{-48}	N.A.	N.A.
HgE	1.6×10^{-52}	4×10^{-59}	N.A.
In_2E_3	5.7×10^{-74}	N.A.	N.A.
NiE	3.2×10^{-19}	2×10^{-26}	N.A.
PbE	8×10^{-28}	1×10^{-37}	N.A.
PtE	9.9×10^{-74}	N.A.	N.A.
SbE	2×10^{-26}	N.A.	N.A.
SnE	1×10^{-25}	5×10^{-34}	N.A.
ZnE	1.6×10^{-24}	3.6×10^{-26}	N.A.

Figure 1. (A) Thermodynamic scheme of a CE reaction initiated by different phosphines or phosphites (R_3P). Reproduced with permission from ref 114. Copyright 2015 John Wiley and Sons. (B) A small collection of multidentate ligands, commonly employed in organometallic chemistry. Each molecule has a different binding preference to metal cations, which may allow, in principle, for the modulation of the solvation energy of cations involved in CE reactions. Adapted with permission from ref 120. Copyright 2014 John Wiley and Sons.

ations can be used, for example, to explain the well-known spontaneous CE reaction between CdSe NCs and Cu^+ ions in polar solvents.[80,92,93] While the K_{SP} of CdSe is known ($K_{SP} = 4 \times 10^{-35}$), no K_{SP} data is apparently available for Cu_2Se, but we expect its solubility to be lower than that of the corresponding Cu_2S ($K_{SP} = 2.5 \times 10^{-48}$). For this reason, it is possible to realize why the formation of Cu_2Se is favored in the CE exchange reaction involving CdSe NCs and Cu^+ ions. Using the same argument, one can rationalize why CdTe NCs ($K_{SP} = 1 \times 10^{-42}$) undergo CE with Hg^{2+}, Ag^+, and Cu^+ ions in polar solvents.[94−97] Indeed, even if the solubility product constants of HgTe, Ag_2Te, and Cu_2Te are not available in the literature, one should expect them to be lower than those of HgSe ($K_{SP} = 4 \times 10^{-59}$), Ag_2Se ($K_{SP} = 3 \times 10^{-54}$), and Cu_2S ($K_{SP} = 2.5 \times 10^{-48}$), respectively, and thus much lower than that of CdTe.

2.2.3. Ligands in CE. Water and alcohols are particularly suitable for CE reactions in which the acidity of the in-going cations is lower than the one of the out-going cations. On the other hand, also nonpolar solvents have been shown to work in many different CE transformations, if coupled with proper Lewis bases in the form of ligands. In these reactions, a fine-tuning of the affinity between the outgoing cations and the ligands is required. Unfortunately, the hardness values can be used only as a guideline and every specific CE process has to be studied and optimized by choosing proper ligands.

As a general trend, soft acids as Cu^+, Ag^+, and Pb^{2+} have been extracted and replaced by harder ones, such as Cd^{2+}, Zn^{2+}, In^{3+}, Sn^{2+}, and Sn^{4+} in metal chalcogenides and pnictides using either tri-*n*-octylphosphine (TOP), tri-*n*-butylphosphine (TBP)[29,30,64,72,79,80,92,93,98−115] or carboxylates[41,88,116−118] as soft bases. Since phosphines (R_3P) have been widely exploited in most of these CE reactions, Gui et al. dedicated a study on their activity in CE reactions between N_2E (E = chalcogen and N = Ag or Cu) NCs and M^{2+} ions in solution, which can generalized by the following reaction scheme:[114]

$$N_2E(s) + M^{2+} + yR_3P \rightarrow ME(s) + 2N^+(R_3P)_x \qquad (5)$$

These compounds are able bind metal ions by donating their P lone pair and forming a monodentate terminal metal−PR_3 group (σ-bonding, see Figure 1a). Differently from amine ligands, capable only of σ-bonding, phosphines can be also good π acceptors, and therefore, they can coordinate metal cations through π-backbonding, to an extent that depends on the nature of the R groups. For these reasons, phosphines can be very high field ligands and can form strong metal−ligand (M−L) bonds. The particular interest in R_3P arises from the fact that their affinity to metal cations can be easily modulated in a systematic and predictable way over a wide range by tuning the electron-donor power and steric effect of R groups.[119] Moreover, as spectator ligands, R_3P could be also used to stabilize metal−ligand (M-L) units as they are able to form $(R_3P)_n$ Metal−Ligand complexes.[120] Using the $Ag_2S \rightarrow CdS$ CE reaction as a case study, Gui et al. could rank the activity of many different phosphines: triethyl phosphine > trimethyl phosphite > triethyl phosphite > tributyl phosphine > triphenyl phosphine > trioctyl phosphine > tri-*p*-tolylphosphine > tris(*o*-methoxyphenyl) phosphine. Thus, by varying the phosphine molecules used in the CE transformation, Gui et al. could prove a good control over the residual amount of Ag^+ ions inside the product CdS NCs.

In addition to tertiary phosphines, also amines and carboxilates have been shown to be fundamental ligands in many CE reactions as they behave as strong and weak Lewis bases, respectively. For example, the exchange between CdSe and Pb^{2+} ions was found to be triggered by the presence of oleylamine (OA) that promotes the extraction of Cd^{2+} ions by forming a stable Cd-OA complex.[121] This can be easily understood by considering that Cd^{2+} is a harder Lewis acid if compared to Pb^{2+} and OA is a hard base, so that the Cd-OA coupling results in a more stable acid−base combination than Pb-OA. On the other hand, CE reactions involving PbSe or PbS NCs with Cd^{2+} ions, when performed in a nonpolar solvent, are made possible by the presence of an oleate moiety that, being a weak base, promotes the extraction of Pb^{2+} cations.[41,122−127] Amines with long alkyl chains (such as OA or octadecylamine)

have also been shown to trigger CE between ZnSe or ZnTe NCs and Cd^{2+}, Mn^{2+}, and Pb^{2+} ions. This is due to the fact that such amines bind preferentially Zn^{2+} ions which are slightly harder than Cd^{2+}, Mn^{2+}, and Pb^{2+} ones (see Table 2).[42,64,100,128−130] Similarly, OA has been successfully employed to drive CE reactions involving TiS_2 nanodiscs and Cu^+, Ag^+, Mn^{2+}, and Cd^{2+} ions to form the corresponding metal sulfides.[131] In analogy with phosphines, the activity of amines can be tuned over a relatively broad range depending on the groups bound to the N atom and on their steric hindrance. As it is possible to see in Table 2, primary (RNH_2), secondary (R_2NH), ternary (R_3N), and aromatic amines have quite different values of hardness, ranging from 4.4 of aniline ($C_6H_5NH_2$) up to 6.3 of trimethyl amine (($CH_3)_3N$).

A logical consequence of the discussion above is that the "library" of ligands that can effectively work in CE reactions is likely to expand in the near future, and this will be beneficial for improving the control over such reactions and/or to access new ones. For example, multidentate ligands, which have never been tested in CE reactions, could be used for finely tuning CE reactions in organic media, allowing, in principle, to increase the solvation of exiting cations.[120] Bidentate diamine ligands, such as ethylenediamine, indeed, have been widely employed in metal−organic chemistry as they can coordinate transition-metal ions in a chelating mode to form stable complexes.[132−134] A small collection of such ligands is shown in Figure 1b.

Thiols, thioethers and disulfides (R_2S_2) might also turn out to be valuable ligands in CE reactions. Coordination complexes of transition metal ions with sulfur-containing ligands are ubiquitous in nature. It is also well-known that many organometallic compounds (containing heavy metals) owe their toxicity to a strong affinity for sulfur, which causes them to bind to biologically important thiol groups. Logically, then, molecules containing thiol groups have been used in antidotes to poisoning by such organometals.[135] Moreover, the use of thiols in colloidal synthesis is widespread. As it is possible to see in Table 2, thiols are extremely soft bases, while thioethers, for example ($CH_3)_2S$, exhibit typical hardness values that are similar to those of phosphines. These sulfur based ligands could be tested as complementary soft Lewis bases, being, in principle, able to promote CE reactions in which soft acids have to be extracted. This could be particularly beneficial in those CE reactions in which phosphines are not desirable as they might etch metal chalcogenide NCs by extracting either $Se^{2−}$ or $S^{2−}$ anions out of them.[136,137]

3. MECHANISMS AND KINETICS OF CE

Even if a CE reaction is thermodynamically favored, kinetic factors, such as activation energy barriers and/or ions diffusivity, play a key role in determining its feasibility and the nature of the final products. At present, several aspects related to CE reactions in NCs are debated. When a host NC is exposed to a solution of guest cations, the latter can diffuse inside the NCs lattice, either via an interstitial or via a vacancy-assisted mechanism. Depending on their diffusivity, the guest ions can either probe the whole host NCs or they can only access the outer surface layer. At a later stage, the fast replacement of cations that leads to the nucleation of the product phase occurs at the sites that are energetically favored/allowed. During this step, host cations are expelled from the NCs through an out-diffusion or kick-out mechanism and become solvated by the ligand molecules present in the solution.

The region(s) where the CE take place, also called the "reaction zone", can include the whole surface of the NC or a fraction of it. When the transformation front includes the whole NC surface, the intermediate steps of a CE reaction are represented by core−shell or graded core−shell NHCs, depending on the solubility of reactant and product materials (see section 5.3.2). When the nucleation of the product occurs at specific sites of the host NC surface (such as the tips of a NR or the corners of a polyhedral NC) the intermediate steps observed in CE are represented by multi domain hetero-structures (such as Janus-like, striped or segmented hetero-structures). All these structures will be discussed in detail in section 5.3. Once a reaction zone is formed, the CE reaction proceeds then toward the remaining unexchanged part of the NC trough solid state ions diffusion. This step, in most cases, is the rate-limiting one and it strongly influences the outcome of the CE reaction.[42,94,138] Many factors influence the rate at which the solid state diffusion can take place: the possibility of cations to diffuse through interstitial sites, the presence of vacancies (even on the surface), dislocations, stacking faults, and possibly grain boundaries inside the NC.[40,88,104,137,139]

3.1. Solid-State Diffusion via Vacancies

In a recent work, Groenveld et al. proposed a detailed description of the solid state diffusion process taking place during a CE reaction.[42] Their suggested model, specifically conceived for the transformation of ZnSe to CdSe NCs, can be generally extended to many of the known CE transformations. It is noteworthy to specify that ZnSe and CdSe structures are completely miscible, so that CE, in this case, occurs trough the formation of $Cd_xZn_{1−x}Se$ solid solutions, meaning that both Zn^{2+} and Cd^{2+} ions can coexist in the same crystal domain (this will be discussed more extensively in section 5.1). Once a reaction zone has formed, two solid-state diffusion fluxes allow the reaction to proceed: inward diffusion of Cd^{2+} and outward diffusion of Zn^{2+}. In bulk ionic crystals, solid state diffusion processes are promoted by point defects that are able to move through the crystal and to act as "vehicles for diffusion" of atoms.[139]

Of particular interest for CE reactions are diffusion-relevant point defects such as Frenkel pairs. A Frenkel pair forms when a cation moves from its lattice position to an interstitial site, creating a cation vacancy and a self-interstitial (V_{Zn} and Zn_i in the present discussion, respectively), guaranteeing global charge neutrality (see Figure 2). In the specific case of ZnSe, Frenkel defects have been shown to promote self-diffusion of zinc ions in the bulk. The formation of these defects is strongly temperature-dependent as they minimize the Gibbs free energy of the crystal itself.[139] At a given temperature, the concentration of Frenkel pairs (n_{FP}) can be expressed as

$$n_{FP} \propto e^{-\Delta H_{FP}/2kT}$$

where ΔH_{FP} is the formation enthalpy of a Frenkel defect, k is the Boltzmann constant, and T is the temperature. Once formed, both Zn_i and V_{Zn} can move through the solid by hopping from site to site, which requires further activation energy.

Depending on the temperature at which the CE is performed, different scenarios can be distinguished: at low temperature (for which n_{FP} is negligible) both inward and outward cation diffusions are precluded, therefore CE either cannot take place or it is limited to the outer surface layer of the NCs. In the specific case of ZnSe NCs exchanged with Cd^{2+}
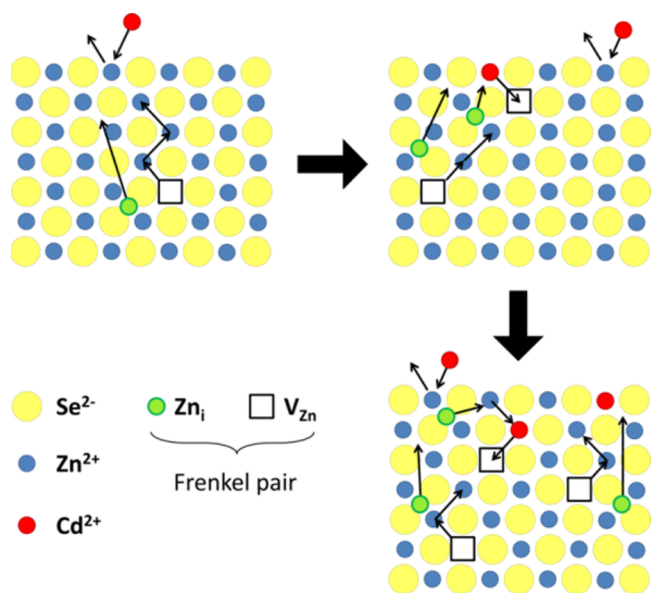
Figure 2. Sketch of the mechanism proposed by Groenveld et al.[42] for CE of ZnSe NCs with Cd^{2+} ions. Fast CE takes place at the NC surface and it is followed by the relatively slower thermally activated solid-state diffusion. The ion diffusion is driven by Frenkel pairs (Zn_i-V_{Zn}), so that the outward diffusion flux consists of interstitial zinc cations (Zn_i) moving toward the NC surface, while the incoming Cd^{2+} cations diffuse inwardly by hopping into the V_{Zn}.

ions, this is observed at 150 °C and NHCs form that consist of a ZnSe core coated with a thin CdSe shell (one monolayer). At higher temperatures, n_{FP} is sufficiently high to allow solid-state diffusion processes to occur. The host cations migrate to the surface as interstitials (Zn_i) and are exchanged by Cd^{2+} guest cations, which hop to the closest available vacancy (V_{Zn}) and thus diffuse inward. Once CE takes place at the surface, the Frenkel pair is annihilated, shifting the equilibrium toward the formation of additional Zn_i-V_{Zn} pairs. At the same time, a concentration gradient establishes driving the Cd^{2+} flux inward

(via V_{Zn}) and the Zn^{2+} flux outward (as Zn_i). In Figure 2 a schematic representation of the solid-state diffusion is depicted. In some cases, this gradient has been shown to keep on driving the ions interdiffusion even after the removal of host NCs from the guest cations solution.[94] When the concentration of Frenkel defects is sufficiently high (at high T), the Zn^{2+} for Cd^{2+} exchange at the surface occurs simultaneously with solid-state diffusion processes within the NC.

The generation of Frenkel pairs is not the only process through which vacancies can form. Wang et al., in a more recent study, highlighted the relatively low energy required to create a cationic vacancy in ionic NCs.[39] For example, the calculated Pb^{2+}-vacancy formation energy in a PbS NC (passivated with Cl^- ions) can be as high as 0.96 eV (93.6 kJ/mol) on the edge of a {111} facet, and surprisingly low, that is 0.09 eV (8.7 kJ/mol), on the edge of a {100} facet. The removal of a surface cation and the consequent creation of a surface vacancy obviously require less energy than the formation of a Frenkel defect. It is well-known, indeed, that adatoms, corner atoms, and atoms at terrace steps of a crystal surface possess high energy since they are less tightly bound. The presence of ligands, as Cl^- species in the model of Zherebetskyy et al.,[39] can further reduce the energy required to extract such surface atoms. Motivated by similar considerations, Casavola et al. studied the chemical transformation of PbSe to CdSe and proposed a surface-vacancy assisted mechanism.[41,140,141] The PbSe-CdSe system is different from the ZnSe-CdSe one since PbSe and CdSe are not miscible, meaning that Cd^{2+} and Pb^{2+} cannot coexist in the same crystal domain. After the initial surface exchange and the formation of a first CdSe layer, a surface vacancy is allegedly formed and then it diffuses through the CdSe shell to the PbSe/CdSe interface. This happens via multiple moves of Cd^{2+} ions to the closest vacant sites (see Figure 3a,b). Next, a Pb atom can jump into the vacancy, thereby leaving the PbSe core. Then, through multiple vacancy-assisted hops the Pb atom can reach the surface of the CdSe shell, after which it is exchanged for a Cd atom (see Figure 3c–f).
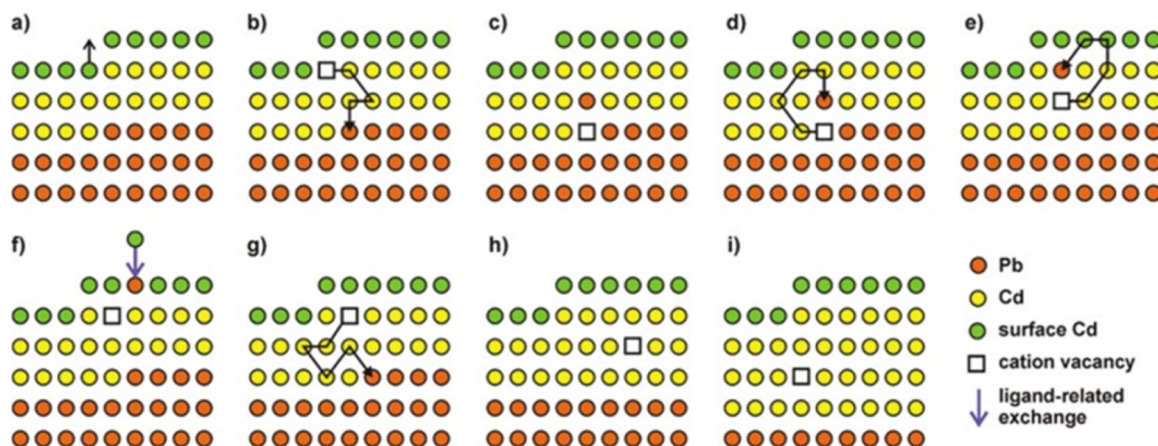
Figure 3. Schematic of a plausible mechanism of the CE reaction between PbX NCs and Cd^{2+} ions. The sketch represents a two-dimensional projection of the PbSe-CdSe interface with Pb (orange) and Cd (yellow) atom positions. Light green dots represent surface Cd atoms; Se anions are not shown. (a) The formation of a cation vacancy at the surface is followed by (b) diffusion of the vacancy to the PbSe-CdSe interface. (c−e) Next, the Pb atom can diffuse to the interface by means of vacancy-assisted migration, whereby many (Cd-associated) vacancy jumps are required to enable (f) diffusion of Pb to the surface, where it undergoes a ligand-enabled Cd-for-Pb exchange. (b−g) This process continues until (h) the Pb layer is completely replaced by Cd atoms, after which (i) the next Pb layer is replaced. (b, d, e, g) only one of many possible vacancy diffusion paths is shown. Reproduced from [Casavola, M.; van Huis, M. A.; Bals, S.; Lambert, K.; Hens, Z.; Vanmaekelbergh, D. Anisotropic Cation Exchange in PbSe/CdSe Core/Shell Nanocrystals of Different Geometry *Chem. Mater.* **2012**, *24*, 294−302]. Copyright 2012 American Chemical Society.

Differently from the Zn-to-Cd exchange, here the "immiscibility rule" forces the vacancy to travel from the NC surface to the PbSe-CdSe interface and then back, in order to enable CE. HAADF-STEM tomography on these systems confirmed that Pb/Cd intermixing occurs only at the PbSe/CdSe interfacial layer. Interestingly, Lechner et al. could experimentally detect, through SAXS analysis, the presence of a submonolayer of Pb atoms bound on top of the Cd based shell.[38] This finding directly supports the proposed exchange mechanism: the Pb^{2+} ions have to diffuse toward the particle surface, where they are subsequently exchanged by the Cd^{2+} ions within the solution. The process, in this specific system, proceeds in a layer-by-layer fashion (see Figure 3g−i). The interfacial "corner" Pb atoms in the incomplete Pb/Cd atomic plane are in an energetically unfavorable position: consequently, the removal of such Pb atoms requires much less energy than the removal of a Pb atom from a continuous atomic plane. This is believed to occur because the rock-salt PbSe and the zinc-blend CdSe structures have different cation coordinations (octahedral and tetrahedral, respectively). The same explanation might apply to many CE reactions in which the intermediate structures consist of heterostructures having two domains of different materials sharing a flat interface.

The surface vacancy-assisted mechanism has been also directly demonstrated by Justo et al. in studying the PbS-CdS system.[40] They exposed PbS NCs with either a full Pb coverage or surface Pb vacancies (i.e., having a partial Pb-surface coverage) to Cd^{2+} ions. While no exchange was observed at room temperature for PbS NCs with full excess Pb coverage, the NCs with partial surface coverage exhibited a self-limiting adsorption of Cd, forming PbS|CdS core|shell structures with restricted shell thickness. At higher temperatures, they observed a similar limiting shell thickness for both NCs when using an excess of cadmium. Moreover, in the case of PbS NCs with partial surface coverage, a complete exchange occurred only when working with reduced amount of Cd. This suggests that the CE reaction can run to completion only at low Cd loading, that is, when the surface vacant sites on PbS NCs are not "poisoned" by an excess of Cd^{2+} ions adsorbed on the NCs surface. These findings support the hypothesis that surface vacancies not only facilitate the adsorption of guest cations from the solution phase, but they also enable the exchange of ions between the inner lattice sites and the surface. This, in turn, demonstrates that surface reactions can indeed limit the rate of a CE reaction and they can play a fundamental role in the kinetics of the overall transformation.

It must be emphasized, however, that thermally activated CE processes are hardly driven by surface vacancies or by Frenkel defects alone but most likely by both types of defects at the same time. In these reactions, the temperature can be used as a sensitive parameter to tune the CE kinetics and consequently to tailor both the composition and the elemental distribution profile of the product.[42,100] On the other hand, elevated temperatures may alter the materials stability or trigger secondary processes, such as red-ox reactions, etching, sintering, etc. Equally importantly, at high temperature, the exchange might proceed close to thermodynamic equilibrium, preventing kinetically controlled access to metastable or nonequilibrium structures, which instead represent an interesting feature of CE as a synthetic tool (see section 4).

3.1.1. CE in Systems with High Density of Vacancies.
Vacancies are often present in compound nanostructures that are synthesized under wet chemical conditions, as their

composition is never perfectly stoichiometric. Aside from this, there are classes of materials which, already in the bulk, can exist in a wide range of stoichiometries of the component ions. This is the case of the entire family of copper chalcogenides, namely, copper sulfides ($Cu_{2-x}S$), selenides ($Cu_{2-x}Se$), and tellurides ($Cu_{2-x}Te$). Colloidal NCs of these materials can be easily synthesized with control over the shape and size with the additional possibility of manipulating the density of copper vacancies,[97,142,143] and have been tested in many CE reactions. Our group recently studied these NCs, with particular focus on $Cu_{2-x}Se$ and $Cu_{2-x}S$ ones, to explore the role of vacancies in CE reactions. In a first work, we investigated CE in copper selenide NCs with Zn^{2+} and Cd^{2+} ions by comparing the reactivity of close-to-stoichiometric (that is, Cu_2Se) NCs with that of substoichiometric ($Cu_{2-x}Se$) ones.[137] Under identical reaction conditions, CE in Cu_2Se NCs was found to proceed much slower than in the corresponding $Cu_{2-x}Se$ NCs (see Figure 4a,b). Moreover a small excess of guest cations was found to be sufficient to achieve full exchange in $Cu_{2-x}Se$ NCs, while under the same CE conditions, the Cu_2Se NCs still contained a considerable fraction of Cu ions. The evident conclusion of the work was that Cu vacancies in copper chalcogenide NCs
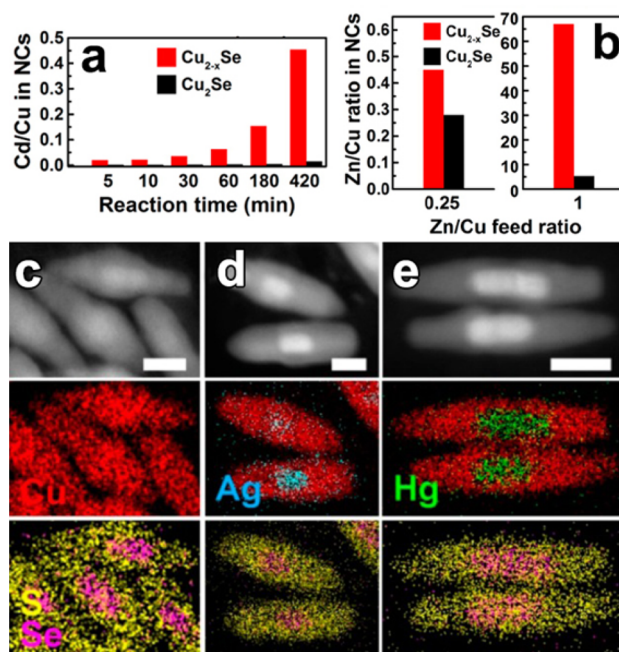
Figure 4. (a) Diagrams displaying the evolution of the Cd/Cu ratio in the heavily substoichiometric ($Cu_{2-x}Se$, red) and close to stoichiometric (Cu_2Se, black) NCs over the time of the $Cu^+ \rightarrow Cd^{2+}$ CE reaction at RT using a Cd/Cu feed ratio of 0.5. (b) Diagrams displaying the dependence of the Zn/Cu ratio in the vacant (red) and stoichiometric (black) NCs on the Zn/Cu feed ratio in overnight CE reactions at RT. Reproduced from [Lesnyak, V.; Brescia, R.; Messina, G. C.; Manna, L. Cu Vacancies Boost Cation Exchange Reactions in Copper Selenide Nanocrystals *J. Am. Chem. Soc.* **2015**, *137*, 9315−9323]. Copyright 2015 American Chemical Society. (c−e) CE in $Cu_{2-x}Se/Cu_{2-x}S$ NRs with Ag^+ and Hg^{2+} ions. HAADF-STEM images of groups of (c) pristine, (d) Ag^+, and (e) Hg^{2+} partially exchanged $Cu_{2-x}Se/Cu_{2-x}S$ NRs with the corresponding STEM-EDS elemental maps. Scale bars are 20 nm. Reproduced from [Miszta, K.; Gariano, G.; Brescia, R.; Marras, S.; De Donato, F.; Ghosh, S.; De Trizio, L.; Manna, L. Selective Cation Exchange in the Core Region of Cu2-xSe/Cu2-xS Core/Shell Nanocrystals *J. Am. Chem. Soc.* **2015**, *137*, 12195−12198]. Copyright 2015 American Chemical Society.
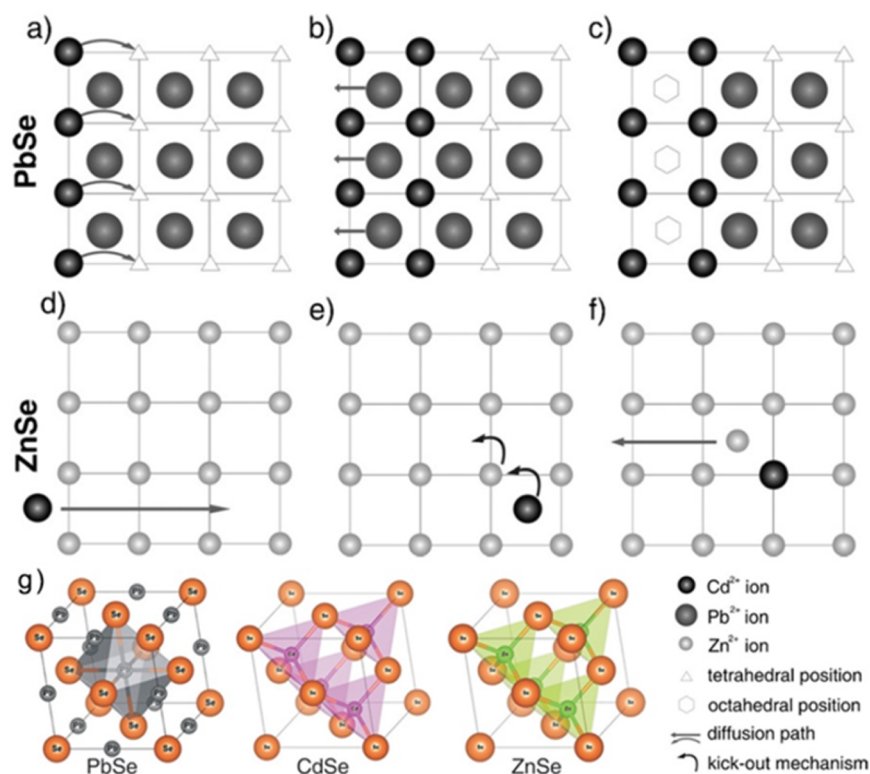
Figure 5. Exchange mechanism for the CE with cadmium in (a−c) PbSe and (d−f) ZnSe NCs.(g) The lattice structures involved in these CE experiments. Adapted with permission from ref 145. Copyright 2015 John Wiley and Sons.

accelerate the exchange process, most likely by offering to the exchanging ions several alternative pathways for diffusion, even at low temperature.

In another work, we studied CE reactions between $Cu_{3-x}P$ NCs and In^{3+} ions in order to synthesize InP NCs.[104] Copper phosphide NCs are naturally substoichiometric in copper, and therefore, in analogy with copper chalcogenides, they are characterized by a high density of Cu vacancies. Our findings were that $Cu_{3-x}P$ NCs can undergo total CE, to form InP NCs, at mild conditions and by employing only a small excess of In^{3+} ions. On the other hand, CE reactions to prepare III−V semiconductor NCs have been shown to require much higher temperatures and a high excess of guest cations (for the Cd_3P_2 → InP CE reaction, for example, a In/Cd feed ratio of 100 was required to get full exchange) since the diffusivity of ions in covalent semiconductors can be orders of magnitude lower than that in ionic systems.[144] This brought us to conclude that CE reactions in $Cu_{3-x}P$ NCs are strongly favored and assisted by Cu vacancies.

In a recent work, we demonstrated that that Cu vacancies in copper chalcogenide NCs not only boost CE reactions, but also can provide sufficient mobility for the guest cations to initiate the exchange in the preferred zone of the host crystal.[65] To prove this point, we used core|shell $Cu_{2-x}Se|Cu_{2-x}S$ nanorods as starting seeds, Ag^+ or Hg^{2+} ions as guest cations and methanol as polar solvent. At the early stages of the CE transformation, the guest cations diffused through the $Cu_{2-x}S$ shell and selectively replaced Cu^+ ions in the $Cu_{2-x}Se$ core region (see Figure 4c−e). The preferential exchange in the core is driven by thermodynamic factors, which favor the formation of metal selenides over the corresponding sulfides (see section 2.2.2). Nearly identical CE transformations were performed on CdSe|CdS core|shell NRs with Cu^+ or Ag^+ ions. In such

reactions, the thermodynamic driving force should likewise promote the initial selective replacement of the selenide core region. In this case, however, CE starts with a partial replacement of cadmium ions from the sulfide shell, while the core region remains unaltered. These control experiments suggests that, most likely, it is the high ions diffusivity in copper chalcogenide NCs, promoted by Cu vacancies, that enables guest cations to probe the whole host structure, such that they initiate the exchange where it is mostly thermodynamically favored. On the contrary, in cadmium chalcogenide NHCs this is not possible. This work suggests that in CE reactions involving nanoscale systems with high ionic diffusivity, the reaction zone that is formed at the beginning of the transformation might not be necessarily limited to the surface of a NC, but it could involve any region of the host material.

### 3.2. Solid-State Diffusion via Interstitials

Bothe et al., in a recent study, proposed a model in which the ion diffusion and exchange processes are exclusively mediated by interstitial lattice sites.[145] This conclusion was reached by studying two model CE reactions that involve the exposure of PbSe or ZnSe NCs to Cd^{2+} ions. Both CE processes, as seen in the previous section, had been previously explained as mediated by vacancies.[40−42] In this model, instead, the relatively small Cd^{2+} ions (ionic radius 78 pm) are assumed to be diffusing in both ZnSe and PbSe structures by occupying tetrahedral interstitial sites. Moreover, in the PbSe → CdSe CE transformation the interstitial sites of the rock-salt PbSe lattice represent the lattice sites of the developing CdSe crystal, while in the ZnSe → CdSe case the exchange has to take place on the existing tetrahedral sites of the zb-ZnSe lattice. By monitoring the kinetics and the temperature-dependent behavior of these CE reactions, Bothe et al. extrapolated activation energy values

in the range of 30−40 kJ/mol, which are in good agreement with an ion exchange transformation occurring without the creation of vacancies. A vacancy-mediated CE in bulk materials would require higher energies, of the order of 10^2 kJ/mol. Motivated also by the fact that these ions have short diffusion pathways and that the concentration of vacancies in these NCs is rather low at RT, the authors proposed an interstitial-mediated mechanism to rationalize such CE reactions (see Figure 5). In the PbSe → CdSe reaction, Cd^{2+} ions start occupying tetrahedral interstitial sites in the PbSe lattice, while at the same time the Pb^{2+} ions out-diffuse by hopping through the octahedral interstitial sites. Clearly, this process is completely controlled by diffusion and the activation energies involved are, thus, the ones for the diffusion through the interstitial sites. In the ZnSe → CdSe transformation, Cd^{2+} ions can diffuse through both octahedral and unoccupied tetrahedral sites by replacing Zn^{2+} ions in their respective lattice positions by a kick-out mechanism. Zinc ions, now occupying interstitials, will then leave the crystal by diffusion through interstitials. For these reactions, it was proposed that the rate-determining step is not the diffusion but the ion exchange. In this case, in fact, the exchange has small activation energy as it is believed to proceed through a kick-out mechanism, that is, without any vacancy creation.

3.3. Cooperativity in CE Transformations in NCs

CE in many cases was assumed to be a diffusion-limited transformation. In some systems, however, as pointed out by White et al., sharp and instantaneous CE transformations, evidencing some sort of cooperativity, are observed.[43,146,147] A typical feature of a cooperative system is the "all-or-nothing" behavior: rather than progressively transforming through intermediate steps, the system makes a sudden sharp transition from the initial to the final state in response to a specific input. The CE transformation of CdSe to Ag_2Se (or to Cu_2Se) NCs seems to follow such behavior. At the early stages of the process, the incorporation of guest cations (Ag^+ or Cu^+) into a NC lattice has a relatively low probability of occurrence. However, once this initial step does take place, it activates the NC for further doping. Each doping event increases the affinity of the same NC for the subsequent guest ions incorporation, until a critical doping concentration is reached. Then, the NC is ready to transform by taking up every available Cu^+ or Ag^+ ion, which results in a cascade of guest ion incorporation events and in an abrupt phase transition from a doped CdSe NC to Cu_2Se or Ag_2Se. Thus, at the intermediate steps of the CE reaction, each NC has either a CdSe composition (with some Ag^+ or Cu^+ dopants) or it has transitioned to a fully exchanged Ag_2Se or Cu_2Se NC, thus exhibiting the typical "all-or-nothing" behavior of a cooperative system. Optical monitoring such reaction with single NC resolution revealed that indeed each CdSe NC waits a specific amount of time, of the order of few hundred milliseconds, before making a sudden transition to the Ag_2Se phase.[43,147]

Ott et al. recently proposed a detailed microscopic model (based on density-functional theory calculations and dynamical simulations of CE) that is in line with the co-operative behavior observed by Jain and co-workers.[115,148] The model, specifically built for the CdSe → Ag_2Se transformation, considers as first step the entrance of Ag^+ ions in the CdSe lattice as interstitials (Ag^+_{int}), followed by their rapid diffusion, still through interstitial sites, toward the central region of the lattice (see Figure 6a). As the concentration of Ag^+_{int} ions increases, their
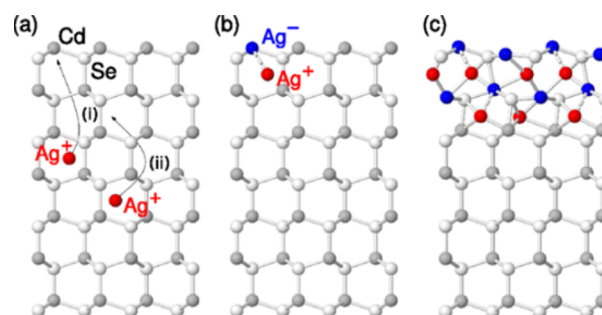

Figure 6. Microscopic model of Ag doping and CE of CdSe NCs. (a) At low concentration, the Ag^+ ions diffuse through interstitial sites (Ag^+_{int}). As their concentration in the lattice increases, their mutual repulsion pushes them toward the NC surface, where a Cd kick-out reaction can occur [step (i)]. The substitutional Ag^-_{Cd} created by the kick-out reaction attracts the remaining Ag^+_{int} [step (ii)]. (b) An electrostatically bound complex is then formed by two Ag at the surface, generating a nucleus of Ag_2Se. (c) At even higher Ag concentrations, all interstitial and Cd sites at the surface become occupied with Ag. This fully substituted domain closely resembles the naumannite crystal structure of Ag_2Se. Reproduced with permission from ref 148. Copyright 2014 American Physical Society.

mutual repulsion becomes dominant and drives the ions toward the surface. At this stage, to compensate electrically for the positive charge accumulating near the surface, a "kick-out reaction" occurs, in which an Ag^+_{int} ion moves onto a Cd site forming a Ag^-_{Cd}. The Cd^{2+} ion can immediately leave the NC by out-diffusing from the NC to the surrounding solution. At the same time, the Ag^-_{Cd} attracts a mobile Ag^+_{int}, generating a Ag_2 pair around a Se anion, that is a Ag_2Se nucleus (see Figure 6b). The formation of such Ag_2 pair triggers a cascade of CE steps through Coulomb interactions, as the formation of contiguous regions of electrostatically bound Ag_2 pairs is strongly favored. The model explains why initial Ag^+_{int} doping of a NC strongly enhances further silver doping within the same NC, causing eventually a sharp transition from a lightly doped CdSe NC to the Ag_2Se phase (a typical example of co-operative behavior).

A common feature of the transformations from CdSe to Ag_2Se or to Cu_2Se and those involving CE of $Cu_{2-x}Se/Cu_{2-x}S$ NRs with Ag^+ or Hg^{2+} ions (discussed in section 3.1.1) is that the guest ions appear to be able to probe the whole host NC and to start the CE in a "preferred" region. While in CdSe this is possible through the high diffusivity of Ag^+ and Cu^+ ions via interstitials, in copper chalcogenides the fast ion diffusion is favored by the high density of vacancies. These examples support the idea that the reaction zone, which is established at the beginning of a CE transformation, might not be necessarily limited to the surface of a NC, as commonly believed.

3.4. Influence of Crystal Structure on CE Reactions

In the simplified discussion of section 2, the overall CE reaction was reduced to a model that consists of the dissolution of a starting AX crystal to form A^+ cations and X^- anions which, upon reaction with B^+ cations, generate a BX crystal. In an actual CE reaction, the host AX crystal is not dissolved and the X^- anion framework can be thought as a rigid skeleton with a limited flexibility that sustains the whole reaction, while the cations diffuse in and out. The activation barrier for the diffusion and the exchange of cations depends on many factors, including structural differences between the reactant and the product phases. It is therefore important, before performing a
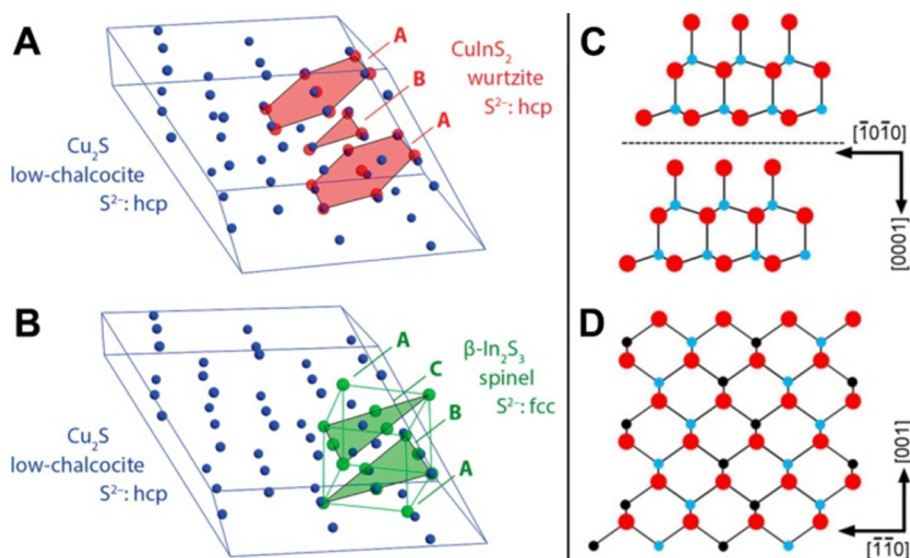
Figure 7. (A and B) Comparison of the anionic sublattice of low-chalcocite $Cu_{2-x}S$ with wurtzite $CuInS_2$, evidencing that the anionic sublattice of low chalcocite $Cu_{2-x}S$ (blue spheres) is compatible with that of wurtzite $CuInS_2$ (red spheres) since both sublattices have an hcp arrangement (A). Comparison of low-chalcocite unit cell (blue spheres) with In_2S_3 (green spheres). The spinel In_2S_3 structure has a fcc anionic sublattice, where the C layer has to dislocate by 58% of a S−S distance in order to fit in the low-chalcocite lattice (B). Reproduced from [van der Stam, W.; Berends, A. C.; Rabouw, F. T.; Willhammar, T.; Ke, X.; Meeldijk, J. D.; Bals, S.; de Mello Donega, C. Luminescent CuInS2 Quantum Dots by Partial Cation Exchange in Cu2−xS Nanocrystals *Chem. Mater.* **2015**, *27*, 621−628]. Copyright 2015 American Chemical Society. (C) Description of the In−Se layer shown in [0−1−10] projection of the In_2Se_3 structure (bigger dark circle, Se; smaller light circle, In). (D) [110] projection of $CuInSe_2$ structure (smaller dark circle: Cu). Adapted with permission from ref 91. Copyright 2011 IOP Publishing. All rights reserved.

CE reaction, to compare the starting AX and the final BX crystal structures. If the anion framework of the expected BX crystal structure can be accessed only by a severe deformation of the starting AX lattice, the AX → BX conversion might not take place or it might result in deformed BX NCs.[66] For example, the CE involving $Cu_{2-x}Se$ NCs and Sn^{4+} ions cannot proceed to the expected $SnSe_2$ phase, but it reaches a composition limit of Cu_2SnSe_3.[149] This can be rationalized by considering that the initial $Cu_{2-X}Se$ NCs have a *fcc* anion sublattice, while $SnSe_2$ has a trigonal crystal structure characterized by a stack of $SnSe_2$ layers bound together by weak Se−Se van der Waals bonds. Therefore, even if the exchange between Cu^+ and Sn^{4+} cations is promoted by a proper choice of ligands, complete CE in this case would entail a pervasive reorganization of the anion framework, which is not possible under the mild reaction condition at which the exchange is carried out. Harsher conditions on the other hand, were found to trigger redox reactions.[149]

Similarly, van der Stam et al. demonstrated that $Cu_{2-x}S$ NCs with hexagonal crystal phase (low-chalcocite) can undergo CE with In^{3+} ions up to a $CuInS_2$ stoichiometry.[103] The resulting NCs exhibit a wurtzite crystal structure whose anion sublattice, in line with that of the starting low-chalcocite $Cu_{2-x}S$ NCs, has a hexagonal close-packed arrangement. On the other hand, In_2S_3 can exist in three different crystal structures, denoted as α, β, and γ, all of them characterized by an fcc stacking of S^{2-} anions and differing from each other only in the ordering of the In^{3+} cations. Hence, the anion sublattice is intrinsically different from that of hexagonal $Cu_{2-x}S$ and of wurtzite $CuInS_2$, preventing the full conversion from $Cu_{2-x}S$ to In_2S_3 (see Figure 7A,B).

Gupta et al. demonstrated that the exchange between wurtzite CdSe nanorods and Hg^{2+} ions in water, even if thermodynamically favored (see Table 3 and section 2.2.2) on the basis of the much lower solubility product of HgSe relative

to that of CdSe, was strongly limited.[150] This was attributed to the differences between the two end point structures of the transformation: wurtzite CdSe on the starting side and cubic HgSe on the end side. In order for the full exchange to take place, the Se^{2-} framework would have to be deformed, creating a high-strain field in the NCs. Eventually the entering Hg^{2+} ions would experience repulsive elastic forces from the host CdSe lattice, and this explains why their inclusion was limited up to a composition corresponding to $Cd_{0.9}Hg_{0.1}Se$. There are nonetheless cases of CE transformations in which a significant reorganization of the crystal structures takes place. Yuho et al. reported, for example, a CE transformation from trigonal In_2Se_3 NCs to tetragonal $CuInSe_2$ NCs at room temperature in water.[91] Similarly to $SnSe_2$, In_2Se_3 has a layered structure consisting of alternating sheets (Se−In−Se−In−Se) held together by van der Waals bonds (see Figure 7C,D). During the CE process, Cu^+ ions both substitute In^{3+} cations and occupy "vacant sites" within the In_2Se_3 layers (see the dashed line in Figure 7C). The reorganization of the lattice upon inclusion of Cu^+ ions produces a small volume expansion of the unit cell (~5%) and the cleavage of weak Se−Se van der Waals bonds. It is remarkable that, in this specific system, these requirements are fulfilled even at RT.

Along the same lines, in a recent work of ours, we observed that the CE transformation from covellite CuS to cinnabar HgS, which requires a marked reorganization of the crystal lattice of the starting NCs, can take place already at room temperature.[151] The covellite (CuS) structure is formed by Cu−S layers stitched together by S−S covalent bonds. Every Cu−S layer, in turn, is composed by a trilayer motif made of a layer of triangular CuS_3 units between two layers of CuS_4 tetrahedra. Even if the transformation from CuS to HgS should be promoted by a polar solvent (see section 2.2.2), no exchange was observed by exposing the CuS NCs to Hg^{2+} ions in methanol. The formation of a HgS phase requires, in fact, not
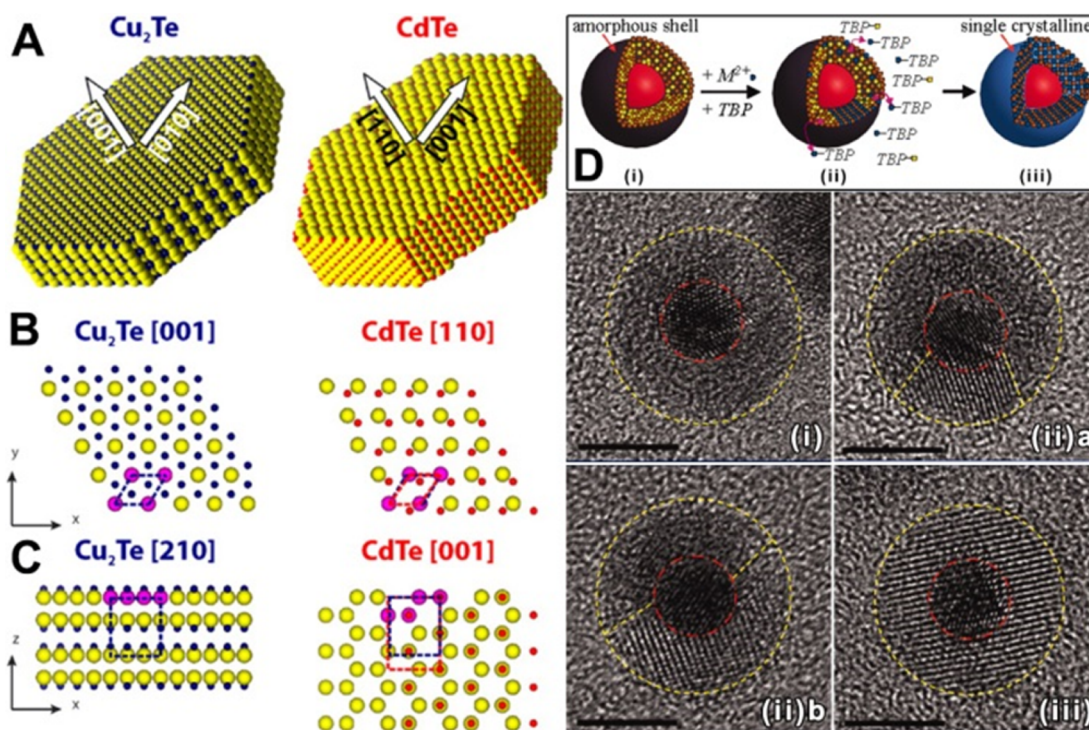
Figure 8. (A) Sketches of the Cu$_2$Te and CdTe disks, with arrows indicating the respective crystal orientations. (B and C) Schematic views of slabs of the Cu$_2$Te and CdTe structures, evidencing a few atomic layers of the nanodisks, according to the respective phases and orientations determined by HRTEM. Each Te anion (larger yellow spheres) in the (001) plane of Cu$_2$Te forms an hexagonal lattice (cell indicated by blue dashed lines) with the three neighboring anions (magenta) on the same plane. The (110) anionic sublattice in wurtzite CdTe still resembles a distorted hexagon in projection (red dashed lines). However, the Te atoms of the original Cu$_2$Te structure have to move considerably in the z-direction to accommodate for the Cd atoms and form the two (110) layers in wurtzite CdTe. The volume occupied by the same number of Te atoms is included within the blue and red frames in Cu$_2$Te and CdTe, respectively. Reproduced from [Li, H.; Brescia, R.; Povia, M.; Prato, M.; Bertoni, G.; Manna, L.; Moreels, I. Synthesis of Uniform Disk-Shaped Copper Telluride Nanocrystals and Cation Exchange to Cadmium Telluride Quantum Disks with Stable Red Emission *J. Am. Chem. Soc.* **2013**, *135*, 12270−12278]. Copyright 2013 American Chemical Society. (D) Schematic of the CE transformation from Metallic|Ag$_2$X core|amorphous-shell nanoparticles to Au|MX core|monocrystalline-shell HNCs promoted by TBP molecules. (Bottom) Series of high-resolution TEM images highlighting different synthetic stages (indicated with (i), (ii), and (iii)) in the CE reaction from Au|Ag$_2$S to Au|CdS NCs. The scale bar is 5 nm in all the images. Red and yellow dashed lines are guides for the eye, distinguishing the core and shell boundaries, respectively. Adapted with permission from ref 106. Copyright 2010 The American Association for the Advancement of Science.

only a simple replacement of Cu$^+$ with Hg^{2+} ions, but also a chemical reduction of a fraction of the sulfur anions (2/3) in order to break the covalent S−S bonds. The transformation from covellite to hexagonal cinnabar HgS phase (although with a low yield) was made possible at RT in the presence of a mild reducing agent (i.e., ascorbic acid) that provided the required electrons to reduce the disulfide bonds. In another work, we observed that hexagonal Cu$_2$Te disk-shaped NCs could be converted into wurtzite CdTe ones.[109] This CE reaction, interestingly, preserved the NCs morphology, even if a substantial reconstruction of the anion sublattice took place. As it possible to notice in the sketches of Figure 8A−C, a reorientation of the c-axis must take place when going from Cu$_2$Te to CdTe nanodisks. This is accomplished by a displacements of Te anions, mainly along the z direction, resulting in a splitting of a pristine (001) Te-plane of Cu$_2$Te into the (110) Te "bilayer" of CdTe. The temperature, in this particular CE reactions, is believed to play a fundamental role in supplying the system with enough energy for the reorganization of the lattice and, consequently, for the cation replacement. Indeed, while above 150 °C the reactions required only 5 min to reach completion, almost no exchange was observed when working at 50 °C, even after 24h.

As shown in the previous examples, the crystal phase resulting from a CE reaction can be sometimes hard to predict. This is especially true in some systems in which during CE there is a transition from an amorphous to a monocrystalline structure: Zhang et al. studied CE reactions taking place on an amorphous Ag$_2$X (X=S, Se, Te) shell grown onto preformed metallic NC. By exchanging the Ag$^+$ ions of the shell with M^{2+} ions (M= Cd, Zn, Pb), the resulting MX shell was monocrystalline (see Figure 8D, top panel).[106] The alkyl phosphine used in the synthesis, TBP, was believed to make the CE reaction possible (by selectively solvating the Ag$^+$ ions) and to promote the reorganization of the MX crystalline lattice to form a monocrystalline domain, even at low temperature (i.e., 50 °C). As it is possible to appreciate from HRTEM micrographs, reported in Figure 8D, the CE takes place from a certain site on the Ag$_2$X surface and then gradually transforms the amorphous domain into a monocrystalline MX one.

3.5. Effects of Volume Change

In the previous section we have shown various examples of CE reactions in which the morphology of the host NCs is retained, even if a strong deformation of their anion framework occurs. There are also reported examples of CE transformations in which the crystal structure is retained, albeit with a large change in the volume of the structure. The morphology retention of

NCs, in these cases, may not be assured anymore as the volume change ($\Delta V/V$) can have various deleterious effects on the product NCs. Depending on the degree of lattice stress developed in the exchanged NCs, the formation of voids or a fragmentation can be observed. This was seen, for example, by Wark et al. when studying CE reactions between CdE (E=S, Se and Te) NCs and Pd^{2+} or Pt^{2+} ions.[66] The volume change in almost all these transformations is approximately −30%. As shown in Figure 9, the CdSe → PdSe (Figure 9 c → d) and
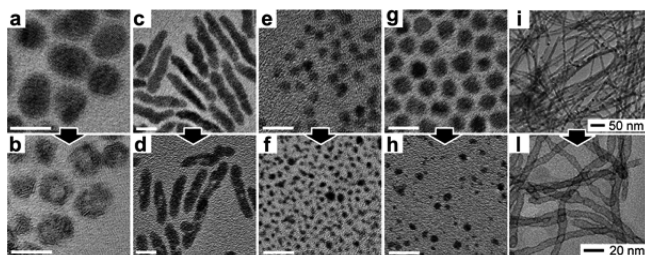
Figure 9. TEM images of the reactant CdE (E = S, Se, and Te) and fully exchanged product NCs. In the Figure, each reactant-product pair is indicated by an arrow connecting the two panels: (a → b) CdTe-PtTe, (c → d) CdSe-PdSe, (e → f) CdS-PtS, (g → h) CdSe-PtSe, (i → l) CdTe-PtTe₂. Scale bars in a–h are 10 nm. (a–h) Reproduced from [Wark, S. E.; Hsia, C.-H.; Son, D. H. Effects of Ion Solvation and Volume Change of Reaction on the Equilibrium and Morphology in Cation-Exchange Reaction of Nanocrystals *J. Am. Chem. Soc.* **2008**, *130*, 9550−9555]. Copyright 2008 American Chemical Society. (i−l) Reproduced from [Moon, G. D.; Ko, S.; Xia, Y.; Jeong, U. Chemical Transformations in Ultrathin Chalcogenide Nanowires *ACS Nano* **2010**, *4*, 2307−2319]. Copyright 2010 American Chemical Society.

CdTe → PtTe (Figure 9 a → b) reactions yielded NCs characterized by voids, especially when starting from larger NCs. This was attributed to the release of stress accumulated in the NCs lattice during the CE reaction, as a consequence of the large volume change. In the CdS → PtS (Figure 9 e → f) and CdSe → PtSe (Figure 9 g → h) cases, fragmentation of the NCs occurred. The fragmentation was tentatively explained by considering a continuous pealing-off of the ion-exchanged parts from the main body of the reacting NC, due to the excessive lattice mismatch at the heterointerface. Similarly, Moon et al. showed that the exposure of CdTe nanowires to Pt^{4+} ions leads to the formation of PtTe₂ nanotubes (see Figure 9 i → l).[31] Also in this case, the void formation was not attributed to the Kirkendall effect (see section 4.1) but to the release of the mechanical stress accumulated during the reaction.

4. MATERIALS

As it is possible to see from Table 4, many materials are now accessible via CE reactions on NCs, emphasizing how such a synthetic tool has been refined over the last years. As regarding binary compounds, most of the work has been done on metal chalcogenide NCs, with most efforts on metal sulfides and selenides. Few CE reactions, on the other hand, have been reported on metal telluride NCs. This might be due to the weak M-Te bonds (i.e., low lattice energy, see section 2) that make the whole anion lattice less rigid and thus more prone to deformation or dissolution during a CE reaction. Also, much less has been reported on metal oxides. This can be tentatively explained considering that, in general, the M-O bonds are much shorter than the M-X (X = S, Se, and Te) bonds, hindering, in many cases, the diffusion of cations in oxides NCs.[152] CE

Table 4. List of Reactant and Product Materials of Known CE Reactions in NCs

class	reactant	shape	product
oxides	CuO	sphere	NiO, CoO, Fe₂O₃, Mn₃O₄[153]
selenides	CdSe	rod, sphere, wire, sheet	Cu₂Se,[75,92,154] Ag₂Se[28,76,78,155] PdSe, PtSe,[66] PbSe[118,121,156]
	PbSe	rods, cubes	CdSe[41,145]
	Cu₂₋ₓSe	rod, sphere, cube	ZnSe,[92] Ag₂Se,[157] SnSe[149]
	SnSe	sphere	PbSe[158]
	ZnSe	sphere	Ag₂Se,[159] PbSe,[89,130] CdSe[145]
	Ag₂Se	wire, sphere, rod	CdSe,[28,29,99] Cd₁₋ₓZnₓSe[111]
sulfides	CdS	sphere, rod, wire, platelet	CuS,[77] Cu₂S,[88,117,160−163] PdS, PtS,[66] PbS[118,164]
	CuS	sphere	Ag₂S[87]
	ZnS	rod, sphere	Cu₂S,[49] PbS[118]
	Ag₂S	sphere	CdS[114]
	Cu₂S	Sphere, rod, platelet, wire	ZnS,[107,160] CdS, PbS,[88,117,160] Au₂S,[165] Ag₂S[162]
	PbS	sphere	CdS[40]
selenide-sulfide	Cu₂₋ₓ(SᵧSe₁₋ᵧ)	sphere, platelet	Cd(SᵧSe₁₋ᵧ),[105,166] Zn(SᵧSe₁₋ᵧ)[166]
	CdSe|CdS	core|shell	Cu₂Se|Cu₂S[73,79,80,93,160,167,168]
	Cu₂Se|Cu₂S	core|shell	PbSe|PbS,[79,160] ZnSe|ZnS,[93,160] CdSe|CdS,[80]
tellurides	CdTe	wire, sphere, tetrapod	PbTe,[118] Ag₂Te,[28] PtTe₂,[31] PdTe, PtTe,[66] Cu₂Te[97]
	Cu₂Te	platelet	CdTe[109]
pnictides	Cd₃As₂	sphere	InAs, GaAs[144]
	Cd₃P₂	sphere	InP, GaP[144]
	Cu₃P	platelet	InP[104]
lantanide fluorides	GdF₃, EuF₃	sphere	LaF₃[169]
	NaYF₄	sphere	LaF₃[169]
	Ln:CaF₂ (Ln = Yb, Ho, Er, Tm)	cube, sphere	Ln:NaGdF₄[170]
hybrid metal-chalcogenide	Se|Ag₂Se	core|shell sphere	Se|ZnSe, Se|CdSe, Se|PbSe[30,98]
	Au|Ag₂S	core|shell rod, sphere	Au|CdS[112,171]
	Au|Ag₂X (X = S, Se, Te)	core|shell sphere	Au|CdSe, Au|CdTe, Au|PbS, Au|ZnS, Au|Cd(SₐSe₁₋ₐ)[106]

reactions are even more challenging in pnictides: in these systems, the bonds are much more covalent than those in metal chalcogenides. In order to promote a CE reaction in such materials high temperatures are required, but such harsh conditions may lead to the dissolution of the starting NCs.

CE reactions have been exploited even in complex structures, such as the so-called nano heterostructures (NHCs) (see Table 4). In these cases, the anion frameworks of the different sections of the NHCs remain unaltered while all the original cations are replaced with new desired ones. As a few examples, spherical, dot-in-rod and platelet-like CdSe\|CdS core\|shell NHCs have been transformed into the corresponding Cu₂Se\|Cu₂S NHCs and subsequently to PbSe\|PbS, ZnSe\|ZnS, or back to CdSe\|CdS NHCs, with complete morphology preservation.[79,80,93,160,167,168] This is assured by the topotactic nature of CE transformations that, in some cases, also leads to unexpected results, such as metastable crystal structures. For example, the CE reaction of wurtzite (wz) CdSe NCs with Cu^+ ions produces an unknown hexagonal (hex) Cu₂Se phase.[92]
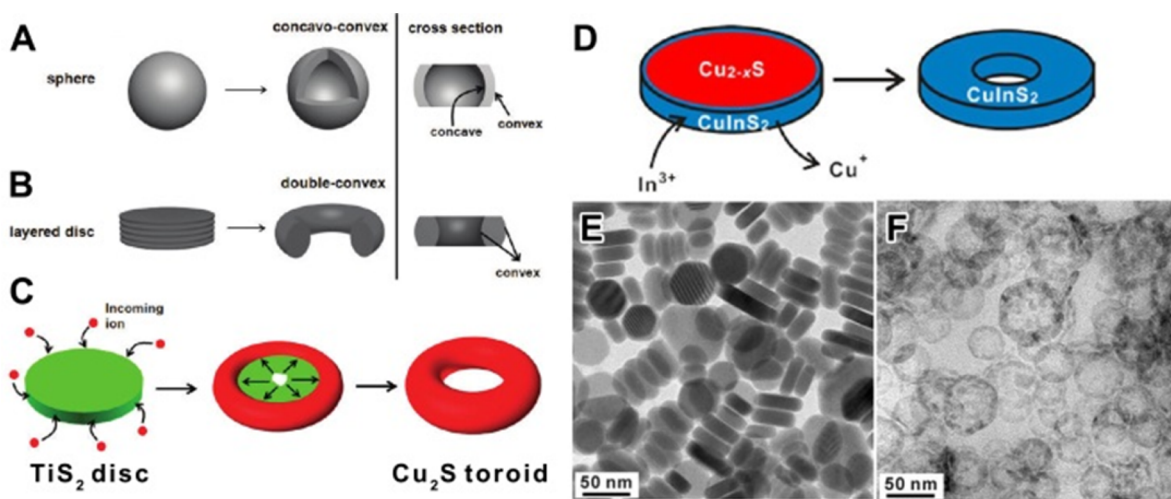
Figure 10. (A) Concavo-convex curvature formed as a consequence of a transformation from a sphere to a hollow sphere. (B) Double-convex curvature from a layer-structured disc to a toroid. (C) Schematic illustration of 2D layered nanocrystals, regioselectively reacting with incoming ions, to form a toroid as the final product. Reproduced from [Jeong, S.; Han, J. H.; Jang, J.-t.; Seo, J.-w.; Kim, J.-G.; Cheon, J. Transformative Two-Dimensional Layered Nanocrystals *J. Am. Chem. Soc.* **2011**, *133*, 14500−14503]. Copyright 2011 American Chemical Society. (D) Schematic representation of the Kirkendall Effect occurring in the transformation of $Cu_{2-x}S$ NDs into hollow $CuInS_2$ NDs. Schematic TEM images of (E) the template $Cu_{2-x}S$ NCs and (F) $CuInS_2$ nanocrystals resulting from ion exchange with InI_3 (150 °C), revealing large central holes and related thickness variations. Reproduced from [Mu, L.; Wang, F.; Sadtler, B.; Loomis, R. A.; Buhro, W. E. Influence of the Nanoscale Kirkendall Effect on the Morphology of Copper Indium Disulfide Nanoplatelets Synthesized by Ion Exchange *ACS Nano* **2015**, *9*, 7419−7428]. Copyright 2015 American Chemical Society.

Similarly, metastable hex-CdTe phase formed when starting from hex-Cu_2Te NCs, and wz-InP NCs resulted from the CE transformation of hex-Cu_3P NCs by exchanging Cu^+ with In^{3+} ions.[104,109] As highlighted in the introduction, important recent reviews on CE reactions have already discussed most of the above-mentioned cases and have given a comprehensive overview on this topic.[28,32−34] This second part of the review, with the aim of being complementary to those works, will focus only on those complex structures that were made accessible by CE transformations. More specifically, we will provide an overview of the nanostructures that can be prepared with partial replacement of the original cations, with a special attention on the morphology of the resulting products (see section 5). Also, we decided to include those CE transformations that do not proceed topotactically, resulting, consequently, in NCs with complex morphologies, such as hollow nanostructures (see next Section).

4.1. Kirkendall Effect in CE Reactions: Hollow NCs

CE reactions naturally involve the diffusive motion of two different cation species, which, in general, have different intrinsic diffusion coefficients. Two ions fluxes take place during such transformations: one flux corresponds to that of the outgoing host cations, while the other refers to ingoing guest ions. If one cation species diffuses much faster than the other, a net mass flow accompanies the interdiffusion process, which is balanced by an opposite flow of vacancies. In bulk materials, these vacancies can condense forming voids, or they can annihilate at dislocations. This phenomenon, discovered by Kirkendall and co-workers in the 1940s studying a copper-brass diffusion couple, is indeed known as the Kirkendall effect.[139] If the outgoing cations of a NC diffuse much faster than the ingoing cations, a significant flow of vacancies can be established, favored by the high surface-to-volume ratio of the NC.[172] Within the small volume of a transforming NC, the supersaturated vacancy cloud is likely to coalesce into a single void, with the consequent formation of a hollow structure. The

Kirkendall effect has been demonstrated in some CE reactions and has led to exotic nanostructures such as toroids, hollow tubes and ring-like morphologies.

4.1.1. $TiS_2 \rightarrow Cu_2S$, CdS. Jeong et al. studied the CE reactions between 2D layered TiS_2 nanodiscs (NDs) and copper(I) ions.[131] TiS_2 consists of S−Ti−S layers stacked in the (001) direction and offering preferential nanometer sized channels for the ion diffusion. Upon exposure to excess of copper ions at relatively low temperature (100 °C), TiS_2 NDs transform into Cu_2S toroidal nanostructures. The transformation starts at the edges of the 2D NDs with the nucleation of the Cu_2S phase. While the CE process proceeds inward, the sulfur ions most likely migrate outward, through nanometer-sized channels of the TiS_2 structure, eventually producing a hole in the middle of the original NDs and forming a toroid (see Figure 10B,C). The same process was observed to take place using Cd^{2+} ions as guest cations, with the consequent formation of CdS toroidal NCs. This final morphology is unconventional, since usually the hollow nanostructures obtained with shape-transformative reactions, for example of spherical NCs, result in concavo-convex curvature (see Figure 10A). This unique shape obtained through CE reaction is made possible as a consequence of the different diffusivities of the in-going and out-going cations coupled with anion migration through the layered structure of TiS_2. It is noteworthy that the whole ion diffusion produces, upon CE, a monocrystalline material (hexagonal Cu_2S) whose crystal structure is templated by the starting TiS_2.

4.1.2. $Cu_{2-x}S \rightarrow CuInS_2$. Mu et al. prepared $CuInS_2$ hollow NDs starting from $Cu_{2-x}S$ NDs and In^{3+} ions.[110] The CE in this system takes place from the edges of the NDs and proceeds toward the core. The formation of an internal void is not directly correlated to intrinsic ions diffusion rates, but it is governed by the availability of In^{3+} ions at the NCs surface. More specifically, a high reaction barrier for In^{3+} entry at the NCs edges decreases the effective rate of indium incorporation,

allowing for the out-diffusion of Cu^+ (and S^{2-}) to outcompete the in-diffusion of In^{3+}. Hollow-centered $CuInS_2$ nanorings form under these conditions (see Figure 10D−F). In contrast, low reaction barriers for In^{3+} entry at the NDs edges provide higher rate of indium incorporation in the lattice, balancing the fluxes of ingoing and outgoing ions. In this case, no formation of voids is observed and the NDs preserve their morphology. Remarkably, Mu et al. observed that this reaction barrier can be modulated experimentally by varying the temperature and the nature of the In-complex used in the CE reaction. Therefore, the variation of these two synthetic parameters could either promote or suppress the nanoscale Kirkendall effect, effectively regulating the final NCs morphology.

4.1.3. $Co_3O_4 \rightarrow Zn_xCo_{3-x}O_4$. Tian et al. reported the formation of hollow single crystal $Zn_xCo_{1-x}Co_2O_4$ nanocubes as a result of the in situ CE reaction between Co_3O_4 nanocubes and Zn^{2+} ions (see Figure 11).[173] The transformation
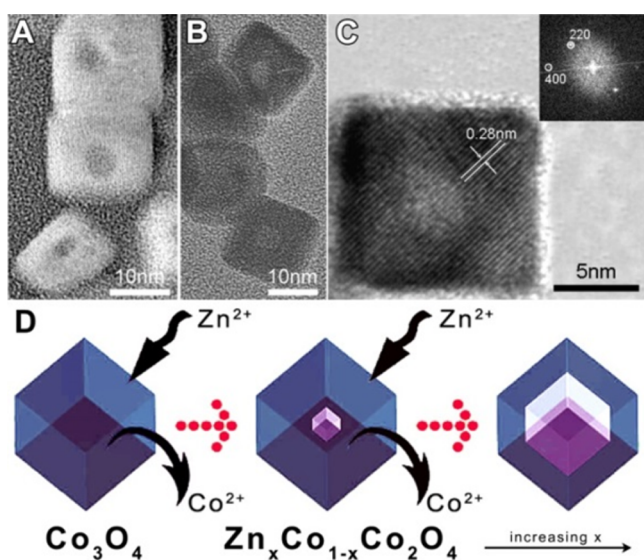
Figure 11. High-magnification (A) dark and (B) bright-field TEM images of $Zn_xCo_{1-x}Co_2O_4$ hollow nanocubes. (C) HRTEM image of a single hollow nanocube along with its FFT (inset). (D) Illustration of the nanoscale differential diffusion (CE) and the hollowing process. Reproduced from [Tian, L.; Yang, X.; Lu, P.; Williams, I. D.; Wang, C.; Ou, S.; Liang, C.; Wu, M. Hollow Single-Crystal Spinel Nanocubes: The Case of Zinc Cobalt Oxide Grown by a Unique Kirkendall Effect *Inorg. Chem.* **2008**, *47*, 5522−5524]. Copyright 2008 American Chemical Society.

represents actually the last step of a hydrothermal synthetic route in which, at the beginning, Co_3O_4 nanocubes with a cubic spinel like crystal lattice form. The Zn^{2+} ions in the reaction solution, then, start replacing the Co^{2+} ions in tetrahedral positions and progressively transform the host crystal lattice to $Zn_xCo_{1-x}Co_2O_4$. The zinc content in the NCs slowly varies with time, up to a maximum value of x = 0.75, with the corresponding formation of a void in the center of each NC (see Figure 11). The formation of hollow NCs, comes, most likely, as a consequence of the fast out-diffusion of Co^{2+} and a less efficient in-diffusion of Zn^{2+} which produce a net mass transport between the inner part and the more external part of the Zn−Co−O spinel nanocubes. The end products of this process (i.e., Kirkendal effect) are hollow nanocubes that are surprisingly monocrystalline, as shown by HRTEM images of Figure 11a-c.

5. PARTIAL CE

The outcome of partial exchange experiments depends mostly on the miscibility of reactant and product materials. In the case of miscible materials, either alloy or doped NCs can be produced, otherwise multi domain NHCs, such as core|shell or segmented NCs, are observed. All these structures are listed in Table 5. Thus, the phase diagrams of reactant-product solid solutions have to be carefully consulted in order to predict a desired nano architecture.[37]

5.1. Partial CE with Miscible Phases

The direct synthesis of alloy NCs requires a deep understanding of the specific reactivities of the precursors employed, together with the correct choice of ligands for the size and shape control of the resulting NCs. It is easy to understand that, in many cases, the simultaneous control over the composition, size distribution and morphology of alloy NCs, especially when quaternary or even quinary systems need to be prepared, can be extremely challenging. A useful method to sidestep these problems has recently emerged; it consists of first growing binary/ternary compound NCs using well-established synthesis procedures, and then using such NCs as templates for CE reactions in order to include other cations species. A wide range of alloyed metal chalcogenide NCs realized by CE have been demonstrated (see Table 5). Starting from Cu-based chalcogenides, for example, ternary, quaternary and even quinary systems, such as Cu−Zn−Sn−Se-S, have been produced with a fine control over the composition. The alloying, in almost all the reported systems, is exclusively exploited to achieve control over the optical properties of the corresponding NCs, as it allows, for example, to tune the absorbance or, in specific cases, the photoluminescence of the products.

5.1.1. Cd-Based Chalcogenides. ZnSe NCs and ZnTe magic size clusters, both in the zinc-blende (zb) crystal structure, have been alloyed with Cd^{2+} to get ternary NCs.[42,63,64,100,129] As this CE transformation is thermally activated (see section 3.1), the process is particularly sensible to the reaction temperature that can be used to govern the final NCs composition. Sheng et al., working with ZnSe NCs in water (that is at 95 °C), could tune the PL of the resulting $Cd_xZn_{1-x}Se$ NCs from 375 to 480 nm.[63] By performing the reaction in organic media at higher temperatures (up to 250 °C-300 °C), the exchange could be pushed further, achieving eventually the total conversion of ZnSe to CdSe: the PL of the alloy NCs could be shifted up to almost 600 nm (see Figure 12B).[42,64,100] Analogously, the reverse CE (that is, from CdS to ZnS) enabled the fabrication of alloy $Zn_xCd_{1-x}S$ structures. If the reaction was performed at relatively low temperature (100 °C), the Zn^{2+} ions started replacing Cd^{2+} ions gradually from the surface of the NCs, yielding composition-gradient $Zn_xCd_{1-x}S$ NCs.[177] These NCs showed enhanced PL emission, as a consequence of the fact that the composition-gradient Cd−Zn−S shell optimally alleviates the lattice strain caused by the lattice mismatches between the CdS core and the Zn-based shell.

Hg^{2+} ions can be easily inserted in zb-CdTe NCs through partial CE at RT to form the corresponding ternary Cd−Hg−Te alloy NCs.[96,181,182] As CdTe and HgTe are completely miscible and have nearly identical lattice constants (a_{CdTe} = 6.48 Å, a_{HgTe} = 6.46 Å) the amount of Hg in $Hg_xCd_{1-x}Te$ NCs can be easily tuned from x = 0 to x = 1. The Cd^{2+} by Hg^{2+} CE in CdTe NCs does not change the lattice parameters or the

**Table 5. List of Nanostructures Accessible via Partial CE Transformations**

class	reactant	shape	product	morphology
oxides	Co_3O_4	cube	$Zn_xCo_{1-x}Co_2O_4$[173]	alloy
	Fe_3O_4	sphere	$Co-Fe-O$[174]	
	$FeO|CoFe_2O_4$	core|shell	$Fe_{1-x}Co_xO_4|CoFe_2O_4$[174]	
selenides	CdSe	sphere, rod	$Cd_xHg_{1-x}Se$[90,96,150]	
	$Cu_{2-x}Se$	sphere	$Cu_{2-4y}Sn_ySe$[149]	
	ZnSe	sphere	$Zn_xCd_{1-x}Se$,[42,63,64,100,145]	
	In_2Se_3	sphere	$CuInSe_2$[91]	
sulfides	In_2S_3	sphere	Cu_xInS_2[175]	
	CdS	sphere, wire	$Zn_xCd_{1-x}S$,[176,177] $Hg_xCd_{1-x}S$[96]	
	Cu_2S	sphere	$CuInS_2$,[102,103,110] $Cu-In-Zn-S$[102]	
	$AgInS_2$	sphere	$Ag-In-Zn-S$[178,179]	
	$Cu_{1-x}InS_2$	sphere	$Cu-In-Zn-S$[113]	
	Cu_2SnS_3	sphere	Cu-M−Sn-S (M = Zn, Fe, Co, Ni, Cd)[180]	
selenide-sulfide	$Cu_{2-x}(Se_yS_{1-y})$	platelet	$Cu-Zn-Se-S$	
			$Cu-Sn-Se-S$	
			$Cu-Zn-Sn-Se-S$[108]	
	$Cu_2Se|Cu_2S$	core|shell	$CuInSe_2|CuInS_2$[168]	
tellurides	CdTe	sphere, rod	$Cd_xHg_{1-x}Te$[96,181,182]	
	ZnTe	wire	$Cd_xZn_{1-x}Te$[129]	
lantanide fluorides	NdF_3	sphere	$La_xNd_{1-x}F_3$	
	GdF_3		$Eu_xGd_{1-x}F_3$[169]	
	$KLnF_4$ (Ln=Y, Yb, Er, Gd)	rod	$NaLnF_4$[183]	
lantanide fluorides	$NaYF_4$:Yb,Tm	sphere	$NaYF_4$:Yb,Tm-$NaGdF_4$[184]	core|shell
selenides	CdSe	sphere	$CdSe|PdSe$[66]	
	PbSe	sphere, rod, cubes, star-shaped	$PbSe|CdSe$[41,122−124,126,145,185,186]	
selenide-sulfide	$CuInSe_xS_{2-x}$	sphere	$CuInSe_xS_{2-x}|CdSe_xS_{2-x}$[187]	
sulfides	PbS	sphere, rod	$PbS|CdS$[38,40,88,116,122,126,188,189]	
	CdS	sphere, wire	$CdS|PbS$,[37] $CdS|HgS$,[36] $CdS|Cu_{2-x}S$[161,162]	
	$CuInS_2$	sphere	$CuInS_2|ZnS$[190]	
	Cu_2S	sphere	$Cu_2S|Au_2S$[165]	
tellurides	PbTe	sphere	$PbTe|CdTe$[127]	
selenides	CdSe	sphere, rod	$CdSe/PbSe$[118,121]	segmented
	$Cu_{2-x}Se$	sphere	$Cu_{2-x}Se/SnSe$,[149] $Cu_{2-x}Se/CdSe$, $Cu_{2-x}Se/ZnSe$[137]	
sulfides	Cu_2S	sphere, wire	Cu_2S/ZnS, Cu_2S/CdS,[107] Cu_2S/Ag_2S[162]	
	CdS	rod, sphere, wire	CdS/PbS,[72,118] CdS/Ag_2S,[71] CdS/Cu_2S,[70,162] CdS/PdS, CdS/PtS,[66] CdS/Pd_4S[191]	
	TiS_2	disc	TiS_2/Cu_2S[131]	
tellurides	CdTe	rod	$CdTe/Cu_{2-x}Te$[192]	
oxides	YVO_4	sphere	Eu^{3+}:YVO_4[193]	doping
selenides	CdSe	sphere	Ag:CdSe[115]	
selenides	ZnSe	sphere	$Ag:Zn_xCd_{1-x}Se$[89]	
			$Cu:Zn_xCd_{1-x}Se$[89,100]	
selenides	ZnSe	sphere	Cu:ZnSe[159]	
selenide-sulfide	CdSe|ZnS	sphere	^{64}Cu:CdSe|ZnS[194]	
tellurides	ZnTe	cluster	Mn:ZnTe[128]	

particle size but greatly alters the band gap energy of the corresponding alloy NCs, since the two end points of this transformation (CdTe and HgTe) have very different band gap energies (the band gap energy of CdTe is 1.5 eV whereas that of HgTe is −0.15 eV). Consequently the PL emission of such NCs can be tuned from 600 nm to almost 1000 nm depending on the amount of Hg incorporated (see Figure 12c,d).

The transformation of binary CdSe to ternary alloy $Cd_xHg_{1-x}Se$ NCs via Cd by Hg CE is strongly influenced by the crystal structure of the starting NCs.[90,96,150] This is due to the fact that HgSe crystallizes only in a zinc-blende phase, while CdSe can exist either in cubic zinc-blende or wurtzite

structures. Consequently, zb-CdSe NCs can be easily converted at RT to isostructural alloy $Cd_xHg_{1-x}Se$ NCs with precise control over the composition.[90,96] On the other hand, wz-CdSe NCs have been shown to incorporate a limited amount of Hg^{2+} ions, requiring at the same time longer reaction times.[90,150] Gupta et al. showed, for example, that in wz-CdSe NRs the inclusion of Hg^{2+} ions is limited to a composition of $Cd_{0.9}Hg_{0.1}Se$ (see also Section 3.4) with the resulting NCs exhibiting many stacking faults.[150] This was attributed to the poor miscibility of the two end point structures, as the wurtzite Cd−Hg−Se bulk alloy structure can incorporate at maximum 20% of Hg.[195] By increasing the amount of Hg^{2+}, the bulk alloy
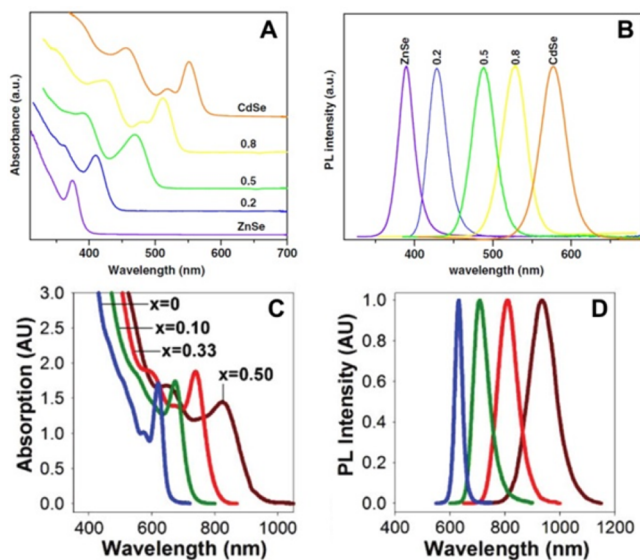
Figure 12. Normalized UV−vis (left panels) and PL spectra (right panels) of: (A and B) ∼3 nm ZnSe and cation-exchanged $Cd_xZn_{1-x}Se$ NCs; (C and D) 4 nm CdTe and cation-exchanged $Hg_xCd_{1-x}Te$ NCs. (A and B) Reproduced with permission from ref 64. Copyright 2007 IOP Publishing. All rights reserved. (C and D) Reproduced from [Smith, A. M.; Nie, S. Bright and Compact Alloyed Quantum Dots with Broadly Tunable Near-Infrared Absorption and Fluorescence Spectra through Mercury Cation Exchange *J. Am. Chem. Soc.* **2011**, *133*, 24−26]. Copyright 2011 American Chemical Society.

adopts a zinc-blende structure. Similarly, Prudnikau et al. observed that upon exposure of wz-CdSe NRs to Hg^{2+} ions, defective nonluminescent alloy structures formed at the early stage of the CE reaction.[90] Notably, at longer reaction times (i.e., 24h at RT) these structures were found to gradually undergo structural reorganization forming eventually zb-$Cd_xHg_{1-x}Se$ NCs (as predicted by the corresponding phase diagram[195]) with PL emission in the NIR (up to 850 nm).

5.1.2. Cu-Based Chalcogenides. Numerous recent works have shown that Cu-based chalcogenide NCs are able to incorporate many different guest cations forming quaternary or even quinary alloy systems with finely tunable optical properties. It is worth to note that, even if the possibility of different materials to form alloys is known (such as Cu_2Se and $SnSe_2$), not all the compositions allowed by CE experiments can be predicted by phase diagrams.[149] Indeed, NCs with metastable compositions and with hitherto unexplored optical proprieties have been recently shown in various reports on CE, as will be shortly discussed below.

Different groups demonstrated that Cu_2S NCs or NPLs with hexagonal crystal lattice can be partially exchanged to form ternary Cu−In−S NCs with wurtzite structure.[102,103,110] In turn, the ternary alloy NCs, having either hexagonal or tetragonal crystal structure, can be further transformed into quaternary Cu−In−Zn-S or Cu−In−S|ZnS core|shell-like NCs with precise control over the composition and with enhanced PL emission.[102,113] Remarkably, the direct transformation of Cu_2S NCs into quaternary Cu−In−S NCs can be achieved in one-step CE by exposing the starting NCs to both In^{3+} and Zn^{2+} ions (see Figure 13A).[102] Being $AgInS_2$ and $CuInS_2$ both chalcopyrite ternary solids belonging to I−III−VI$_2$ class of semiconductors, the CE reactions working on the latter have been shown to work also on the former yielding quaternary Ag−In−Zn-S NCs.[178,179] Tang et al., for example,
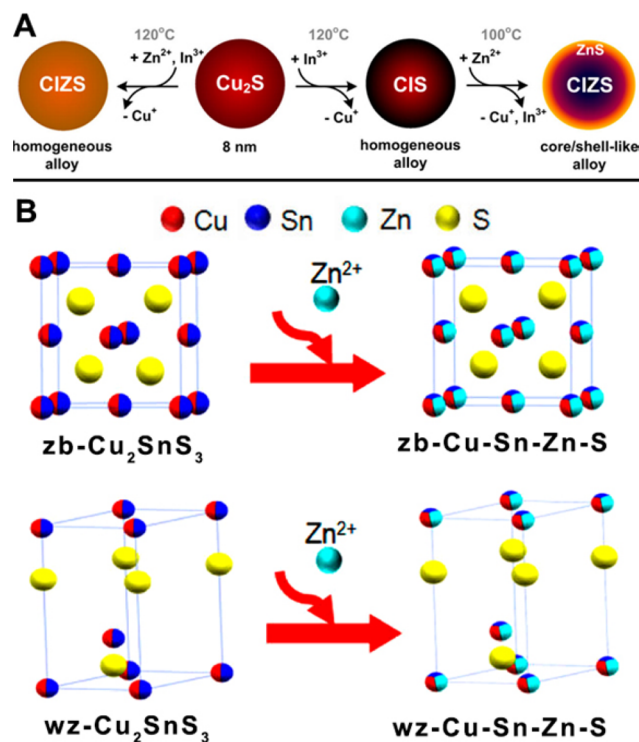

Figure 13. (A) Transformations of spherical Cu_2S NCs into ternary and quaternary alloy NCs. The sequential introduction of In^{3+} and Zn^{2+} ions leads to the formation of Cu−In−S[196] NCs and core|shell-like Cu−In−Zn-S (CIZS) NCs, respectively. The simultaneous introduction of indium and zinc produces homogeneous CIZS NCs (left). Reproduced from [Akkerman, Q. A.; Genovese, A.; George, C.; Prato, M.; Moreels, I.; Casu, A.; Marras, S.; Curcio, A.; Scarpellini, A.; Pellegrino, T. et al. From Binary Cu2S to Ternary Cu−In−S and Quaternary Cu−In−Zn−S Nanocrystals with Tunable Composition via Partial Cation Exchange *ACS Nano* **2015**, *9*, 521−531]. Copyright 2015 American Chemical Society. (B) Schematic representation of the lattice conservation during CE reactions between zb- or wz-Cu_2SnS_3 NCs and Zn^{2+} ions. Reproduced from [Wang, Y.-X.; Wei, M.; Fan, F.-J.; Zhuang, T.-T.; Wu, L.; Yu, S.-H.; Zhu, C.-F. Phase-Selective Synthesis of Cu2ZnSnS4 Nanocrystals through Cation Exchange for Photovoltaic Devices *Chem. Mater.* **2014**, *26*, 5492−5498]. Copyright 2014 American Chemical Society.

showed that Ag−In−Zn-S NCs can be prepared by CE from $AgInS_2$ NCs with a fine control over the Zn concentration, from 36.4 to 56.5%.[179]

In a similar manner, in a recent work from our group, we demonstrated that $Cu_{2-x}Se_yS_{1-y}$ nanoplatelets (NPLs) with hexagonal chalcocite-like structure can be partially exchanged with either Sn^{4+} or Zn^{2+} ions and form ternary alloys.[108] Also, if the tin and zinc precursors are used together in the partial CE reaction, it is possible to insert both ions at the same time to get quinary Cu−Sn−Zn-Se(S) NCs. The bandgap of the alloy NPLs can be tuned from 1.0 to 2.1 eV depending on the composition. As an example, $Cu_{0.26}Zn_{0.25}Sn_{0.06}Se_{0.3}S_{0.13}$ NPLs, having the highest Zn content and the lowest Sn content, are characterized by a wide band gap (2.1 eV), which narrows down by reducing Zn and increasing Sn amount (1.3 eV for $Cu_{0.29}Zn_{0.14}Sn_{0.12}Se_{0.33}S_{0.12}$). The incorporation of only tin ions into $Cu_{2-x}Se_yS_{1-y}$ NPLs produces a further narrowing of their band gap from 1.5 to 1.0 eV. An analogous behavior was observed by us in spherical $Cu_{2-x}Se$ NCs with a cubic structure (berzelianite), which can accommodate Sn^{4+} ions and form

ternary Cu−Sn−Se systems when partially exchanged.[149] Interestingly, the same NCs, if exposed to Zn^{2+} ions, undergo CE, but in this case NHCs are formed (see section 5.3.1.6).[137] The crystal structure of the host NCs, evidently, has a major role in accommodating the guest ions and in dictating the outcome of the CE. On the other hand, Wang et al. demonstrated that both zinc-blende and wurtzite Cu_2SnS_3 NCs can be partially exchanged with numerous guest ions, such as Zn^{2+}, Fe^{3+}, Co^{2+}, Ni^{2+}, and Cd^{2+}, forming, independently from the initial crystal structure, single crystal alloy NCs (see Figure 13B).[180]

5.1.3. Iron Oxides. The formation of alloy NCs prepared by partial CE has almost exclusively concerned metal chalcogenide systems (see Table 5). The only example of alloying in oxide NCs was reported by Heiss et al. when exposing Fe_3O_4 NCs to Co^{2+} cations to give Co−Fe−O alloy NCs.[174] The alloying is promoted by the structural similarity between Fe_3O_4 (more precisely written as $Fe^{2+}Fe^{3+}_2O_4$) and metal-doped spinel-type ferrites, $M^{2+}Fe^{3+}_2O_4$ (M=Co, Ni or Mn). Ideally, a complete replacement of Fe^{2+} ions, occupying the octahedral sites of the inverse spinel structure of Fe_3O_4, with Co^{2+} cations would lead to the $CoFe_2O_4$ structure. Heiss et al. observed indeed that partial Co^{2+}-for-Fe^{2+} CE of Fe_3O_4 NCs resulted in homogeneous alloy NCs with size and shape preservation (see Figure 14a,b). The Co alloying, on the other
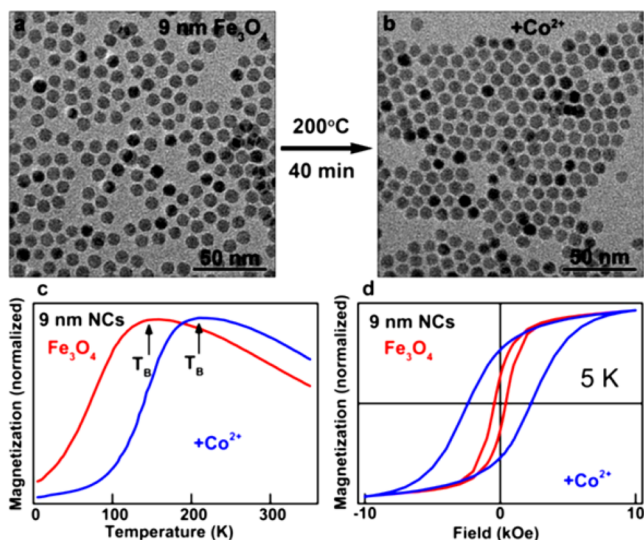
Figure 14. TEM images of small Fe_3O_4 NCs with a mean diameter of 9 nm before (a) and after (b) partial CE with Co^{2+} (performed at 200 °C for 40 min). The size, shape and size distribution of the parental Fe_3O_4 NCs are preserved after the exchange process. (c) The blocking temperature T_B increases from 130 to 210 K. (d) The opening of the hysteresis loop observed a 5 K increase from 836.6 to 4674.8 Oe. Reproduced from [Sytnyk, M.; Kirchschlager, R.; Bodnarchuk, M. I.; Primetzhofer, D.; Kriegner, D.; Enser, H.; Stangl, J.; Bauer, P.; Voith, M.; Hassel, A. W. et al. Tuning the Magnetic Properties of Metal Oxide Nanocrystal Heterostructures by Cation Exchange *Nano Lett.* **2013**, 13, 586−593]. Copyright 2013 American Chemical Society.

hand, had a strong influence on the magnetic properties of the resulting NCs due to strong spin−orbit couplings at the Co^{2+} sites and the concomitant increase of the magnetic anisotropy (see Figure 14c,d).

5.2. Doping with Partial CE

When partial CE reactions are performed using a severe substoichiometric amount of guest ions, few "impurities" can be added to each host NC. This process is commonly defined as doping, even if, compared to doped bulk semiconductors, the concentration of dopants is enormously higher. Doping in direct synthesis requires a fine balance or precursor reactivity, as the impurities have to be incorporated in a controlled way during the growth of the NCs. At the same time, a precise control over the size and shape of the NCs is required in order to have a homogeneous sample. One additional challenge in the synthesis of doped NCs is the so-called "self-purification" process, in which the host matrix tends to expel the dopant ions to the NC surface during the synthesis, especially when working at high temperatures.[197] One key advantage of the CE approach is that it enables the temporal separation of the growth stage of the NCs from that of the inclusion of impurities. The original sample, eventually, can be compared with that after the doping process, allowing a more direct study of the doping effects. That would be otherwise hard to produce through a direct approach.

Sahu et al. prepared lightly doped Ag:CdSe NCs by adapting a standard CE procedure normally used to convert CdSe into Ag_2Se NCs.[115] Ag can be added as electronically active impurity in CdSe NCs, which led to a strong enhancement of their PL emission, with the maximum intensity peaking around 2 Ag per NC (see Figure 15A). Additional Ag ions were found to decrease the PL intensity from this maximum. A further increase in Ag incorporation eventually led to the nucleation of a Ag_2Se phase. Acharya et al. observed instead the formation of Cu-doped $Cd_xZn_{1-x}Se$ NCs by exchanging simultaneously Cu^+ and Cd^{2+} ions with Zn^{2+} ones in preformed ZnSe NCs (see Figure 15B,C).[100] Such doping procedure is quite challenging as a fine-tuning of copper incorporation can be achieved only through the proper choice of the relative concentration of Cu- and Cd-precursors, as well as the reaction temperature. This is due not only to the fact that Cu^+ and Cd^{2+} ions have different substitution rates in ZnSe NCs, but also because Cu^+ ions can be easily inserted in ZnSe, but not in CdSe. Consequently, at the early stage of the CE, both Cd^{2+} and Cu^+ ions are exchanged with zinc. As long as the CE proceeds with the further inclusion of cadmium, copper ions are progressively ejected from the NCs (see Figure 15C). The Cu:$Cd_xZn_{1-x}Se$ tunability covers the range from 500 to 750 nm, accompanied by the composition tunable spectral broadening which arises due to tailoring of the band gap of the host (see Figure 15B).

Direct and sequential hydrazine-promoted CE approaches have been demonstrated by Haibao et al. to produce Cu:ZnSe NCs and Cu- or Ag-doped $Cd_{1-x}Zn_xSe$ NCs.[89] In the first step, ZnSe NCs were exposed to Ag^+ (or Cu^+) ions to get alloyed Zn−Ag−Se (or Zn−Cu−Se) NCs. This was followed by a second CE reaction with Cd^{2+} ions that resulted in Ag- or Cu-doped $Cd_{1-x}Zn_xSe$ NCs (see Figure 15D). The final amount of dopants concentration could be controlled by tuning the concentration of Ag^+ or Cu^+ ions inserted in ZnSe NCs during the first step, while keeping fixed the amount of Cd^{2+} ions used in the second step. Starting from 3.3 nm ZnSe NCs, the PL emission of the resulting Ag-doped ZnCdSe NCs could be tuned from 515 to 660 nm, while Cu-doped ZnCdSe ternary NCs exhibited a much broader tunable spectrum range, covering emission from 550 to 790 nm.

The potentialities of CE reactions have been also exploited to prepare more elaborate doped systems. Sun et al. for example
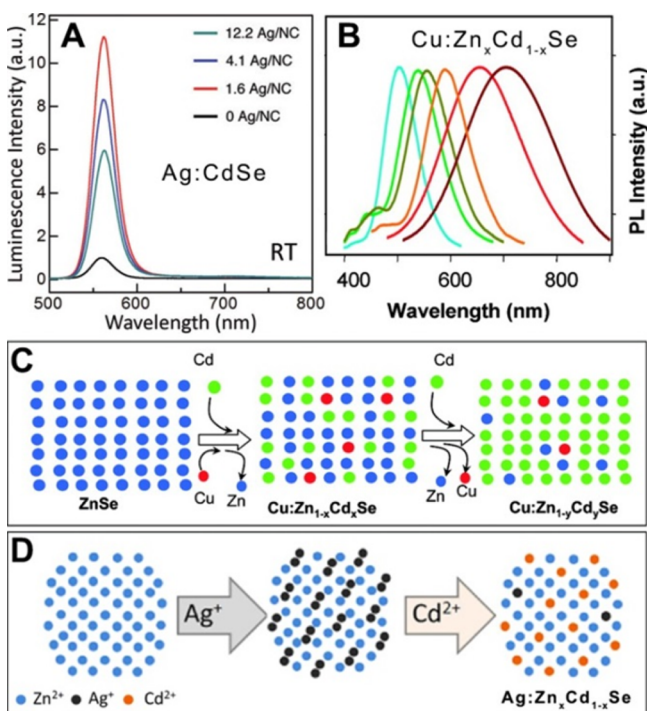
Figure 15. (A) Room-temperature PL emission spectra of 3.1 nm-diameter CdSe NCs dispersed in hexane with no Ag (black), 1.6 Ag/NC (0.3% Ag, red), 4.1 Ag/NC (0.74% Ag, blue), and 12.2 Ag/NC (2.22% Ag, green). The excitation wavelength was 350 nm. (B) PL spectra (normalized) of Cu-doped alloyed $Cd_xZn_{1-x}Se$ NCs. Cu precursors are incorporated along with the Cd precursor. The excitation wavelength is 350 nm. Reproduced from [Sahu, A.; Kang, M. S.; Kompch, A.; Notthoff, C.; Wills, A. W.; Deng, D.; Winterer, M.; Frisbie, C. D.; Norris, D. J. Electronic Impurity Doping in CdSe Nanocrystals *Nano Lett.* **2012**, *12*, 2587−2594]. Copyright 2012 American Chemical Society. (C) Sketch of the formation of Cu:$Cd_xZn_{1-x}Se$ NCs trough the one-pot CE reaction used by Acharya et al. Dopants are incorporated together with Cd ions, and ejected when the amount of Cd increases with the progress of the reaction. In the alloy composition, x is greater than y. Reproduced from [Acharya, S.; Pradhan, N. Insertion/Ejection of Dopant Ions in Composition Tunable Semiconductor Nanocrystals *J. Phys. Chem. C* **2011**, *115*, 19513−19519]. Copyright 2011 American Chemical Society. (D) Schematic of the sequential CE approach used by Haibaoet al. to synthesize Ag (or Cu)-doped $Cd_xZn_{1-x}Se$ NCs. In both (C and D) the arrangement of the colored balls represents the placement of cations in the crystal lattice. Adapted with permission from ref 89. Copyright 2014 IOP Publishing. All rights reserved.

synthesized ^{64}Cu-doped CdSe|ZnS NCs by inserting positron-emitting [64]Cu^{2+} radionuclides in core|shell CdSe|ZnS NCs through CE.[194] Meijerink et al., on the other hand, observed that CE reactions can even work for doping extremely small (less than 2 nm) ZnTe nanoclusters.[128] The exposure of ZnTe nanoclusters to Mn^{2+} ions resulted, indeed, in doped Mn:ZnTe systems whose PL spectra showed a red 620 nm emission characteristic of manganese impurities in bulk ZnTe. As a last example, Du et al. exploited CE reactions to dope YVO_4 NCs (10−15 nm in size) with Eu^{3+} ions, forming Eu^{3+}:YVO_4 NCs.[193] All these complex systems, obviously, give credit to CE reactions as a powerful tool to prepare nanostructures that would be otherwise extremely hard to synthesize through a direct approach.

## 5.3. Partial CE with Immiscible Phases

The systems discussed in this section deal with materials that are known to be immiscible in the bulk. Partial CE, in these cases, leads to the formation of NHCs made of two (or more) different domains sharing, usually, a sharp epitaxial interface. The spatial arrangement of the two materials within each NC strongly depends on kinetic and thermodynamic factors and it is hardy predictable a priori. The final architecture is mainly governed by the relative activation barriers for CE to initiate at different facets of the NC and by the energetics of the interface(s) between the two materials, as the reaction front proceeds through the NC. The diffusion rates of the exchanging ions can play a dominant role in determining the morphology of the intermediate CE structures which, in turn, can be dictated by kinetic rather than by thermodynamic factors. The observed morphologies can be divided in two main groups: core|shell and segmented NHCs. As a general trend, core|shell NHCs are formed when CE proceeds following a isotropic-like cations substitution, without the generation of a significant strain between the two materials (see section 5.3.2). On the other hand, segmented NHCs, such as Janus-like, striped and sandwich-like ones are characterized by the presence of a preferred interface between the two materials that minimizes both the interface energy and the strain of the different domains (see section 5.3.1). It is easily understood that the shape of the starting NCs plays a pivotal role in determining the morphology of the intermediate NHCs, since different types of surfaces, and thus, different entry points for the entering cations, are exposed to the reaction solution. Wark et al. showed, for example, that wz-CdSe NCs and NRs, when partially exchanged with Pd^{2+} ions, produce core|shell or segmented NHCs, respectively.[66] Also, it is important to underline that the NHCs formed upon CE do not always exhibit morphologies that can be explained by simple considerations based on interfacial energy, strain or ions diffusivities. The presence of point, line or planar defects in the host NCs, in fact, may lead to unpredicted structures: these defects can act as preferential nucleation points for the new phase, or as preferential entry/diffusion channel for the guest cations.[70,88,162] These cases are discussed in section 5.3.3.

5.3.1. Segmented Heterostructures. The synthesis of NHCs, consisting of two or more components within each particle, has been for long exploited to create multifunctional materials and to control the electronic coupling between nanoscale units. Typically the synthesis of such NHCs implies the nucleation and growth of a secondary material on specific facets of seed NCs. While this seeded-growth methodology has been applied to a wide range of material combinations, one of the major drawbacks is that that the desired heterogeneous nucleation on the existing NCs surface often competes with homogeneous nucleation of separate NCs of the secondary material. CE reactions have been exploited as an alternative reaction tool for synthesizing NHCs. Thanks to this approach, a portion of the seed NCs can be transformed into a new composition or structural phase, therefore circumventing any separate homonucleation. Moreover, as the CE process in most of the cases is topotactic, the different materials share a common anion sublattice and have a sharp epitaxial interface. This, of course, makes such NHCs particularly suitable for applications.

Segmented NHCs seem to form in CE reactions as a result of the presence of a specific interface between the reactant and the product materials that minimizes both the interface energy and

the strain. In all the systems in which segmented structures are formed upon partial CE, the ion mobility is usually high enough to favor the arrangements of the resulting domains in the "lowest energy" configuration. Typically, once the product material nucleates at preferred sites on the surface of the host NC, the CE proceeds further only from there. The ion exchange tends to favor specific crystallographic directions, with the consequent formation of NHCs whose domains exhibit a preferential low energy interface. As a general trend, when the host NCs have a rod-like shape, the CE tends to initiate at the tip regions of the NRs,[37,70,191] while in case of NDs the nucleation of the product phase has a stronger tendency to take place at the lateral edges.[104,131,151] In case of spherical NCs the CE can start from just one site, generating Janus-like nanoarchitectures,[118,137,149] from two diametrically opposite sites, forming sandwich-like NHCs,[107] or even from multiple random points, forming polycrystalline NCs.[149]

5.3.1.1. CdX/Cu$_2$X (X = S, Te) Systems. CdS/Cu$_2$S is among the most studied binary systems prepared with CE reactions. As no miscibility is allowed in the whole compositional range, Cu-partial exchange of CdS (or *vice versa*) produces binary NHCs. Sadtler et al. provided a detailed study of partial CE reactions involving CdS NRs and Cu$^+$ ions.[70] In these reactions, Cu$^+$ ions start replacing cadmium preferentially at one or both ends of each NR, so that one or two orthorhombic Cu$_2$S domains grow inward starting from the tip regions. The result of this process is the formation of segmented Cu$_2$S/CdS NHCs in which the two materials share flat interfaces perpendicular to the elongation direction of the NRs (see Figure 16). As the
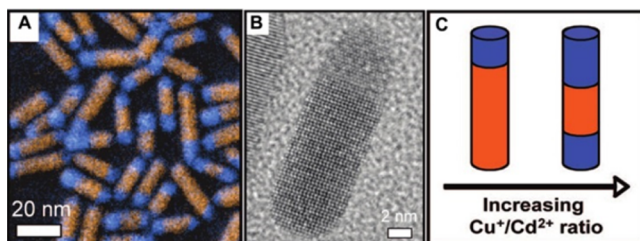
Figure 16. (A) Color-composite EFTEM image of CdS/Cu$_2$S binary NRs, where the orange regions correspond to the Cd energy-filtered mapping and blue regions correspond to the Cu mapping. (B) high-resolution TEM image of a CdS/Cu$_2$S NR, (C) Sketch representing the development of the morphology of binary NRs produced by CE for increasing amounts of Cu$^+$ added to CdS NRs. Reproduced from [Sadtler, B.; Demchenko, D. O.; Zheng, H.; Hughes, S. M.; Merkle, M. G.; Dahmen, U.; Wang, L.-W.; Alivisatos, A. P. Selective facet reactivity during cation exchange in cadmium sulfide nanorods *J. Am. Chem. Soc.* **2009**, *131*, 5285−5293]. Copyright 2009 American Chemical Society.

hexagonal sulfur sublattices of wurtzite CdS and orthorhombic Cu$_2$S are almost identical and the lattice volume contracts just by 8% when going from CdS to Cu$_2$S, the morphology and size of NRs is preserved upon such conversion.

The elastic contributions to the interface formation energies are small in this system and the relative values of the chemical formation energies determine the stability of the different CdS-Cu$_2$S interfaces. The S sublattices of the two different crystal structures are perfectly aligned along the [001] axis of the orthorhombic Cu$_2$S cell that corresponds to the [0001] axis of the hexagonal CdS lattice. The interfaces with the lowest energy of formation are perpendicular to the elongation direction of the NR (*c* axis). This explains why the CE selectively starts at the tips of the rod and why Cu$_2$S/CdS

interfaces parallel to the cross section of the NRs are observed most often by TEM. Moreover, the probability of nucleation of Cu$_2$S at the (000−1) end facet is slightly lower if compared to the (0001) facet, which justifies why in some NRs the CE takes places at only one tip, while in some other cases asymmetric Cu-CE is observed.

Analogous NHCs were recently observed by Kriegel et al. when exposing zb-CdTe NRs to Cu$^+$ ions.[192] In such CE reactions the exchange took place preferentially from just one side of the parent CdTe NRs, yielding CdTe/Cu$_{2-x}$Te NHCs. Also in this case, even if CE in most NRs started from only one of the NRs' tips, in some other NRs CE was observed to start simultaneously from both tips.

5.3.1.2. CdS/Ag$_2$S System. Another important combination of materials, represented by the Ag$_2$S−CdS binary system, has been deeply investigated in colloidal NCs using CE. Robinson et al., for example, found that CdS NRs transform to Ag$_2$S/CdS striped superstructures (n-n junctions) after partial CE with Ag$^+$ ions.[71,198] Differently from the Cu$_2$S/CdS case, the addition of low amounts of Ag$^+$, rather than leading to a preferential exchange at the tips, produces instead small Ag$_2$S regions that are dispersed randomly over the surface of the starting CdS NR. This is due to the negative chemical formation energies for each of the CdS/Ag$_2$S attachments that favor, initially, the creation of Cd−S−Ag interfacial bonds on both ends and sides of the CdS NRs. By increasing the amount of silver ions, the Ag$_2$S domains coalesce and form regular segments spanning the diameter of the NR, with flat interfaces parallel to the NR cross section (see Figure 17). As the Ag$_2$S domains grow further, the elastic strain originating at the Ag$_2$S/CdS interface becomes a more important contribution to the total formation energy, driving the ripening of the Ag$_2$S regions in order to reduce the interfacial area. Surprisingly, the system does not tend to the lowest energy structure, that would consist in a full phase segregation of the CdS and Ag$_2$S regions to the opposite ends of the NR (as in the case of Cu$_2$S/CdS NRs), but the Ag$_2$S segments remain separated from each other. This separation is stabilized by the large interfacial strain that leads to a repulsive elastic interaction between segments that decreases with increasing separation between them. Differently from the CdS-Cu$_2$S case, thus, here the factor that governs the morphology of the resulting NHCs is the interfacial strain, rather than the interface energy.

5.3.1.3. CdX/PbX (X = S, Se, Te) Systems. The CdX/PbX system (X = S, Se, Te) represents one of the most studied systems in CE reactions (see also section 5.3.2.1). As PbX and CdX materials are immiscible, partial exchange of Cd^{2+} with Pb^{2+} ions results in segmented CdX/PbX NHCs. In a recent work, Lee et al. showed that the transformation of CdSe NRs, upon exposure to Pb^{2+} ions, leads to rock-salt (rs) PbSe NRs with intermediate structures represented by wz-CdSe/rs-PbSe heterojunctions.[121] The replacement of Cd^{2+} ions was found to take place anisotropically from the tips of the NRs and forming interfaces parallel to the (0001) plane of wz-CdSe NRs, exactly as in the CdS/Cu$_2$S case (see Figure 18A,B).[70] These interfaces were proven to minimize the interfacial energy between the two materials as the {111} facets of rs-PbSe form nearly strain-free interface with {0001} facets of wz-CdSe. The lattice mismatch at the {111}$_{PbSe}$/{0001}$_{CdSe}$ interface is estimated around 0.74%, implying the high stability of this particular epitaxial interface. Interestingly, as in the case of CdS-Cu$_2$S system, the CE process initiates at both tips of CdSe NRs, and then it proceeds faster along the (000−1) planes. In the case of Cd-to-
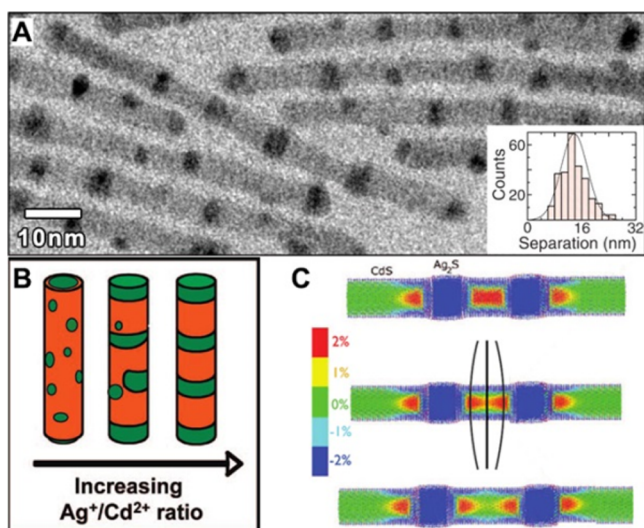
Figure 17. (A) TEM image of Ag$_2$S-CdS superlattices formed through partial CE. (Inset) Histogram of Ag$_2$S segment spacing (center-to-center). The average spacing is 13.8 ± 3.8 nm. Adapted with permission from ref 71. Copyright 2007 The American Association for the Advancement of Science. (b) Sketch representing the development of the morphology of binary nanorods produced by CE at increasing amounts of Ag$^+$ added to CdS NRs. Reproduced from [Sadtler, B.; Demchenko, D. O.; Zheng, H.; Hughes, S. M.; Merkle, M. G.; Dahmen, U.; Wang, L.-W.; Alivisatos, A. P. Selective facet reactivity during cation exchange in cadmium sulfide nanorods *J. Am. Chem. Soc.* **2009**, *131*, 5285–5293]. Copyright 2009 American Chemical Society. (C) Color maps of the z-component of strain in the interatomic bonds, for a 4.8 nm diameter Ag$_2$S/CdS striped NR. The segment separations are 6, 8, and 10 nm. The color map limits indicate a strain ranging from −2% (compression, blue) to 2% (tension, red). The atoms are pulled in opposite directions (indicated by the black lines at the center of the second rod), which leads to an increased interaction energy when the segments separation decreases. Reproduced from [Demchenko, D. O.; Robinson, R. D.; Sadtler, B.; Erdonmez, C. K.; Alivisatos, A. P.; Wang, L.-W. Formation Mechanism and Properties of CdS-Ag$_2$S Nanorod Superlattices *ACS Nano* **2008**, *2*, 627–636]. Copyright 2008 American Chemical Society.

Cu conversion in CdS NRs this asymmetry was explained as resulting from the lack of inversion symmetry about the *c* axis in the wz-CdS lattice; namely, the densities of dangling bonds and their geometries are not equal at the (0001) and (000−1) end facets of the NRs, hence the two facets have different energies. Analogously, as the (000−1) facet of CdSe NRs is more reactive than the (0001) one, the Cd-to-Pb exchange appears to be facet-selective.

Using similar reaction conditions, Zhang et al. prepared zb-CdS/rs-PbS and zb-CdSe/rs-PbSe Janus-like NHCs upon partial CE.[118] In this case too, even if starting from cubic CdX NCs, the CE proceeds anisotropically: it is initiated at specific sites or planes and then forms sharp (111)$_{PbE}$/(111)$_{CdE}$ interfaces (see Figure 18c). The presence of only one interface in all the Janus-like NHCs, again, proves that the process tends to proceed by minimizing both strain and interface energy. The specific (111)$_{PbE}$/(111)$_{CdE}$ interface suits this requirements as it is composed by a Se atomic layer sandwiched by a Pb layer on one side and a Cd layer at the other side along the <111> direction.

5.3.1.4. CdS/Pd$_4$S System. Shemeshet al. reported the synthesis of CdS/Pd$_4$S segmented NRs by exposing CdS NRs to Pd^{2+} ions in the presence of oleylamine at 200 °C.[191]
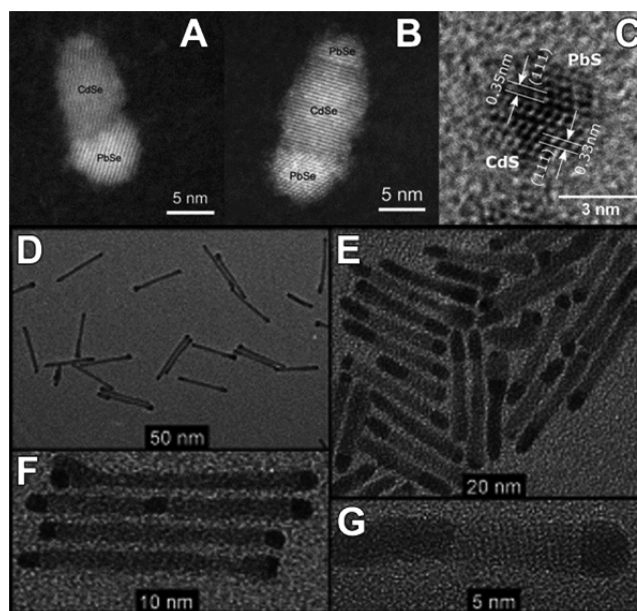
Figure 18. (A,B) HAADF images of w-CdSe/rs-PbSe NRs obtained with Cd-to-Pb partial conversion of CdSe NRs. The NHC have either only one or both tip converted into PbSe, in the latter case with different extents of conversion. The resulting clear PbSe/CdSe interfaces are parallel to the (0001) plane of w-CdSe. Reproduced from [Lee, D.; Kim, W. D.; Lee, S.; Bae, W. K.; Lee, S.; Lee, D. C. Direct Cd-to-Pb Exchange of CdSe Nanorods into PbSe/CdSe Axial Heterojunction Nanorods *Chem. Mater.* **2015**, *27*, 5295–5304]. Copyright 2015 American Chemical Society. (C) Janus-like spherical NC where approximately half of each QD is made PbS and half is CdS. The resulting c PbS/CdS interface is parallel to the (111) plane of both cubic structures. Reproduced from [Zhang, J.; Chernomordik, B. D.; Crisp, R. W.; Kroupa, D. M.; Luther, J. M.; Miller, E. M.; Gao, J.; Beard, M. C. Preparation of Cd/Pb Chalcogenide Heterostructured Janus Particles via Controllable Cation Exchange *ACS Nano* **2015**, *9*, 7151–7163]. Copyright 2015 American Chemical Society. (D–G) CdS/Pd$_4$S hybrid nanostructures: (D) tip growth of Pd$_4$S on 5.9 nm diameter nanorods; (E) more extensive growth of Pd$_4$S on a sample of CdS nanorods with a broad size distribution; (F) close-up of the sample shown in (D); (G) HRTEM of a single CdS/Pd$_4$S NR from the sample shown in (E). Adapted with permission from ref 191. Copyright 2010 John Wiley and Sons.

Surprisingly, while the direct exchange of Cd^{2+} with Pd^{2+} ions would produce a PdS phase, in this particular work the formation of a Pd$_4$S phase, in which Pd is present both in the +2 and 0 oxidation states, was observed. The process itself, consequently, can be thought as a combination of a high-temperature reduction of Pd^{2+} to Pd^0 (driven by the oleylamine) and the simultaneous replacement of Cd^{2+} ions with both palladium species. Interestingly, the formation of Pd$_4$S, as in the case of CdS/Cu$_2$S and CdX/PbX systems, starts either at one or at both tips of the initial CdS NRs (see Figure 18D−G). The growth of the new phase produces segmented CdS/Pd$_4$S structures in which the two domains share flat interfaces perpendicular to the elongation direction of the NRs, most likely to ensure a minimal interface energy and strain. As the reactivity of the crystallographically anisotropic ends of the wz-CdS NRs is different, also in this case the formation of the Pd$_4$S domains was not symmetrical on both sides of the NRs.

5.3.1.5. Cu$_{2-x}$S/ZnS and Cu$_{2-x}$S/CdS Systems. Ha et al. reported the formation of dual-interface NHCs by exposing roxybite Cu$_{2-x}$S NCs to Zn^{2+} ions.[107] The CE starts with the
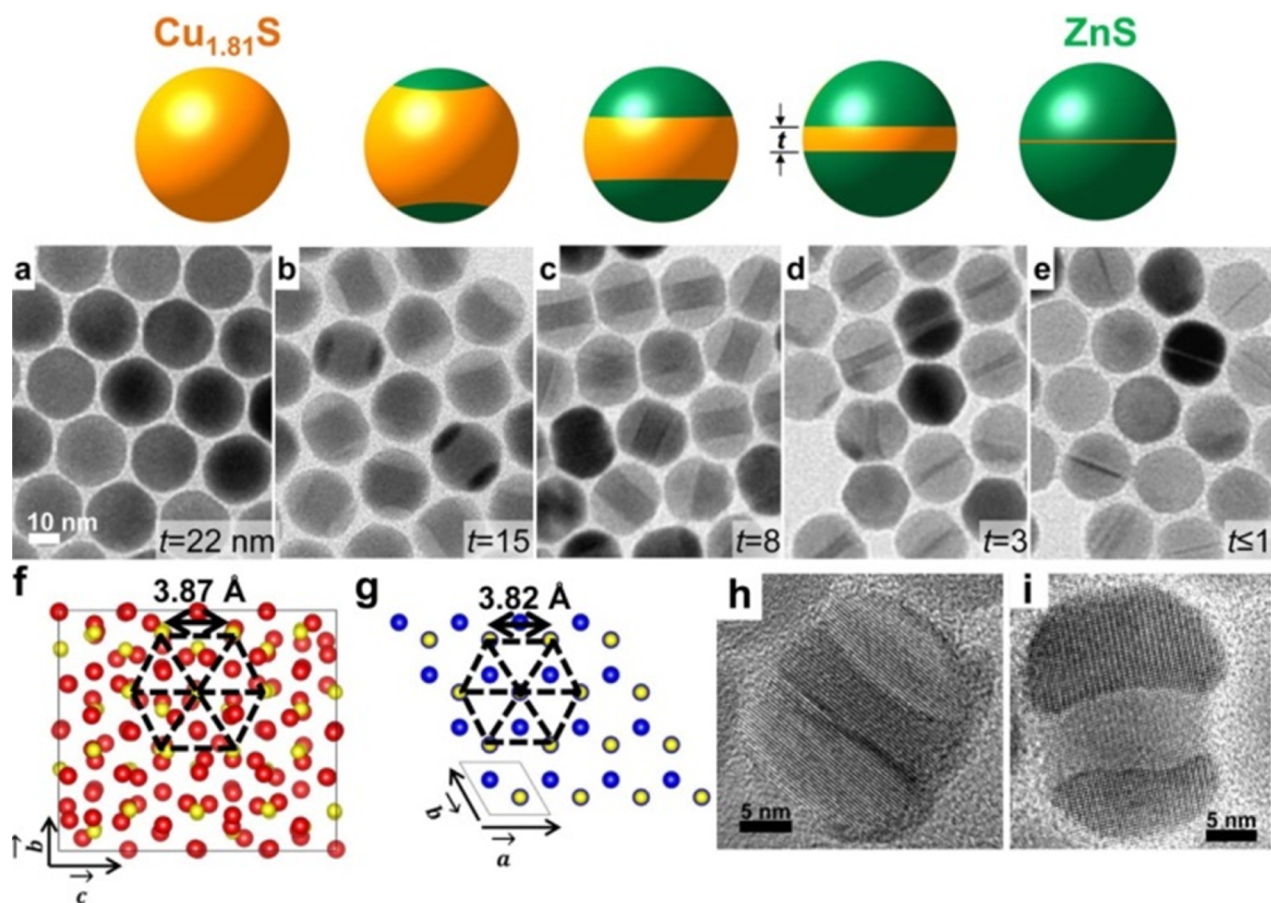
Figure 19. CE transformation of spherical $Cu_{2-x}S$ NCs into dual-interface NHCs with ZnS caps. Schematic (top panel) and TEM images (a−e) show the composition change from the initial copper sulfide NC (a) into a ZnS with a residual copper sulfide thin disk (e). The copper sulfide disk thickness (t) is indicated. (f,g) Atomic models of the $Cu_{1.81}S$ roxbyite (100) plane (f) and wz-ZnS (001) plane (g). The sulfur atoms are shown in yellow. HRTEM images of $Cu_{2-x}S/ZnS$ (h) and $Cu_{2-x}S/CdS$ (i) dual-interface NHCs showing the convex curvature of ZnS caps (h) and concave curvature of CdS caps (i) on the copper sulfide central layer. The opposite curvature is due to the reversal of the interfacial strain for the ZnS (copper sulfide is in compression) versus the CdS (copper sulfide is in tension) caps. Reproduced from [Ha, D.-H.; Caldwell, A. H.; Ward, M. J.; Honrao, S.; Mathew, K.; Hovden, R.; Koker, M. K. A.; Muller, D. A.; Hennig, R. G.; Robinson, R. D. Solid−Solid Phase Transformations Induced through Cation Exchange and Strain in 2D Heterostructured Copper Sulfide Nanocrystals *Nano Lett.* **2014**, *14*, 7090−7099]. Copyright 2014 American Chemical Society.

symmetrical nucleation of two ZnS grains on opposite sides of each spherical copper sulfide NC (see Figure 19). As ZnS domains grow, the copper sulfide region in the center of the NC eventually becomes a disk-like 2D layer (see Figure 19c− e), whose thickness can be tuned by controlling the extent of CE. In the presence of an excess of Zn^{2+} the CE leads to fully converted ZnS NCs preserving the spherical shape and size of the initial copper sulfide NCs. As revealed by HAADF and HRTEM characterizations, the $Cu_{2-x}S/ZnS$ NHCs exhibit atomically sharp interfaces along the <100> direction of $Cu_{2-x}S$ and <001> direction of ZnS, with no intermixing of zinc and copper ions. These particular epitaxial interfaces minimize the interface energy as the sulfur sublattices shared by $Cu_{1.81}S$ roxbyite (triclinic) and wz-ZnS are well-matched. Indeed, even if roxbyite copper sulfide has a low symmetry crystal structure, its sulfur sublattice along the (100) or (−100) planes is hexagonal, with maximum deviations of ±0.35 Å from the sulfur sublattice spacing in wz-ZnS along the (001) or (00− 1) planes (see Figure 19f−g). Along the other planes, a poor match between the two crystal structures was found. Additionally, the dual interface formation in this specific systems can be explained by considering that the atomic arrangements of the

(100) and (−100) planes of the roxbyite phase are extremely similar, providing a comparable chemical environment for the CE, and, thus, similar interface energies with the ZnS domains. The presence of such favorable epitaxial matching with only a few atomic planes is likely the reason why $Cu_{1.81}S/ZnS$ NHCs do not form a core−shell structure. The strain in $Cu_{1.81}S/ZnS$ NHCs however plays a minor role in determining the arrangements of the different domains, since the lattice constant of the sulfur sublattice in ZnS (001/00−1) is only 1.1% smaller than that of the sulfur sublattice in roxbyite (100/ −100). This lattice mismatch results in the formation of curved interfaces between copper sulfide and ZnS (see Figure 19h) and the strain relaxation occurs only by the development of atomic steps along the interfaces. It is interesting to notice that the same CE procedure was shown to work with Cd^{2+} ions and led again to the formation of dual-interface $Cu_{1.81}S/CdS$ NHCs. As the CdS sulfur sublattice spacing is 6.8% larger than that of roxbyite copper sulfide, the stress at the interface is reversed with respect to the $Cu_{1.81}S/ZnS$ NHCs case; therefore, an opposite curvature develops (see Figure 19i).

5.3.1.6. $Cu_{2-x}Se/MSe$ (M═Cd,Sn,Zn) Systems. The replacement of Cu^+ ions in berzelianite $Cu_{2-x}Se$ spherical NCs with

Zn^{2+}, Cd^{2+}, and Sn^{2+} produces, as intermediates, Janus-like $Cu_{2-x}Se/MSe$ NHCs.[137,149] This indicates that the MSe phase nucleates at one location of the NCs and grows from there at the expenses of the residual $Cu_{2-x}Se$ domain, forming a single epitaxial interface. In all the cases, the appearance of a Janus-like architecture suggests that once a MSe nucleus is formed on a given location on the host NC surface, the CE reaction can proceed only from there and creates a single interface between the two different materials. The possibility of a simultaneous formation of multiple MSe nuclei on the surface of a single NC, with the consequent increase of the overall interface energy, is rarely observed, but is not statistically impossible, and it leads to the formation of polycrystalline NHCs, as shown in Figure 20F.[149] The Cd^{2+}-for-Cu^+ partial CE in $Cu_{2-x}Se$ spherical NCs
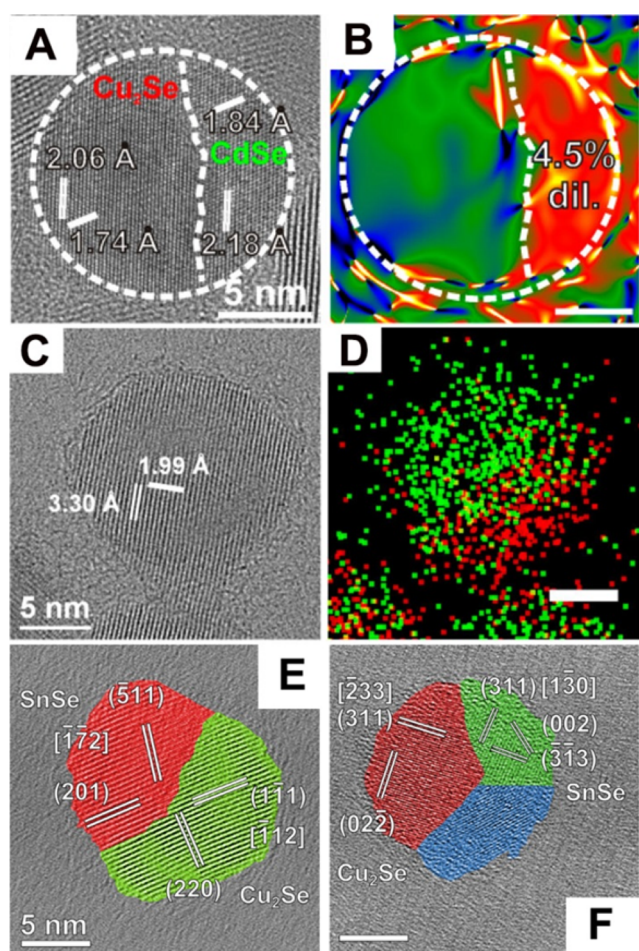

Figure 20. HRTEM images of (A) $Cu_2Se/CdSe$, (C) $Cu_2Se/ZnSe$, and (E) $Cu_2Se/SnSe$ Janus-like NCs. (B) Mean dilation map as obtained by geometric phase analysis of the $Cu_2Se/CdSe$ NC in panel A. (D) STEM-EDS map of the $Cu_2Se/ZnSe$ NC shown in panel C. (F) HRTEM image a polycrystalline $Cu_{2-x}Se/SnSe$ NC exhibiting different domains ($Cu_{2-x}Se$ in green, SnSe in red and light blue). Scale bars in all the HRTEM images are 5 nm. (A−D) Reproduced from [Lesnyak, V.; Brescia, R.; Messina, G. C.; Manna, L. Cu Vacancies Boost Cation Exchange Reactions in Copper Selenide Nanocrystals *J. Am. Chem. Soc.* **2015**, *137*, 9315−9323] Copyright 2015 American Chemical Society. (E and F) Reproduced from [De Trizio, L.; Li, H.; Casu, A.; Genovese, A.; Sathya, A.; Messina, G. C.; Manna, L. Sn Cation Valency Dependence in Cation Exchange Reactions Involving Cu2-xSe Nanocrystals *J. Am. Chem. Soc.* **2014**, *136*, 16277−16284]. Copyright 2014 American Chemical Society.

produces $Cu_{2-x}Se/CdSe$ Janus-like NCs with a clear distinction between the sphalerite CdSe ($a = 6.1$ Å) and the berzelianite Cu_2Se ($a = 5.8$ Å) domains. In these structures, interestingly, the HRTEM analysis enables for the detection of a 4.5 (± 0.9)% mean dilation in the CdSe domain relative to the Cu_2Se one (see Figure 20A,B).[137] The CE between $Cu_{2-x}Se$ NCs and Zn^{2+} ions, on the other hand, produces $Cu_2Se/ZnSe$ NHCs whose morphological attribution is more complex as neither HRTEM nor XRD analyses can directly prove that pure Cu_2Se and ZnSe domains form.[137] The mismatch between the berzelianite Cu_2Se and sphalerite ZnSe ($a = 5.7$ Å) is indeed so low that HRTEM analysis of a single NHC cannot detect any variation in the lattice parameter (see Figure 20C). On the other hand, STEM-EDS mapping of such NCs indicates the presence of two distinct domains, one Cu-rich and the other Zn-rich (see Figure 20D). As these two materials are completely immiscible in the bulk, these NHCs are most likely $Cu_2Se/ZnSe$ Janus-like NCs (see Figure 20D).

Differently from the systems discussed above, the substitution of Cu^+ ions with Sn^{2+} ions in $Cu_{2-x}Se$ NCs produces a significant distortion of the Se^{2-} anion sublattice, leading to the formation of an orthorhombic SnSe phase.[149] This distortion is responsible, in the case of partial CE, for the formation of $Cu_{2-x}Se/SnSe$ Janus-like NCs characterized by clean interfaces, but exhibiting an imperfect epitaxial relationship: as can be seen from Figure 20E, there is a visible angular distortion between the (220) planes of $Cu_{2-x}Se$ and the (−511) planes of SnSe, which is also affected by a lattice mismatch of the order of 10%. The formation of Janus-like NHCs in this system can be attributed, most likely, to the high energy required for the nucleation of the SnSe phase. A local distortion of $Cu_{2-x}Se$ the anion sublattice is indeed necessary to enable the large Sn^{2+} ions to form the orthorhombic SnSe phase.

5.3.1.7. TiS_2/Cu_2S System. Jeong et al. showed that layered TiS_2 nanoplatelets can undergo CE with Cu^+ ions, leading to unconventional intermediate structures: TiS_2/Cu_2S core-crown-like NCs.[131] The formation of the Cu_2S phase starts and propagates from the edges of the TiS_2 NDs in a heteroepitaxial manner. The interface between the two materials is not atomically flat, but the two lattices are precisely aligned, as found by HRTEM analysis (see Figure 21). On the edge of TiS_2 NDs, the (002) planes of Cu_2S are indeed parallel to the (001) planes of TiS_2. Clearly, the presence of a preferential interface is lacking in this system and the reactive peripheral edges of TiS_2 offer nonselective nucleation and growth points for the product material. The role of the strain in TiS_2/Cu_2S NHCs is hardly computable as the morphology of the starting Ti_2S NCs is not retained during the CE process. Indeed, in this case even a reorganization of the anion framework accompanies the overall transformation. The initial disc-like shape transforms into a toroid; a highly symmetric, double-convex geometrical structure with a hole in its center (see section 4.1.1). The very same process seems to apply even when working with other guest cations such as Ag^+, Mn^{2+} and Cd^{2+}, which consistently resulted in similar intermediate nanostructures of TiS_2/Ag_2S, TiS_2/MnS and a fully converted toroid of CdS, respectively.

5.3.2. Core|Shell Heterostructures. The synthesis of core| shell structures typically involves the epitaxial growth of a second semiconductor onto seed NCs, either in a single-step or in multistep reactions. In wet chemical approaches, the inorganic shell growth requires, in general, relatively high temperatures, i.e. above 150 °C, at which undesirable
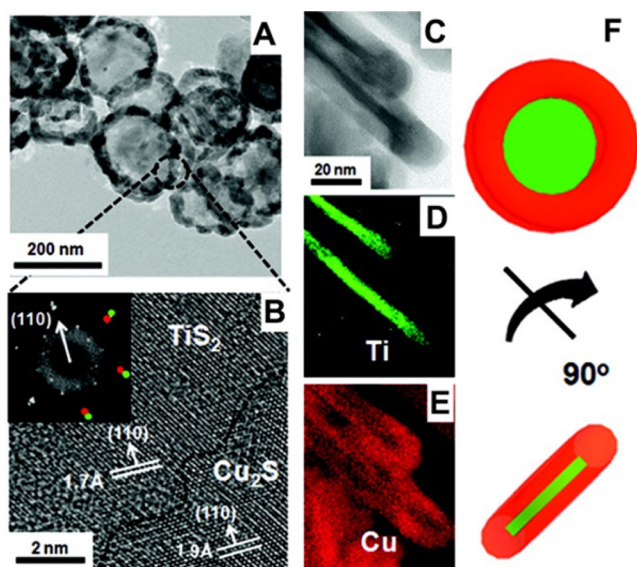
Figure 21. (A) Large-area TEM image of TiS_2/Cu_2S core-crown-like NHCs. (B) High-magnification image of the interface between TiS_2 and Cu_2S showing that the (110) planes of Cu_2S with a 1.9 Å lattice fringe are oriented in the same direction as the (110) planes of TiS_2 with a 1.7 Å lattice fringe. The FFT pattern (inset) shows green and red dots corresponding to TiS_2 and Cu_2S, respectively. (C−E) Side-view TEM image (C) and EELS elemental analysis (D and E) of a core-crown-like NHCs. Ti is shown in green and Cu in red. (F) Schematic rotation of a TiS_2/Cu_2S NHC by 90°, showing both planar and side-view images. Reproduced from [Jeong, S.; Han, J. H.; Jang, J.-t.; Seo, J.-w.; Kim, J.-G.; Cheon, J. Transformative Two-Dimensional Layered Nanocrystals *J. Am. Chem. Soc.* **2011**, *133*, 14500−14503]. Copyright 2011 American Chemical Society.

homogeneous nucleation of the shell material NCs or degradation of the starting seeds can occur: for example, lead chalcogenides NCs might undergo Ostwald ripening. Also, the growth of a monocrystalline shell might be hindered once the shell thickness becomes larger than the critical layer thickness (about two monolayers) due to the existence of strain-induced defects.[199] This is particularly true when growing a shell onto quasi-spherical core NCs, as they are characterized by highly curved surfaces and they expose many different crystallographic facets.

Pioneering works, dating back to the nineties, demonstrated that CE reactions could lead, in some cases, to core|shell structures (for example exposing CdS QDs either to Pb^{2+} or Hg^{2+} ions) with tunable layer thickness.[36,37] Recently, CE reactions have emerged as an alternative strategy to synthesize many core|shell NHCs of compounds such as PbX|CdX, CdX|PbX (where X = S, Se, or Te), and $CuInS_2$|ZnS NCs (see Table 5). CE reactions can be used to overcome the problems connected to the traditional seeded-growth approach, as they can be performed at relatively low temperature, with consequent preservation of the starting NC seeds.[122] Also, as the cation replacement proceeds in most cases topotactically, strain-induced effects can be minimized and in principle monocrystalline shells with tunable thickness can be prepared.

Differently from the segmented NHCs, the core|shell NCs formed upon CE seem to be metastable (i.e., kinetically driven), and under annealing or beam irradiation they transform into bidomain NHCs sharing one single interface that minimizes both interface energy and strain (see the discussion below). This suggests that this kind of architecture

forms when the diffusivity of the ions involved in the CE is sufficiently slow to allow, statistically, the nucleation of the product material unselectively on the whole surface of the parent NCs. This is also favored by the absence of a specific interface that has an overwhelming lower energy with respect to the other interfaces. The growth of the product phase, therefore, proceeds from the surface to the inner core of each NC, with the consequent increment of the shell thickness and of the interface energy. Even if the shell growth can be thought as the result of an isotropic replacement of host cations with new ones, it has been demonstrated that this process is rather anisotropic. There is always, in fact, a favored interface, having the lowest energy, that preferentially forms, with consequent heterogeneity in shell thickness and in core position, size and shape.[122,127,186]

5.3.2.1. PbX-CdX System. Cd-exchanged PbX NCs are among the most studied core|shell systems that can be prepared by CE. As shown in section 5.3.1.3 the intermediate structures formed upon Cd^{2+} for Pb^{2+} exchange are typically segmented CdX/PbX heterojunctions, while the opposite reaction, that is, the replacement of Pb^{2+} ions with Cd^{2+} in PbX NCs, leads, surprisingly, to PbX|CdX core|shell NCs (see Figure 22a−c).
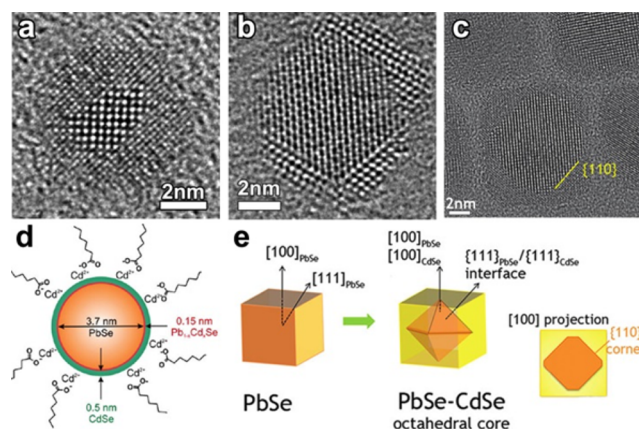
Figure 22. HR-TEM images of (a) spherical PbTe|CdTe, (b) spherical and (c) cubic PbSe|CdSe core|shell NCs observed in the (a,c) [100] and (b) [100] directions. (d) Schematic representation of a typical PbSe|CdSe core|shell QD. (e) Sketch of the structural transformation from pure PbSe cube-shaped NCs to core|shell PbSe|CdSe NHCs with a nearly octahedron PbSe core. The PbSe is indicated in orange, CdSe in yellow. (a,b) Reproduced from [Lambert, K.; Geyter, B. D.; Moreels, I.; Hens, Z. PbTe|CdTe Core|Shell Particles by Cation Exchange, a HR-TEM study *Chem. Mater.* **2009**, *21*, 778−780]. Copyright 2009 American Chemical Society. (c,e) Reproduced from [Casavola, M.; van Huis, M. A.; Bals, S.; Lambert, K.; Hens, Z.; Vanmaekelbergh, D. Anisotropic Cation Exchange in PbSe/CdSe Core/Shell Nanocrystals of Different Geometry *Chem. Mater.* **2012**, *24*, 294−302]. Copyright 2012 American Chemical Society. (d) Reproduced from [Abel, K. A.; FitzGerald, P. A.; Wang, T.-Y.; Regier, T. Z.; Raudsepp, M.; Ringer, S. P.; Warr, G. G.; van Veggel, F. C. J. M. Probing the Structure of Colloidal Core/Shell Quantum Dots Formed by Cation Exchange *J. Phys. Chem. C* **2012**, *116*, 3968−3978]. Copyright 2012 American Chemical Society.

This suggests that the two processes have different dynamics, i.e. the ions have different mobilities, which leads to different CE pathways. It is also important to consider that, while CE from CdX to PbX entails the reorganization of the overall NC lattice, from either wz-CdX or zb-CdX to rs-PbX, the inverse reaction (discussed in this section) always implies the

transformation of a rs-PbX structure into a zb-CdX one. In this last case PbX and CdX materials have both a cubic crystal structure, with almost no lattice mismatch between them, and no relevant strain is generated at their interface.[41,122,127] No preferential interfaces are thermodynamically predominant so that CE can proceed from each surface of the NC toward the inner part, generating core|shell architectures.[127]

Pietryga et al. were the first group to exploit CE reactions in order to achieve inorganic passivation of PbSe NCs with a CdSe shell in 2008.[122] They purposely employed a relatively slow-reacting cadmium precursor allowing for a controlled ion substitution at the surface and, in turn, resulting in a slow, self-limiting growth of a CdSe shell at the expenses of the starting PbSe NCs. Additional works followed this synthetic route and some of them demonstrated that PbS and PbTe, when exposed to Cd²⁺, form similar core|shell struc-tures.[40,41,88,116,123,124,126,127,185,186,188] As a general trend, the formation of PbX|CdX core|shell NCs leads to improved photostability and higher PL quantum efficiencies with respect to the "bare" starting PbX NCs.[38,40,116,122,188] Moreover, when the shell is grown thick enough, the NHCs exhibit also the characteristic absorption and emission features of the CdX material.[40,126,188]

As the direct observation of such core|shell structure was initially challenging, detailed structural characterizations of CdX and PbX domains were published in later works.[38,127,188] For what concerns the exact chemical composition of PbX|CdX NHCs, Abel et al., by combining advanced HRTEM with synchrotron XPS as well as X-ray and neutron scattering methods, demonstrated that the exchange of PbSe NCs with Cd²⁺ ions leads, indeed, to core|shell structures with a purely PbSe core, an outer shell made of pure CdSe (with a Cd-oleate capping layer), and a sharp interface of (strained) $Pb_{1-x}Cd_xSe$ material (see Figure 22d).[185] No hints of the presence of alloyed structures emerged in any analysis.

In the PbS-CdS case, Lechner et al. showed that during the first stages of CE the shell grows at the expenses of the PbS core, preserving its original crystal structure and, thus, originating a metastable rocksalt CdS phase.[38] As the shell gets thicker, the CdS shell transforms into the more stable zinc-blende structure. The growth of the shell, surprisingly, is not isotropic, as expected, but rather anisotropic, as proven by Lambert et al.[127] This finding came as a comparison of *ab initio* calculations of interfacial energies and HRTEM observations of PbTe|CdTe NCs. While similar interface energies, of around 0.20 J/m², were calculated for the {111}, {110}, and {100} facets, mainly {111} interfaces were observed by HRTEM.[125] This suggests that CE in that system is not determined by thermodynamics, but rather by an anisotropic growth mechanism, since preferential interfaces are formed. The same mechanism was found to apply to PbSe|CdSe NHCs.[41,127] More specifically, Casavola et al. showed that, when starting with rs-PbSe NRs or nano cubes, the CE reaction with Cd²⁺ leads to sharp {111}-faceted quantum dot cores of rs-PbSe embedded in a zb-CdSe shell (see Figure 22). The anisotropy of the exchange was tentatively explained by considering that the peculiarity of the {111} interface, with respect to the other interfaces (such as {001} and {110}), is that it consists entirely of either cations or anions. Thus, at the boundary the interfacial Se{111} atomic layer is sandwiched by a Pb{111} layer at one side, and by a Cd{111} layer at the other side providing a stress-free interface.[41,141]

The intrinsic anisotropy of the exchange process leads to a strong increase in the heterogeneity of the cores formed, not only in terms of core size and shell thickness but also at the level of the shape and position of the core. The initial size dispersion of the PbTe cores, for example, increases from 6.6% to 25%. At the same time, the almost spherical PbTe NCs transform into cores with an aspect ratio of about 1:2. The position of these cores can be either at the center or completely at one side of the final NHC. Clearly, this lack of control represents a drawback of an otherwise straightforward core|shell synthesis technique.

PbSe|CdSe core|shell NHCs prepared by CE have been shown to be metastable and to evolve into Janus-like systems upon annealing at temperatures as low as 150 °C under vacuum.[125] Prior to annealing, the spherical NHCs are characterized by a rs-PbSe core with an approximately octahedral morphology (showing eight {111} facets), and a CdSe shell with a zinc-blende crystal structure (see Figure 23A,B). Upon *in situ* annealing, the NHCs preserve their
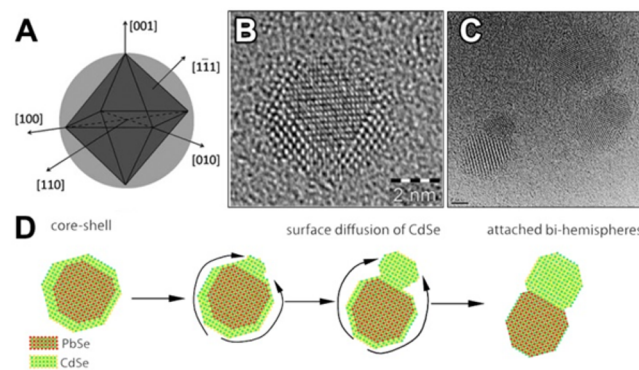
Figure 23. Model of the PbSe|CdSe core|shell NC structure evidencing the octahedral shape of the PbSe core (A). HR-TEM images of a PbSe|CdSe core|shell NC (B) and PbSe/CdSe Janus-like NCs (C). The latter are obtained after thermal annealing at 200 °C of initial core|shell NCs. The bottom-left particle clearly shows that the volume of the CdSe shell was significantly larger than that of the PbSe core, consequently the PbSe/CdSe heterointerface is considerably different from that observed for equal volume bihemispheres, in the sense that it is no longer a flat interface, as can be clearly observed for the two top-right NHCs. (D) The mechanism of the thermally induced structural transformation from core|shell to Janus-like NHC is schematically depicted. Reproduced from [Grodzinska, D.; Pietra, F.; van Huis, M. A.; Vanmaekelbergh, D.; de Mello Donega, C. Thermally induced atomic reconstruction of PbSe/CdSe core/shell quantum dots into PbSe/CdSe bihemisphere heteronanocrystals *J. Mater. Chem.* **2011**, *21*, 11556−11565]. Copyright 2011 American Chemical Society.

original nearly spherical shape, but they undergo a drastic reconstruction whereby the total number of atoms stays constant. Both CdSe and PbSe domains reconstruct to form a Janus-like architecture with a single preferential rs-PbSe{111}/zb-CdSe{111} heterointerface. The mechanism of the thermally induced structural reconstruction is schematically depicted in Figure 23. The formation of perfect bihemispherical NCs requires that the starting volumes of PbSe and CdSe domains must be equal. Obviously, depending on the initial core/shell volume ratios, different shapes of NHCs can be formed after thermal annealing, with consequent different heterointerfaces, as shown in Figure 23C. These annealing experiments prove that the core|shell NHCs that form upon

Cd-for-Pb partial CE are most likely kinetically accessed, and that these systems thermodynamically evolve to Janus-like architectures, with the consequent minimization of the CdSe/PbSe interface, if enough energy is provided.

5.3.2.2. Cu$_{2-x}$S|Au$_2$S System. Wang et al. studied the CE reaction between Cu$_{2-x}$S NCs and gold ions and found that the replacement of copper ions took place gradually from the surface to the core of NCs, yielding eventually Au$_2$S NCs (see Figure 24).[165] This process leads initially to the formation of
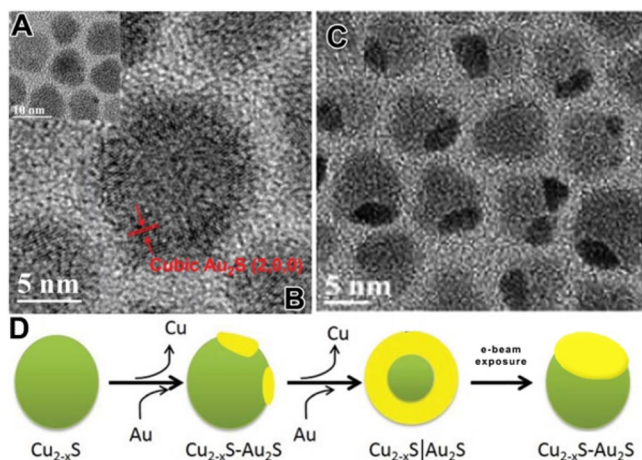
Figure 24. HRTEM images of (A) NCs synthesized exposing Cu$_{2-x}$S NCs to Au ions using (A) nominal 1:4 Au:Cu ratio, and (B) nominal 1:1 Au:Cu ratio (Cu$_{2-x}$S|Au$_2$S NHCs). (C) HRTEM image of Cu$_{2-x}$S–Au$_2$S structures achieved after exposure of Cu$_{2-x}$S|Au$_2$S NHCs to electron beam irradiation. (D) schematic illustration of the CE process and the subsequent evolution of the core|shell structures upon electron beam irradiation. Adapted with permission from ref 165. Copyright 2014 Royal Society of Chemistry.

Au$_2$S islands decorating the host NCs followed by their growth to form a cubic Au$_2$S shell covering the inner hexagonal Cu$_{2-x}$S core. In analogy to the CdS-Ag$_2$S system, the preliminary formation of Au$_2$S islands suggests that the interface energy is sufficiently low to allow a nonspecific nucleation of the new phase along the Cu$_{2-x}$S NCs surface.[71] The growth of the Au$_2$S phase then proceeded from there under kinetic control and led to a core|shell architecture that was found to be metastable: upon exposure to the electron beam of the HR-TEM, such NHCs initiated a transformation to a more stable configuration that resembled that of Janus-like structures (see Figure 24). Hence, when enough energy is provided the system tends to the most stable morphology, in which a single interface is shared between the two materials.

5.3.2.3. CuInS$_2$|MS (M = Cd, Zn) Systems. In some CE reactions the exact morphology of the resulting structures cannot be defined easily. For example, the exposure of CuInS$_2$ (CIS) QDs to Zn^{2+} or Cd^{2+} ions leads to NCs with a blue-shifted and improved PL emission.[113,187,190] More specifically, in both cases the CE process completely eliminates the fast PL component of the parent CuInS$_2$, associated with the surface defects, resulting in uniform single-exponential decay across the whole emission profile. As the size and morphology of the starting NCs is retained, the observed optical improvements have been explained in terms of a reduction of the CuInS$_2$ domain size and the consequent formation of a ZnS or CdS shell. Unfortunately, CIS roquesite, ZnS sphalerite and CdS hawleyite involved in these CE reactions are miscible and have

very similar lattice parameters. Therefore, XRD and HRTEM analyses are of little help in ruling out the formation of alloyed NCs, and in univocally demonstrating the presence of core|shell NCs.[113,190,200] Moreover, as the size of the QDs is extremely small (in the order or 3 nm), any precise element distribution, trough STEM EDX for example, has not been reported yet. Our group, supported mainly by XPS analyses, has proposed that alloyed Cu–In–Zn-S (CIZS) QDS rather than core|shell structures are most likely formed upon CE.[102,113]

5.3.2.4. CdS|Cu$_2$S System. The CE reactions between CdS NRs and Cu$^+$ ions, as it was discussed in section 5.3.1.1, tend to produce segmented CdS-Cu$_2$S NHCs in which the two materials share a low energy interface.[70] On the other hand, CE experiments performed on wz-CdS NWs with Cu$^+$ ions were found to lead to core|shell architectures.[161,162] As an example, Zhang et al. observed CdS|Cu$_2$S core|shell structures upon exposure of 30–40 nm thick and 10 μm long CdS NWs to copper ions (see Figure 25). Both CdS NRs and NWs under
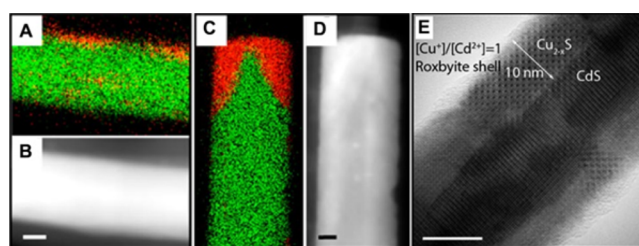
Figure 25. (A–D) EDS mapping for Cd–L (in green) and Cu–K (in red) and corresponding STEM images of CdS–Cu$_{2-x}$S NWs. (A,B) Conversion at the side facets. (C,D) Conversion at the tips of the NWs. (E) HRTEM image of CdS–Cu$_{2-x}$S core–shell NW and. Scale bars in (A–D) are 10 nm. Reproduced from [Zhang, D.; Wong, A. B.; Yu, Y.; Brittman, S.; Sun, J.; Fu, A.; Beberwyck, B.; Alivisatos, A. P.; Yang, P. Phase-Selective Cation-Exchange Chemistry in Sulfide Nanowire Systems *J. Am. Chem. Soc.* **2014**, *136*, 17430−17433]. Copyright 2014 American Chemical Society.

analysis are elongated along the [001] direction, exposing, consequently, the same crystallographic planes to the reaction solution. In the case of NWs, CE takes place preferentially at the tips (as in the case of NRs), but with a non-negligible nucleation of Cu$_2$S islands along the side facets of the wires (see Figure 25D,E). The chemical formation energy of this process was calculated to be approximately 7 times greater than the energy of nucleation of Cu$_2$S of at the CdS NRs tips.[70] In NWs instead, being the lateral surface markedly higher than that of NRs, such nucleation becomes statistically possible. Once the exchange takes place at the tips and at the surface of the NWs, it proceeds from there to the inner part of the crystals through solid state diffusion and eventually produces core|shell structures.

5.3.2.5. ZnSe|CdSe System. The ions diffusion can determine, in some particular circumstances, the formation of core|shell structures, even in case of miscible reactant and product materials. Groeneveld et al., in a recent work, showed that the ZnSe → CdSe CE transformation is a thermally activated isotropic process, and, thus, the reaction temperature can be used to precisely govern both the composition and morphology of the products.[42] More specifically, at 150 °C ZnSe|CdSe core|shell NCs are obtained, while higher temperatures produce either gradient or homogeneous (Zn$_{1−x}$Cd$_x$)Se alloys. This is quite interesting if one considers that ZnSe and

CdSe materials are fully miscible, enabling, in principle, the formation of alloy NCs of any arbitrary composition. At relatively low temperature, i.e., 150 °C, the CE process is most likely limited to the surface of the NCs, as shown by EELS elemental mapping (see Figure 26) leading, unexpectedly, to
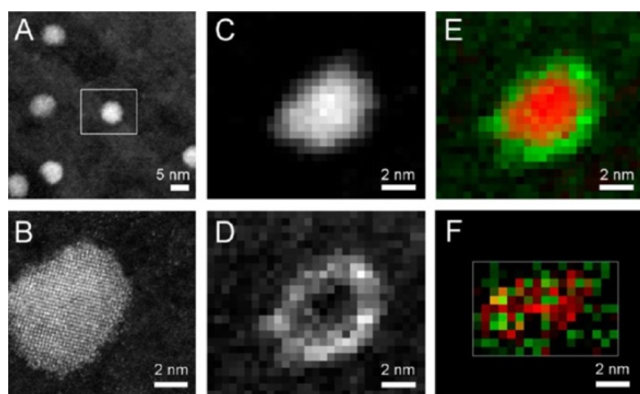
Figure 26. (A) STEM-HAADF images of ZnSe|CdSe core|shell NCs obtained from 5.6 nm ZnSe NCs by Zn^{2+} for Cd^{2+} exchange. The square indicates the region selected for EELS analysis. (B) HR-STEM image of a representative ZnSe|CdSe core|shell NC. Chemical maps for Zn (C) and Cd (D) of the ZnSe|CdSe core|shell NC selected in (A). These maps are combined in (E) to produce a chemical distribution profile of the NC (Zn in red, Cd in green). Panel (F) gives the chemical distribution profile map for a sample obtained by heating the ZnSe/CdSe core|shell NHCs, shown in (A–E) at 250 °C for 20 min. Reproduced from [Groeneveld, E.; Witteman, L.; Lefferts, M.; Ke, X.; Bals, S.; Van Tendeloo, G.; de Mello Donega, C. Tailoring ZnSe–CdSe Colloidal Quantum Dots via Cation Exchange: From Core/Shell to Alloy Nanocrystals *ACS Nano* **2013**, *7*, 7913–7930]. Copyright 2013 American Chemical Society.

core|shell structures with a CdSe shell thickness up to 0.5 nm. These structures, synthesized in a kinetic regime were found to be metastable. Upon thermal treatment at 250 °C, the core| shell NHCs could be converted to the expected alloy $Zn_{1-x}Cd_xSe$ NCs (see Figure 26F).

5.3.2.6. NaYF$_4$:Yb,Tm|NaGdF$_4$ System. Much less work has been done to date on CE reactions involving lantanide-based NCs. Core|shell NCs were reported by van Dong et al. in CE experiments with water-dispersible spherical NaYF$_4$:Yb,Tm NCs and Gd^{3+} ions.[184] The result of the CE reaction is represented by NaYF$_4$:Yb,Tm|NaGdF$_4$ core|shell NCs with a thin, tunable, and uniform NaGdF$_4$ shell (see Figure 27). The presence of a shell in the product NCs could be visualized directly from HAADF images, where the signal difference between the shell and the center gave rise to a contrast, with the shell being brighter (see Figure 27B). Direct proof of the presence of a Gd^{3+} rich shell came from EELS 2D elemental maps in which a stronger Gd^{3+} signal was detected at the edge of each NC (see Figure 27C). In this system too, the interdiffusion of ions appears to govern the shell thickness, so that, by varying the CE reaction temperature from 25 to 100 °C, the shell thickness could be tuned from 0.3 to 1.9 nm. Neither in this case was the shell found to be uniform, most likely because preferred interfaces made the overall process slightly anisotropic.

5.3.3. Defects Driven Heterostructures. The presence of crystal defects, as already anticipated, can alter the outcome of the CE reactions. Dislocations, stacking faults and grain boundaries in host NCs can, indeed, greatly alter the ions
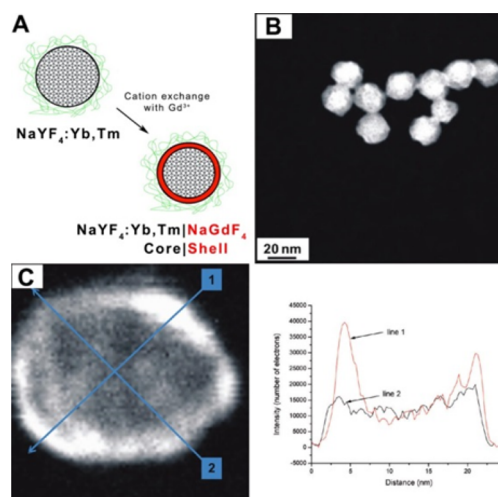
Figure 27. (A) Sketch representing the CE transformation of NaYF$_4$:Yb,Tm NCs exposed to Gd^{3+} ions. (B) HAADF image, and (C) EELS 2D elemental maps and line profiles of Gd^{3+} in NaYF$_4$:Yb,Tm|NaGdF$_4$ core|shell NCs prepared by CE of NaY-F$_4$:Yb,Tm nanoparticles with 10-fold Gd^{3+} ions at 75 °C. Reproduced from [Dong, C.; Korinek, A.; Blasiak, B.; Tomanek, B.; van Veggel, F. C. J. M. Cation Exchange: A Facile Method To Make NaYF4:Yb,Tm-NaGdF4 Core−Shell Nanoparticles with a Thin, Tunable, and Uniform Shell *Chem. Mater.* **2012**, *24*, 1297−1305]. Copyright 2012 American Chemical Society.

diffusion pathways and the energetics involved. Consequently, the morphology of the NHCs, resulting from CE experiments on such NCs, can be substantially different from what expected. Justo et al., for example, observed that the partial CE of polycrystalline PbS NRs with Cd^{2+} ions leads to multiple dot-in-rod PbS/CdS NHCs (see Figure 28A−C).[88] Similarly Casavola et al., when studying the CE transformation of rs-PbSe NRs into zb-CdSe, observed that, in some cases, single CdSe NRs embedding multiple PbSe dots were produced (see Figure 28).[41] In both cases the final NHCs can be seen as NRs made of PbX|CdX core−shell NCs (see Figure 28). These unique nanostructures are believed to form because CE proceeds faster along the grain boundaries that are present in the original PbS NRs. Moreover, the grain boundaries act as preferential nucleation sites for the product CdX phase.

Tan et al. prepared Cu$_2$S NWs bearing multiple twins along the wire and exposed them to Ag^+ cations, which led to the formation of p-n Cu$_2$S−Ag$_2$S striped heterojunctions (see Figure 28D−G).[162] This process was proven not to be driven by any interfacial energy or strain minimization, as in the case of the CdS-Ag$_2$S system. Conversely, it was argued that the twin boundaries in the Cu$_2$S NWs acted as preferred sites for the nucleation of Ag$_2$S segments. Notably, the orientation of the twin planes was shown to have a fundamental role in driving the formation of regular striped Cu$_2$S−Ag$_2$S NHCs. Indeed, while regular Ag$_2$S segments could be grown starting from fcc Cu$_2$S NWs with twin planes perpendicular to the growth direction (see Figure 28E,F), irregular patterning was observed when starting from monoclinic Cu$_2$S NWs having twin planes parallel to the growth direction (see Figure 28G). The presence of stacking faults, on the other hand, induced the degradation of CdSe NRs when exposed to Pb^{2+} ions, as observed by Lee et al.[121] These defects were believed to provide high energy sites (such as corners, edges, or kinks) on side-walls of CdSe NRs which became more prone to CE. Once the exchange started
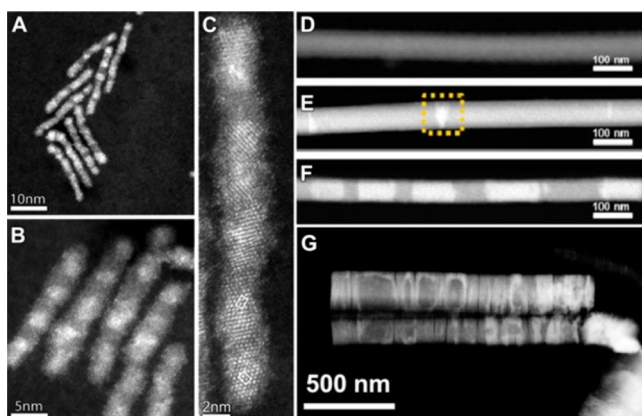
Figure 28. (A−C) STEM-HAADF images of PbS/CdS rods showing multiple PbS QDs inside the rods. The white rectangles in (C) indicate the ⟨110⟩ unit cell. STEM high-angle annular dark-field (HAADF) images of Cu_2S NWs (D) and Cu_2S−Ag_2S superlattice NWs (E−G) formed after Ag-partial CE of (E,F) fcc or (G) monoclinic Cu_2S NWs. The bright stripe regions ar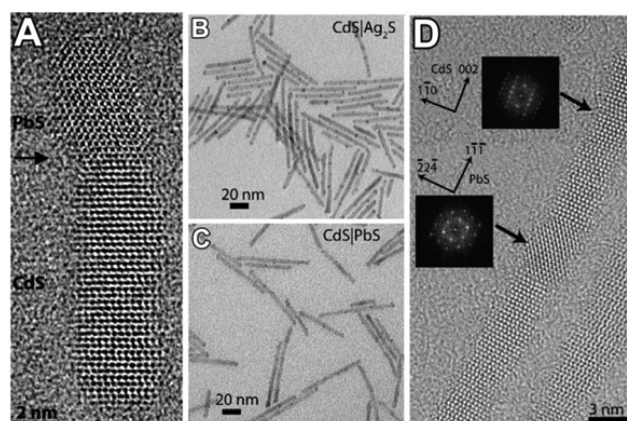e assigned to Ag_2S through EDS chemical mapping, while the darker regions are assigned to Cu_2S. (A−C) Reproduced from [Justo, Y.; Goris, B.; Kamal, J. S.; Geiregat, P.; Bals, S.; Hens, Z. Multiple Dot-in-Rod PbS/CdS Heterostructures with High Photoluminescence Quantum Yield in the Near-Infrared *J. Am. Chem. Soc.* **2012**, *134*, 5484−5487]. Copyright 2012 American Chemical Society. (D−G) Reproduced from [Tan, C.-S.; Hsiao, C.-H.; Wang, S.-C.; Liu, P.-H.; Lu, M.-Y.; Huang, M. H.; Ouyang, H.; Chen, L.-J. Sequential Cation Exchange Generated Superlattice Nanowires Forming Multiple p−n Heterojunctions *ACS Nano* **2014**, *8*, 9422−9426]. Copyright 2014 American Chemical Society.

Figure 29. NHCs with different topologies in chemical composition prepared from wz-CdS NRs. (A) HRTEM image showing epitaxy between rock salt PbS and wurtzite CdS in a segmented CdS/PbS NHC produced using Cu^+ ions in the first partial CE step. TEM images of striped CdS/Ag_2S NHCs (B) that, after exposure to Pb^{2+} ions, are transformed into CdS/PbS NHCs (C). The contrast between Pb and Cd containing regions is less obvious than the contrast between Ag and Cd. (D) HRTEM and FFT images of various segments of striped CdS/PbS NHC clearly demonstrate that PbS sections exist throughout the CdS NRs. The lower FFT image evidence a rock salt structure, while the FFT image of the upper side of the rod is compatible with a wurtzite structure. It is clear how the distribution of the CdS and PbS domains depends on the first partial CE step. Reproduced from [Luther, J. M.; Zheng, H.; Sadtler, B.; Alivisatos, a. P. Synthesis of PbS nanorods and other ionic nanocrystals of complex morphology by sequential cation exchange reactions *J. Am. Chem. Soc.* **2009**, *131*, 16851−16857]. Copyright 2009 American Chemical Society. .

from those sites, multiple unstable wz-CdSe/rs-PbSe were formed that, ultimately, caused the dismantling of the original NRs.

5.4. Engineering Heterostructures through Sequential CE

As shown in the previous sections, partial CE can lead to many different NHCs with specific morphologies. These NHCs, in turn, can be further used in CE reactions in which only one of the two components is converted. Thus, the spatial arrangement of the components of the NHC can be controlled via the first exchange reaction, while the final composition is determined by the second one. By a proper choice of starting NCs seeds and type of CE reaction, it is now possible to finely engineer complex NHCs that are difficult or currently impossible to synthesize through a classical seeded growth approach.

Luther et al., for example, adopted this strategy to prepare CdS-PbS NHCs with different topologies.[117] Partial replacement of Cu-for-Cd ions in CdS NRs was used to synthesize Cu_2S-CdS segmented NHCs in which the Cu_2S region is located at one or both ends of the NRs (see section 5.3.1.1). These structures, in a second step, were exposed to Pb^{2+} ions to yield PbS-CdS NRs in which one or both tips are made of PbS (see Figure 29A). Starting with the same parent CdS NRs, completely different NHCs can be achieved instead by using Ag^+ ions in the first partial CE step. In this case, the first partial CE leads to the formation of small Ag_2S regions distributed along the walls of the CdS NRs and, under careful conditions, to striped NHCs (see Figure 29B and section 5.3.1.2). Then the selective replacement of Ag^+ with Pb^{2+} ions leads to the corresponding PbS-CdS NHCs in which PbS is embedded in CdS (see Figure 29C,D). The same strategy has

been proven to work on wz-CdS NWs to create 1D CdS/PbS heterostructured NWs.[72]

Adel et al. synthesized CdS|CdS/ZnS NRs built in a segment like manner, that is, a CdSe core which is embedded in a CdS rod, which then epitaxially ends with ZnS tips (see Figure 30).[101] This elaborate NHC is realized by exploiting a sequential CE procedure in which first CdSe|CdS core|shell NRs are exposed to Cu^+ ions to get CdSe|CdS/$Cu_{2-x}S$ NHCs. In a second step, the $Cu_{2-x}S$ domains are converted into ZnS. A simple variation of the relative concentration of Cu^+ ions in the first CE step allows for a fine control over the position of the final boundary between CdS and ZnS domains. On the other hand, it is important to underline that a direct Zn-for-Cd CE reaction would have led to NHCs with a completely different topology, most likely to CdSe|$Cd_{1-x}Zn_xS$ core|graded-shell NRs, as suggested by other works.[176,177]

As discussed in section 3.4, Zhang et al. demonstrated that CE reactions can be exploited to prepare NHCs consisting of a metal core and a monocrystalline semiconductor shell with substantial lattice mismatches between them, which cannot be obtained by conventional epitaxial techniques.[106] Their strategy relied on exposing preformed metallic spherical NCs (such as Au, FePt and Pt) covered with an amorphous Ag_2X (X═S, Se and Te) shell to M^{2+} (M = Cd, Pb, Zn) ions in the presence of TBP. As a result, a monocrystalline shell forms around the metallic core, even if the lattice mismatch between the core and the shell materials can be as high as 40%, as in the case of Au|CdS NHCs. In conventional epitaxial techniques it is well-known that some energy is required to accommodate for an epitaxial layer of lattice-mismatched material, since a certain
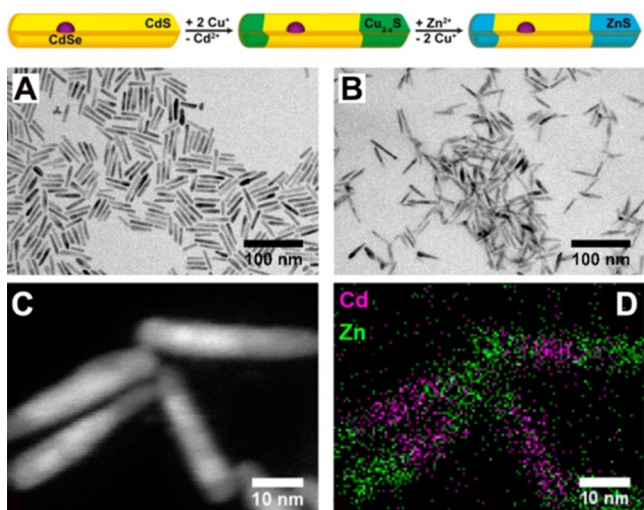
Figure 30. Schematic representation of the sequential CE reactions through which CdSe|CdS NRs are transformed first into CdSe|CdS/ Cu$_{2-x}$S and then into CdSe|CdS/ZnS segment-like NHCs. The TEM images of the original CdSe|CdS (A) and the CdSe|CdS/ZnS (B) samples show that neither the length nor the diameter of the NRs have changed significantly during the sequential ion exchange steps. (C) STEM-HAADF image of several NRs from a sample which has undergone a 50% ion exchange, along with the corresponding EDX mapping (D) showing the spatial distribution of Zn and Cd. The distinct CdS and ZnS sections can be clearly detected. Reproduced from [Adel, P.; Wolf, A.; Kodanek, T.; Dorfs, D. Segmented CdSe@ CdS/ZnS Nanorods Synthesized via a Partial Ion Exchange Sequence *Chem. Mater.* **2014**, *26*, 3121−3127]. Copyright 2014 American Chemical Society.

amount of elastic strain accumulates during its growth. This energy, which depends on both the shell thickness and the extent of lattice mismatch, can be accommodated by the shell material, without the formation of defects, only up to a certain thickness (typically referred to as "critical layer thickness"). Consequently, in conventional epitaxial synthesis the shell material can be grown up to a limited thickness, otherwise strain-induced defects can form, negatively affecting the properties of the resulting heterostructure. Surprisingly, in the procedure reported by Zhang et al. a total absence of a critical layer thickness was observed. The same authors demonstrated that this strategy, if coupled with sequential partial CE reactions, can be used to prepare even more complex NHCs with precise structural and compositional tailoring. For example, as illustrated in Figure 31, Au|(CdS+PbS) core|shell NHCs can be realized by converting the first section of the amorphous Ag$_2$S shell into monocrystalline CdS, followed by the sequential Pb-for-Ag CE that leads to the growth of PbS (see Figure 31).

6. CONCLUSIONS AND PERSPECTIVES

Research on CE reactions in NCs has gone through astonishing developments in recent years, both in understanding the mechanisms and forces involved in these types of reactions and in the complexity in the topology of composition and structure that can be achieved, as was highlighted in this review. With the progress in experimental techniques, for example in high resolution electron microscopy, X-ray photoelectron spectroscopy (using a monochromatic synchrotron beam), X-ray and neutron scattering experiments,[38,185] but also in computational tools, more in depth characterization and modeling of the
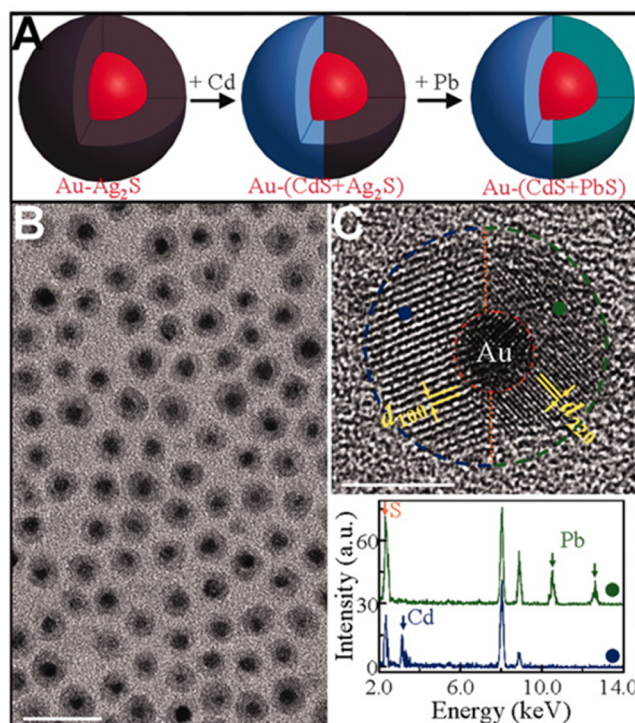
Figure 31. Growth of complex hybrid core|shell NHCs with tailored structures and compositions of the monocrystalline shells. (A−C) Control of the monocrystalline cation species within the shell: the case of Au|(CdS+PbS). (A) Sketch of the growth procedure. (B) Low-resolution TEM image. Scale bar, 20 nm. (C) (top) High-resolution TEM image. Blue and green dashed arc curves highlight the monocrystalline CdS and PbS domains, respectively. CdS and PbS manifest distinct lattice planes that can be assigned to (100) and (220), respectively. Scale bar, 5 nm. (bottom) Single-particle EDS measurements in the CdS and PbS domains. Peaks from Cd, Pb, and S elements are highlighted. Adapted with permission from ref 106. Copyright 2010 The American Association for the Advancement of Science.

process will be possible in the near future. Clearly, there are many questions that remain unanswered or poorly addressed, and they are briefly outlined below.

For example, the role of surface ligands during CE is relatively unexplored. They obviously need to attach and detach dynamically in order to allow for the inflow and outflow of cations, and in many cases there are strong indications that some of the ligands are lost during the process, as the NCs can aggregate. To what extent, for example, they promote or hinder CE? Some ligands coating in the form of polymer shell have been found to block CE altogether.[201] The degradation of the shell by an ionizing radiation such that of an electron beam or an X-ray beam can cause degradation of the ligands to a point that can block CE and even anion exchange on a film of NCs deposited on a substrate, as recently shown by us.[167,202] Then, a natural development in this direction would be the use of various libraries of photopolymerizable or photodegradable ligands able to block CE on specific regions/domains of a NC, in order to create segmented or striped heterostructures. Also, as discussed in this review, there is a wide range of ligands that need to be studied in CE reactions (for example multidentate ligands) in order to improve the solvation of exiting cations.[120,132−134] This, in turn, could not only expand the range of accessible materials, but also optimize the actual

synthetic CE conditions, allowing for a better control over the purity of resulting NCs.

Another major concern in reactions involving CE, somehow connected with the previous discussion, is that lattice defects can form upon exchange, and in addition is in not always clear whether such reactions truly reach completion, or if a fraction of the initial cations is still present in the lattice, compromising the optical/electronic properties of the final NCs. Recent works have started addressing these issues in fluorescent semiconductor NCs.[80,93] Then the logical question is to what extent CE can be truly regarded as an alternative/complementary tool to the direct synthesis of a desired nanostructure, if the exchange can be plagued by the formation of defects and the persistence of residual cations from the parent NC? Are there ways of performing CE such that these defects are eliminated? Addressing these points will require extensive research in the near future.

The capability of CE in accessing NCs in metastable phases, which cannot be prepared otherwise, has already been exploited to a certain extent. However, reports on new metastable materials are continuously reported,[203] and we believe that many unexplored materials, perhaps with novel and/or exotic properties, are yet to be synthesized, and is likely that some of them will only be accessible via CE. Another exciting research direction could be the study of "dry" solid state CE transformations in NHCs. Some systems, like $Cu_3P/CdSe$ NHCs, have been show to undergo CE if annealed under vacuum, by transforming to Cu_2Se NCs through concomitant sublimation of Cd and P.[204] Also, in principle, "sacrificial" NCs can be used as a source of cations to be exchanged with cations of desired host NCs. The possibility of triggering such CE reaction under specific external inputs, such as heat or e-beam irradiation, might represent an alternative route in those cases in which the host NCs are prone to degradation by chemical agents while being processed in solution.[196]

AUTHOR INFORMATION

Corresponding Authors
*E-mail: luca.detrizio@iit.it.
*E-mail: liberato.manna@iit.it.

Notes
The authors declare no competing financial interest.

Biographies

Liberato Manna received his Ph.D. in Chemistry in 2001 from the University of Bari (Italy) and worked at UC Berkeley (USA) as a Visiting Student and subsequently at the Lawrence Berkeley Lab (USA) as a Postdoc until 2003. He was then Scientist at the National Nanotechnology Lab in Lecce (Italy) and he moved to the Istituto Italiano di Tecnologia (IIT), Genova (Italy) in 2009 as Director of the Nanochemistry Department. Since 2010, he has also been part-time Professor at TU Delft (The Netherlands). Currently, he is also Deputy Director of IIT for the Materials and Nanotechnology programs. His research interests include the synthesis and assembly of colloidal nanocrystals, the study of structural, chemical and surface transformations in nanoscale materials, and their applications in energy, photonics, electronics, and biology.

Luca De Trizio graduated in Materials Science in 2008 from the University of Milano Bicocca and obtained his Ph.D. in Nanostructures and Nanotechnology from the same institution in 2013. During his Ph.D., in 2010-2011, he worked as collaborator at the Italian Institute of Technology in Genova with Liberato Manna and, in 2012,

at the Molecular Foundry in the Lawrence Berkeley National Laboratory with Delia Milliron. From 2013 to now, he has been working as a postdoc researcher at the Nanochemistry Department in the Italian Institute of Technology (IIT) in Genova (Italy). His research interests include the synthesis of transparent conductive oxides, luminescent semiconductors, and the study of postsynthetic chemical transformations of nanocrystals.

REFERENCES

(1) Yin, Y.; Alivisatos, A. P. Colloidal nanocrystal synthesis and the organic-inorganic interface. *Nature* **2005**, *437*, 664−670.

(2) Nurmikko, A. What future for quantum dot-based light emitters? *Nat. Nanotechnol.* **2015**, *10*, 1001−1004.

(3) Clifford, J. P.; Konstantatos, G.; Johnston, K. W.; Hoogland, S.; Levina, L.; Sargent, E. H. Fast, sensitive and spectrally tuneable colloidal-quantum-dot photodetectors. *Nat. Nanotechnol.* **2009**, *4*, 40−44.

(4) Alivisatos, A. P.; Gu, W. W.; Larabell, C. *Annual Review of Biomedical Engineering*; Annual Reviews: Palo Alto, 2005; Vol. 7.

(5) Li, Z.-B.; Cai, W.; Chen, X. Semiconductor Quantum Dots for In Vivo Imaging. *J. Nanosci. Nanotechnol.* **2007**, *7*, 2567−2581.

(6) Jain, P.; Huang, X.; El-Sayed, I.; El-Sayed, M. Review of Some Interesting Surface Plasmon Resonance-enhanced Properties of Noble Metal Nanoparticles and Their Applications to Biosystems. *Plasmonics* **2007**, *2*, 107−118.

(7) Klimov, V. I.; Mikhailovsky, A. A.; Xu, S.; Malko, A.; Hollingsworth, J. A.; Leatherdale, C. A.; Eisler, H.-J.; Bawendi, M. G. Optical Gain and Stimulated Emission in Nanocrystal Quantum Dots. *Science* **2000**, *290*, 314−317.

(8) Bruchez, M.; Moronne, M.; Gin, P.; Weiss, S.; Alivisatos, A. P. Semiconductor Nanocrystals as Fluorescent Biological Labels. *Science* **1998**, *281*, 2013−2016.

(9) Brus, L. Electronic wave functions in semiconductor clusters: experiment and theory. *J. Phys. Chem.* **1986**, *90*, 2555−2560.

(10) Talapin, D. V.; Lee, J.-S.; Kovalenko, M. V.; Shevchenko, E. V. Prospects of Colloidal Nanocrystals for Electronic and Optoelectronic Applications. *Chem. Rev.* **2010**, *110*, 389−458.

(11) Efros, A. L.; Efros, A. Interband absorption of light in semiconductor sphere. *Semiconductors* **1982**, *16*, 772−775.

(12) Hergt, R.; Dutz, S.; Müller, R.; Zeisberger, M. Magnetic particle hyperthermia: nanoparticle magnetism and materials development for cancer therapy. *J. Phys.: Condens. Matter* **2006**, *18*, S2919−S2934.

(13) Kovalenko, M. V. Opportunities and challenges for quantum dot photovoltaics. *Nat. Nanotechnol.* **2015**, *10*, 994−997.

(14) Tian, N.; Zhou, Z.-Y.; Sun, S.-G.; Ding, Y.; Wang, Z. L. Synthesis of Tetrahexahedral Platinum Nanocrystals with High-Index Facets and High Electro-Oxidation Activity. *Science* **2007**, *316*, 732−735.

(15) Pang, X.; Zhao, L.; Han, W.; Xin, X.; Lin, Z. A general and robust strategy for the synthesis of nearly monodisperse colloidal nanocrystals. *Nat. Nanotechnol.* **2013**, *8*, 426−431.

(16) Milliron, D. J.; Hughes, S. M.; Cui, Y.; Manna, L.; Li, J.; Wang, L.-W.; Paul Alivisatos, A. Colloidal nanocrystal heterostructures with linear and branched topology. *Nature* **2004**, *430*, 190−195.

(17) Oh, N.; Nam, S.; Zhai, Y.; Deshpande, K.; Trefonas, P.; Shim, M. Double-heterojunction nanorods. *Nat. Commun.* **2014**, *5*, 3642.

(18) Kovalenko, M. V.; Heiss, W.; Shevchenko, E. V.; Lee, J.-S.; Schwinghammer, H.; Alivisatos, A. P.; Talapin, D. V. SnTe Nanocrystals: A New Example of Narrow-Gap Semiconductor Quantum Dots. *J. Am. Chem. Soc.* **2007**, *129*, 11354−11355.

(19) Mauser, C.; Limmer, T.; Da Como, E.; Becker, K.; Rogach, A. L.; Feldmann, J.; Talapin, D. V. Anisotropic optical emission of single

CdSe/CdS tetrapod heterostructures: Evidence for a wavefunction symmetry breaking. *Phys. Rev. B: Condens. Matter Mater. Phys.* **2008**, 77, 153303.

(20) Müller, J.; Lupton, J. M.; Lagoudakis, P. G.; Schindler, F.; Koeppe, R.; Rogach, A. L.; Feldmann, J.; Talapin, D. V.; Weller, H. Wave Function Engineering in Elongated Semiconductor Nanocrystals with Heterogeneous Carrier Confinement. *Nano Lett.* **2005**, 5, 2044–2049.

(21) Talapin, D. V.; Koeppe, R.; Götzinger, S.; Kornowski, A.; Lupton, J. M.; Rogach, A. L.; Benson, O.; Feldmann, J.; Weller, H. Highly Emissive Colloidal CdSe/CdS Heterostructures of Mixed Dimensionality. *Nano Lett.* **2003**, 3, 1677–1681.

(22) Scotognella, F.; Miszta, K.; Dorfs, D.; Zavelani-Rossi, M.; Brescia, R.; Marras, S.; Manna, L.; Lanzani, G.; Tassone, F. Ultrafast Exciton Dynamics in Colloidal CdSe/CdS Octapod Shaped Nanocrystals. *J. Phys. Chem. C* **2011**, 115, 9005–9011.

(23) Pal, B. N.; Ghosh, Y.; Brovelli, S.; Laocharoensuk, R.; Klimov, V. I.; Hollingsworth, J. A.; Htoon, H. 'Giant' CdSe/CdS Core/Shell Nanocrystal Quantum Dots As Efficient Electroluminescent Materials: Strong Influence of Shell Thickness on Light-Emitting Diode Performance. *Nano Lett.* **2012**, 12, 331–336.

(24) Ivanov, S. A.; Nanda, J.; Piryatinski, A.; Achermann, M.; Balet, L. P.; Bezel, I. V.; Anikeeva, P. O.; Tretiak, S.; Klimov, V. I. Light Amplification Using Inverted Core/Shell Nanocrystals: Towards Lasing in the Single-Exciton Regime. *J. Phys. Chem. B* **2004**, 108, 10625–10630.

(25) Kudera, S.; Carbone, L.; Casula, M. F.; Cingolani, R.; Falqui, A.; Snoeck, E.; Parak, W. J.; Manna, L. Selective Growth of PbSe on One or Both Tips of Colloidal Semiconductor Nanorods. *Nano Lett.* **2005**, 5, 445–449.

(26) Costi, R.; Saunders, A. E.; Banin, U. Colloidal Hybrid Nanostructures: A New Type of Functional Materials. *Angew. Chem., Int. Ed.* **2010**, 49, 4878–4897.

(27) Vaneski, A.; Susha, A. S.; Rodríguez-Fernández, J.; Berr, M.; Jäckel, F.; Feldmann, J.; Rogach, A. L. Hybrid Colloidal Heterostructures of Anisotropic Semiconductor Nanocrystals Decorated with Noble Metals: Synthesis and Function. *Adv. Funct. Mater.* **2011**, 21, 1547–1556.

(28) Son, D. H.; Hughes, S. M.; Yin, Y.; Alivisatos, A. P. Cation Exchange Reactions in Ionic Nanocrystals. *Science* **2004**, 306, 1009–1012.

(29) Jeong, U.; Camargo, P. H. C.; Lee, Y. H.; Xia, Y. Chemical transformation: a powerful route to metal chalcogenide nanowires. *J. Mater. Chem.* **2006**, 16, 3893–3897.

(30) Camargo, P. H. C.; Lee, Y. H.; Jeong, U.; Zou, Z.; Xia, Y. Cation Exchange: A Simple and Versatile Route to Inorganic Colloidal Spheres with the Same Size but Different Compositions and Properties. *Langmuir* **2007**, 23, 2985–2992.

(31) Moon, G. D.; Ko, S.; Xia, Y.; Jeong, U. Chemical Transformations in Ultrathin Chalcogenide Nanowires. *ACS Nano* **2010**, 4, 2307–2319.

(32) Moon, G. D.; Ko, S.; Min, Y.; Zeng, J.; Xia, Y.; Jeong, U. Chemical transformations of nanostructured materials. *Nano Today* **2011**, 6, 186–203.

(33) Rivest, J. B.; Jain, P. K. Cation exchange on the nanoscale: an emerging technique for new material synthesis, device fabrication, and chemical sensing. *Chem. Soc. Rev.* **2013**, 42, 89–96.

(34) Fayette, M.; Robinson, R. D. Chemical transformations of nanomaterials for energy applications. *J. Mater. Chem. A* **2014**, 2, 5965–5965.

(35) Gupta, S.; Kershaw, S. V.; Rogach, A. L. 25th Anniversary Article: Ion Exchange in Colloidal Nanocrystals. *Adv. Mater.* **2013**, 25, 6923–6944.

(36) Mews, A.; Eychmüller, A.; Giersig, M.; Schooss, D.; Weller, H. Preparation, characterization, and photophysics of the quantum dot quantum well system CdS/HgS/CdS. *J. Phys. Chem.* **1994**, 98, 934–941.

(37) Zhou, H. S.; Sasahara, H.; Honma, I.; Komiyama, H.; Haus, J. W. Coated Semiconductor Nanoparticles: The CdS/PbS System's Photoluminescence Properties. *Chem. Mater.* **1994**, 6, 1534–1541.

(38) Lechner, R. T.; Fritz-Popovski, G.; Yarema, M.; Heiss, W.; Hoell, A.; Schülli, T. U.; Primetzhofer, D.; Eibelhuber, M.; Paris, O. Crystal Phase Transitions in the Shell of PbS/CdS Core/Shell Nanocrystals Influences Photoluminescence Intensity. *Chem. Mater.* **2014**, 26, 5914–5922.

(39) Zherebetskyy, D.; Zhang, Y.; Salmeron, M.; Wang, L.-W. Tolerance of Intrinsic Defects in PbS Quantum Dots. *J. Phys. Chem. Lett.* **2015**, 6, 4711–4716.

(40) Justo, Y.; Sagar, L. K.; Flamee, S.; Zhao, Q.; Vantomme, A.; Hens, Z. Less Is More. Cation Exchange and the Chemistry of the Nanocrystal Surface. *ACS Nano* **2014**, 8, 7948–7957.

(41) Casavola, M.; van Huis, M. A.; Bals, S.; Lambert, K.; Hens, Z.; Vanmaekelbergh, D. Anisotropic Cation Exchange in PbSe/CdSe Core/Shell Nanocrystals of Different Geometry. *Chem. Mater.* **2012**, 24, 294–302.

(42) Groeneveld, E.; Witteman, L.; Lefferts, M.; Ke, X.; Bals, S.; Van Tendeloo, G.; de Mello Donega, C. Tailoring ZnSe–CdSe Colloidal Quantum Dots via Cation Exchange: From Core/Shell to Alloy Nanocrystals. *ACS Nano* **2013**, 7, 7913–7930.

(43) Routzahn, A. L.; Jain, P. K. Single-Nanocrystal Reaction Trajectories Reveal Sharp Cooperative Transitions. *Nano Lett.* **2014**, 14, 987–992.

(44) Cao, H.; Qian, X.; Wang, C.; Ma, X.; Yin, J.; Zhu, Z. High Symmetric 18-Facet Polyhedron Nanocrystals of Cu_7S_4 with a Hollow Nanocage. *J. Am. Chem. Soc.* **2005**, 127, 16024–16025.

(45) Geng, J.; Liu, B.; Xu, L.; Hu, F.-N.; Zhu, J.-J. Facile Route to Zn-Based II–VI Semiconductor Spheres, Hollow Spheres, and Core/Shell Nanocrystals and Their Optical Properties. *Langmuir* **2007**, 23, 10286–10293.

(46) Saruyama, M.; So, Y.-G.; Kimoto, K.; Taguchi, S.; Kanemitsu, Y.; Teranishi, T. Spontaneous Formation of Wurzite-CdS/Zinc Blende-CdTe Heterodimers through a Partial Anion Exchange Reaction. *J. Am. Chem. Soc.* **2011**, 133, 17598–17601.

(47) Park, J.; Zheng, H.; Jun, Y.-w.; Alivisatos, A. P. Hetero-Epitaxial Anion Exchange Yields Single-Crystalline Hollow Nanoparticles. *J. Am. Chem. Soc.* **2009**, 131, 13943–13945.

(48) Zhang, F.; Shi, Y.; Sun, X.; Zhao, D.; Stucky, G. D. Formation of Hollow Upconversion Rare-Earth Fluoride Nanospheres: Nanoscale Kirkendall Effect During Ion Exchange. *Chem. Mater.* **2009**, 21, 5237–5243.

(49) Dloczik, L.; Könenkamp, R. Nanostructure Transfer in Semiconductors by Ion Exchange. *Nano Lett.* **2003**, 3, 651–653.

(50) Dawood, F.; Schaak, R. E. ZnO-Templated Synthesis of Wurtzite-Type ZnS and ZnSe Nanoparticles. *J. Am. Chem. Soc.* **2009**, 131, 424–425.

(51) Wang, X.; Zhan, S.; Wang, Y.; Wang, P.; Yu, H.; Yu, J.; Hu, C. Facile synthesis and enhanced visible-light photocatalytic activity of Ag_2S nanocrystal-sensitized $Ag_8W_4O_{16}$ nanorods. *J. Colloid Interface Sci.* **2014**, 422, 30–37.

(52) Zhang, Q.; Gao, L. Synthesis of Nanocrystalline Aluminum Nitride by Nitridation of δ-Al_2O_3 Nanoparticles in Flowing Ammonia. *J. Am. Ceram. Soc.* **2006**, 89, 415–421.

(53) Mizusaki, J.; Arai, K.; Fueki, K. Ionic conduction of the perovskite-type halides. *Solid State Ionics* **1983**, 11, 203–211.

(54) Tress, W.; Marinova, N.; Moehl, T.; Zakeeruddin, S. M.; Nazeeruddin, M. K.; Gratzel, M. Understanding the rate-dependent J-V hysteresis, slow time component, and aging in $CH_3NH_3PbI_3$ perovskite solar cells: the role of a compensated electric field. *Energy Environ. Sci.* **2015**, 8, 995–1004.

(55) Stranks, S. D.; Snaith, H. J. Metal-halide perovskites for photovoltaic and light-emitting devices. *Nat. Nanotechnol.* **2015**, 10, 391–402.

(56) Akkerman, Q. A.; D'Innocenzo, V.; Accornero, S.; Scarpellini, A.; Petrozza, A.; Prato, M.; Manna, L. Tuning the Optical Properties of Cesium Lead Halide Perovskite Nanocrystals by Anion Exchange Reactions. *J. Am. Chem. Soc.* **2015**, 137, 10276–10281.

(57) Nedelcu, G.; Protesescu, L.; Yakunin, S.; Bodnarchuk, M. I.; Grotevent, M. J.; Kovalenko, M. V. Fast Anion-Exchange in Highly Luminescent Nanocrystals of Cesium Lead Halide Perovskites (CsPbX$_3$, X = Cl, Br, I). *Nano Lett.* **2015**, *15*, 5635−5640.

(58) Pellet, N.; Teuscher, J.; Maier, J.; Grätzel, M. Transforming Hybrid Organic Inorganic Perovskites by Rapid Halide Exchange. *Chem. Mater.* **2015**, *27*, 2181−2188.

(59) Solis-Ibarra, D.; Smith, I. C.; Karunadasa, H. I. Post-synthetic halide conversion and selective halogen capture in hybrid perovskites. *Chem. Sci.* **2015**, *6*, 4054−4059.

(60) Luo, Y. R. *Comprehensive Handbook of Chemical Bond Energies*; CRC Press: Boca Raton, FL, 2007.

(61) Lide, D. R. *CRC Handbook of Chemistry and Physics, 84th ed.*; Taylor & Francis: London, 2003.

(62) Mu, L.; Feng, C.; He, H. Topological research on lattice energies for inorganic compounds. *MATCH Commun. Math. Comput. Chem.* **2006**, *56*, 97−111.

(63) Sheng, Y.; Wei, J.; Liu, B.; Peng, L. A facile route to synthesize CdZnSe core−shell-like alloyed quantum dots via cation exchange reaction in aqueous system. *Mater. Res. Bull.* **2014**, *57*, 67−71.

(64) Xinhua, Z.; Yaoyu, F.; Yuliang, Z.; Zhenyu, G.; Lei, Z. A facile route to violet- to orange-emitting Cd$_x$Zn$_{1−x}$Se alloy nanocrystals via cation exchange reaction. *Nanotechnology* **2007**, *18*, 385606.

(65) Miszta, K.; Gariano, G.; Brescia, R.; Marras, S.; De Donato, F.; Ghosh, S.; De Trizio, L.; Manna, L. Selective Cation Exchange in the Core Region of Cu$_{2-x}$Se/Cu$_{2-x}$S Core/Shell Nanocrystals. *J. Am. Chem. Soc.* **2015**, *137*, 12195−12198.

(66) Wark, S. E.; Hsia, C.-H.; Son, D. H. Effects of Ion Solvation and Volume Change of Reaction on the Equilibrium and Morphology in Cation-Exchange Reaction of Nanocrystals. *J. Am. Chem. Soc.* **2008**, *130*, 9550−9555.

(67) Parr, R. G.; Pearson, R. G. Absolute hardness: companion parameter to absolute electronegativity. *J. Am. Chem. Soc.* **1983**, *105*, 7512−7516.

(68) Pearson, R. G. Absolute electronegativity and hardness: application to inorganic chemistry. *Inorg. Chem.* **1988**, *27*, 734−740.

(69) Lange, N. A.; Dean, J. A. *Lange's Handbook of chemistry*; McGraw-Hill: New York, 1979.

(70) Sadtler, B.; Demchenko, D. O.; Zheng, H.; Hughes, S. M.; Merkle, M. G.; Dahmen, U.; Wang, L.-W.; Alivisatos, A. P. Selective facet reactivity during cation exchange in cadmium sulfide nanorods. *J. Am. Chem. Soc.* **2009**, *131*, 5285−5293.

(71) Robinson, R. D.; Sadtler, B.; Demchenko, D. O.; Erdonmez, C. K.; Wang, L.-W.; Alivisatos, A. P. Spontaneous superlattice formation in nanorods through partial cation exchange. *Science* **2007**, *317*, 355−358.

(72) Mukherjee, B.; Peterson, A.; Subramanian, V. 1D CdS/PbS heterostructured nanowire synthesis using cation exchange. *Chem. Commun.* **2012**, *48*, 2415−2417.

(73) Miszta, K.; Dorfs, D.; Genovese, A.; Kim, M. R.; Manna, L. Cation exchange reactions in colloidal branched nanocrystals. *ACS Nano* **2011**, *5*, 7176−7183.

(74) Wong, A. B.; Brittman, S.; Yu, Y.; Dasgupta, N. P.; Yang, P. Core−Shell CdS−Cu$_2$S Nanorod Array Solar Cells. *Nano Lett.* **2015**, *15*, 4096−4101.

(75) Yao, Q.; Arachchige, I. U.; Brock, S. L. Expanding the Repertoire of Chalcogenide Nanocrystal Networks: Ag$_2$Se Gels and Aerogels by Cation Exchange Reactions. *J. Am. Chem. Soc.* **2009**, *131*, 2800−2801.

(76) Li, J.; Zhang, T.; Ge, J.; Yin, Y.; Zhong, W. Fluorescence Signal Amplification by Cation Exchange in Ionic Nanocrystals. *Angew. Chem., Int. Ed.* **2009**, *48*, 1588−1591.

(77) Lubeck, C. R.; Han, T. Y. J.; Gash, A. E.; Satcher, J. H.; Doyle, F. M. Synthesis of Mesostructured Copper Sulfide by Cation Exchange and Liquid-Crystal Templating. *Adv. Mater.* **2006**, *18*, 781−784.

(78) Dorn, A.; Allen, P. M.; Harris, D. K.; Bawendi, M. G. In Situ Electrical Monitoring of Cation Exchange in Nanowires. *Nano Lett.* **2010**, *10*, 3948−3951.

(79) Jain, P. K.; Amirav, L.; Aloni, S.; Alivisatos, A. P. Nanoheterostructure Cation Exchange: Anionic Framework Conservation. *J. Am. Chem. Soc.* **2010**, *132*, 9997−9999.

(80) Jain, P. K.; Beberwyck, B. J.; Fong, L.-K.; Polking, M. J.; Alivisatos, A. P. Highly Luminescent Nanocrystals From Removal of Impurity Atoms Residual From Ion-Exchange Synthesis. *Angew. Chem., Int. Ed.* **2012**, *51*, 2387−2390.

(81) Rivest, J. B.; Buonsanti, R.; Pick, T. E.; Zhu, L.; Lim, E.; Clavero, C.; Schaible, E.; Helms, B. A.; Milliron, D. J. Evolution of Ordered Metal Chalcogenide Architectures through Chemical Transformations. *J. Am. Chem. Soc.* **2013**, *135*, 7446−7449.

(82) Yao, J.; Han, X.; Zeng, S.; Zhong, W. Detection of Femtomolar Proteins by Nonfluorescent ZnS Nanocrystal Clusters. *Anal. Chem.* **2012**, *84*, 1645−1652.

(83) Yang, X.; Xue, H.; Xu, J.; Huang, X.; Zhang, J.; Tang, Y. B.; Ng, T. W.; Kwong, H. L.; Meng, X. M.; Lee, C. S. Synthesis of porous ZnS:Ag$_2$S nanosheets by ion exchange for photocatalytic H$_2$ generation. *ACS Appl. Mater. Interfaces* **2014**, *6*, 9078−9084.

(84) Qu, H.; Cao, L.; Su, G.; Liu, W.; Gao, R.; Xia, C.; Qin, J. Silica-coated ZnS quantum dots as fluorescent probes for the sensitive detection of Pb^{2+} ions. *J. Nanopart. Res.* **2014**, *16*, 1−12.

(85) Shi, Y.; Chen, J.; Shen, P. ZnS micro-spheres and flowers: Chemically controlled synthesis and template use in fabricating MS(shell)/ZnS(core) and MS (M = Pb, Cu) hollow microspheres. *J. Alloys Compd.* **2007**, *441*, 337−343.

(86) Qu, Z.; Yan, L.; Li, L.; Xu, J.; Liu, M.; Li, Z.; Yan, N. Ultraeffective ZnS Nanocrystals Sorbent for Mercury(II) Removal Based on Size-Dependent Cation Exchange. *ACS Appl. Mater. Interfaces* **2014**, *6*, 18026−18032.

(87) Pang, M.; Hu, J.; Zeng, H. C. Synthesis, Morphological Control, and Antibacterial Properties of Hollow/Solid Ag$_2$S/Ag Heterodimers. *J. Am. Chem. Soc.* **2010**, *132*, 10771−10785.

(88) Justo, Y.; Goris, B.; Kamal, J. S.; Geiregat, P.; Bals, S.; Hens, Z. Multiple Dot-in-Rod PbS/CdS Heterostructures with High Photoluminescence Quantum Yield in the Near-Infrared. *J. Am. Chem. Soc.* **2012**, *134*, 5484−5487.

(89) Haibao, S.; Chunlei, W.; Shuhong, X.; Yuan, J.; Yujie, S.; Fan, B.; Zhuyuan, W.; Yiping, C. Hydrazine-promoted sequential cation exchange: a novel synthesis method for doped ternary semiconductor nanocrystals with tunable emission. *Nanotechnology* **2014**, *25*, 025603.

(90) Prudnikau, A.; Artemyev, M.; Molinari, M.; Troyon, M.; Sukhanova, A.; Nabiev, I.; Baranov, A. V.; Cherevkov, S. a.; Fedorov, A. V. Chemical substitution of Cd ions by Hg in CdSe nanorods and nanodots: Spectroscopic and structural examination. *Mater. Sci. Eng., B* **2012**, *177*, 744−749.

(91) Yuho, M.; Geon Dae, M.; Jaeyoon, P.; Minwoo, P.; Unyong, J. Surfactant-free CuInSe$_2$ nanocrystals transformed from In$_2$Se$_3$ nanoparticles and their application for a flexible UV photodetector. *Nanotechnology* **2011**, *22*, 465604.

(92) Li, H.; Zanella, M.; Genovese, A.; Povia, M.; Falqui, A.; Giannini, C.; Manna, L. Sequential Cation Exchange in Nanocrystals: Preservation of Crystal Phase and Formation of Metastable Phases. *Nano Lett.* **2011**, *11*, 4964−4970.

(93) Li, H.; Brescia, R.; Krahne, R.; Bertoni, G.; Alcocer, M. J. P.; D'Andrea, C.; Scotognella, F.; Tassone, F.; Zanella, M.; De Giorgi, M.; et al. Blue-UV-Emitting ZnSe(Dot)/ZnS(Rod) Core/Shell Nanocrystals Prepared from CdSe/CdS Nanocrystals by Sequential Cation Exchange. *ACS Nano* **2012**, *6*, 1637−1647.

(94) Gupta, S.; Zhovtiuk, O.; Vaneski, A.; Lin, Y.-C.; Chou, W.-C.; Kershaw, S. V.; Rogach, A. L. Cd$_x$Hg$_{(1−x)}$Te Alloy Colloidal Quantum Dots: Tuning Optical Properties from the Visible to Near-Infrared by Ion Exchange. *Part. Part. Syst. Charact.* **2013**, *30*, 346−354.

(95) Cao, Y.; Zhang, A.; Ma, Q.; Liu, N.; Yang, P. Application of hybrid SiO$_2$-coated CdTe nanocrystals for sensitive sensing of Cu^{2+} and Ag$^+$ ions. *Luminescence* **2013**, *28*, 287−293.

(96) Smith, A. M.; Nie, S. Bright and Compact Alloyed Quantum Dots with Broadly Tunable Near-Infrared Absorption and Fluorescence Spectra through Mercury Cation Exchange. *J. Am. Chem. Soc.* **2011**, *133*, 24−26.

(97) Kriegel, I.; Rodríguez-Fernández, J.; Wisnet, A.; Zhang, H.; Waurisch, C.; Eychmüller, A.; Dubavik, A.; Govorov, A. O.; Feldmann, J. Shedding Light on Vacancy-Doped Copper Chalcogenides: Shape-Controlled Synthesis, Optical Properties, and Modeling of Copper Telluride Nanocrystals with Near-Infrared Plasmon Resonances. *ACS Nano* **2013**, 7, 4367−4377.

(98) Jeong, U.; Kim, J.-U.; Xia, Y.; Li, Z.-Y. Monodispersed Spherical Colloids of Se@CdSe: Synthesis and Use as Building Blocks in Fabricating Photonic Crystals. *Nano Lett.* **2005**, 5, 937−942.

(99) Jeong, U.; Xia, Y.; Yin, Y. Large-scale synthesis of single-crystal CdSe nanowires through a cation-exchange route. *Chem. Phys. Lett.* **2005**, 416, 246−250.

(100) Acharya, S.; Pradhan, N. Insertion/Ejection of Dopant Ions in Composition Tunable Semiconductor Nanocrystals. *J. Phys. Chem. C* **2011**, 115, 19513−19519.

(101) Adel, P.; Wolf, A.; Kodanek, T.; Dorfs, D. Segmented CdSe@CdS/ZnS Nanorods Synthesized via a Partial Ion Exchange Sequence. *Chem. Mater.* **2014**, 26, 3121−3127.

(102) Akkerman, Q. A.; Genovese, A.; George, C.; Prato, M.; Moreels, I.; Casu, A.; Marras, S.; Curcio, A.; Scarpellini, A.; Pellegrino, T.; et al. From Binary Cu_2S to Ternary Cu−In−S and Quaternary Cu−In−Zn−S Nanocrystals with Tunable Composition via Partial Cation Exchange. *ACS Nano* **2015**, 9, 521−531.

(103) van der Stam, W.; Berends, A. C.; Rabouw, F. T.; Willhammar, T.; Ke, X.; Meeldijk, J. D.; Bals, S.; de Mello Donega, C. Luminescent $CuInS_2$ Quantum Dots by Partial Cation Exchange in $Cu_{2−x}S$ Nanocrystals. *Chem. Mater.* **2015**, 27, 621−628.

(104) De Trizio, L.; Gaspari, R.; Bertoni, G.; Kriegel, I.; Moretti, L.; Scotognella, F.; Maserati, L.; Zhang, Y.; Messina, G. C.; Prato, M.; et al. $Cu_{3−x}P$ Nanocrystals as a Material Platform for Near-Infrared Plasmonics and Cation Exchange Reactions. *Chem. Mater.* **2015**, 27, 1120−1128.

(105) Dilena, E.; Dorfs, D.; George, C.; Miszta, K.; Povia, M.; Genovese, A.; Casu, A.; Prato, M.; Manna, L. Colloidal $Cu_{2−x}(S_ySe_{1−y})$ alloy nanocrystals with controllable crystal phase: synthesis, plasmonic properties, cation exchange and electrochemical lithiation. *J. Mater. Chem.* **2012**, 22, 13023−13031.

(106) Zhang, J.; Tang, Y.; Lee, K.; Ouyang, M. Nonepitaxial Growth of Hybrid Core-Shell Nanostructures with Large Lattice Mismatches. *Science* **2010**, 327, 1634−1638.

(107) Ha, D.-H.; Caldwell, A. H.; Ward, M. J.; Honrao, S.; Mathew, K.; Hovden, R.; Koker, M. K. A.; Muller, D. A.; Hennig, R. G.; Robinson, R. D. Solid−Solid Phase Transformations Induced through Cation Exchange and Strain in 2D Heterostructured Copper Sulfide Nanocrystals. *Nano Lett.* **2014**, 14, 7090−7099.

(108) Lesnyak, V.; George, C.; Genovese, A.; Prato, M.; Casu, A.; Ayyappan, S.; Scarpellini, A.; Manna, L. Alloyed Copper Chalcogenide Nanoplatelets via Partial Cation Exchange Reactions. *ACS Nano* **2014**, 8, 8407−8418.

(109) Li, H.; Brescia, R.; Povia, M.; Prato, M.; Bertoni, G.; Manna, L.; Moreels, I. Synthesis of Uniform Disk-Shaped Copper Telluride Nanocrystals and Cation Exchange to Cadmium Telluride Quantum Disks with Stable Red Emission. *J. Am. Chem. Soc.* **2013**, 135, 12270−12278.

(110) Mu, L.; Wang, F.; Sadtler, B.; Loomis, R. A.; Buhro, W. E. Influence of the Nanoscale Kirkendall Effect on the Morphology of Copper Indium Disulfide Nanoplatelets Synthesized by Ion Exchange. *ACS Nano* **2015**, 9, 7419−7428.

(111) Nguyen, A. T.; Lin, W.-H.; Lu, Y.-H.; Chiou, Y.-D.; Hsu, Y.-J. First demonstration of rainbow photocatalysts using ternary $Cd_{1−x}Zn_xSe$ nanorods of varying compositions. *Appl. Catal., A* **2014**, 476, 140−147.

(112) Lambright, S.; Butaeva, E.; Razgoniaeva, N.; Hopkins, T.; Smith, B.; Perera, D.; Corbin, J.; Khon, E.; Thomas, R.; Moroz, P.; et al. Enhanced Lifetime of Excitons in Nonepitaxial Au/CdS Core/Shell Nanocrystals. *ACS Nano* **2014**, 8, 352−361.

(113) De Trizio, L.; Prato, M.; Genovese, A.; Casu, A.; Povia, M.; Simonutti, R.; Alcocer, M. J. P.; D'Andrea, C.; Tassone, F.; Manna, L. Strongly Fluorescent Quaternary Cu−In−Zn−S Nanocrystals Pre-

pared from $Cu_{1−x}InS_2$ Nanocrystals by Partial Cation Exchange. *Chem. Mater.* **2012**, 24, 2400−2406.

(114) Gui, J.; Ji, M.; Liu, J.; Xu, M.; Zhang, J.; Zhu, H. Phosphine-Initiated Cation Exchange for Precisely Tailoring Composition and Properties of Semiconductor Nanostructures: Old Concept, New Applications. *Angew. Chem., Int. Ed.* **2015**, 54, 3683−3687.

(115) Sahu, A.; Kang, M. S.; Kompch, A.; Notthoff, C.; Wills, A. W.; Deng, D.; Winterer, M.; Frisbie, C. D.; Norris, D. J. Electronic Impurity Doping in CdSe Nanocrystals. *Nano Lett.* **2012**, 12, 2587−2594.

(116) Kovalenko, M. V.; Schaller, R. D.; Jarzab, D.; Loi, M. A.; Talapin, D. V. Inorganically Functionalized PbS−CdS Colloidal Nanocrystals: Integration into Amorphous Chalcogenide Glass and Luminescent Properties. *J. Am. Chem. Soc.* **2012**, 134, 2457−2460.

(117) Luther, J. M.; Zheng, H.; Sadtler, B.; Alivisatos, a. P. Synthesis of PbS nanorods and other ionic nanocrystals of complex morphology by sequential cation exchange reactions. *J. Am. Chem. Soc.* **2009**, 131, 16851−16857.

(118) Zhang, J.; Chernomordik, B. D.; Crisp, R. W.; Kroupa, D. M.; Luther, J. M.; Miller, E. M.; Gao, J.; Beard, M. C. Preparation of Cd/Pb Chalcogenide Heterostructured Janus Particles via Controllable Cation Exchange. *ACS Nano* **2015**, 9, 7151−7163.

(119) Tolman, C. A. Steric effects of phosphorus ligands in organometallic chemistry and homogeneous catalysis. *Chem. Rev.* **1977**, 77, 313−348.

(120) Crabtree, R. H. *The Organometallic Chemistry of the Transition Metals*; Wiley: New York, 2014.

(121) Lee, D.; Kim, W. D.; Lee, S.; Bae, W. K.; Lee, S.; Lee, D. C. Direct Cd-to-Pb Exchange of CdSe Nanorods into PbSe/CdSe Axial Heterojunction Nanorods. *Chem. Mater.* **2015**, 27, 5295−5304.

(122) Pietryga, J. M.; Werder, D. J.; Williams, D. J.; Casson, J. L.; Schaller, R. D.; Klimov, V. I.; Hollingsworth, J. a. Utilizing the lability of lead selenide to produce heterostructured nanocrystals with bright, stable infrared emission. *J. Am. Chem. Soc.* **2008**, 130, 4879−4885.

(123) De Geyter, B.; Justo, Y.; Moreels, I.; Lambert, K.; Smet, P. F.; Van Thourhout, D.; Houtepen, A. J.; Grodzinska, D.; de Mello Donega, C.; Meijerink, A.; et al. The Different Nature of Band Edge Absorption and Emission in Colloidal PbSe/CdSe Core/Shell Quantum Dots. *ACS Nano* **2011**, 5, 58−66.

(124) Grodzińska, D.; Evers, W. H.; Dorland, R.; van Rijssel, J.; van Huis, M. A.; Meijerink, A.; de Mello Donegá, C.; Vanmaekelbergh, D. Two-Fold Emission From the S-Shell of PbSe/CdSe Core/Shell Quantum Dots. *Small* **2011**, 7, 3493−3501.

(125) Grodzinska, D.; Pietra, F.; van Huis, M. A.; Vanmaekelbergh, D.; de Mello Donega, C. Thermally induced atomic reconstruction of PbSe/CdSe core/shell quantum dots into PbSe/CdSe bi-hemisphere hetero-nanocrystals. *J. Mater. Chem.* **2011**, 21, 11556−11565.

(126) Lin, Q.; Makarov, N. S.; Koh, W.-k.; Velizhanin, K. A.; Cirloganu, C. M.; Luo, H.; Klimov, V. I.; Pietryga, J. M. Design and Synthesis of Heterostructured Quantum Dots with Dual Emission in the Visible and Infrared. *ACS Nano* **2015**, 9, 539−547.

(127) Lambert, K.; Geyter, B. D.; Moreels, I.; Hens, Z. PbTe|CdTe Core|Shell Particles by Cation Exchange, a HR-TEM study. *Chem. Mater.* **2009**, 21, 778−780.

(128) Eilers, J.; Groeneveld, E.; de Mello Donegá, C.; Meijerink, A. Optical Properties of Mn-Doped ZnTe Magic Size Nanocrystals. *J. Phys. Chem. Lett.* **2012**, 3, 1663−1667.

(129) Groeneveld, E.; van Berkum, S.; van Schooneveld, M. M.; Gloter, A.; Meeldijk, J. D.; van den Heuvel, D. J.; Gerritsen, H. C.; de Mello Donega, C. Highly Luminescent (Zn,Cd)Te/CdSe Colloidal Heteronanowires with Tunable Electron−Hole Overlap. *Nano Lett.* **2012**, 12, 749−757.

(130) Kim, S.; Marshall, A. R.; Kroupa, D. M.; Miller, E. M.; Luther, J. M.; Jeong, S.; Beard, M. C. Air-Stable and Efficient PbSe Quantum-Dot Solar Cells Based upon ZnSe to PbSe Cation-Exchanged Quantum Dots. *ACS Nano* **2015**, 9, 8157−8164.

(131) Jeong, S.; Han, J. H.; Jang, J.-t.; Seo, J.-w.; Kim, J.-G.; Cheon, J. Transformative Two-Dimensional Layered Nanocrystals. *J. Am. Chem. Soc.* **2011**, 133, 14500−14503.

(132) Narayanan, B.; Bhadbhade, M. M. X-Ray Structure Of Thermochromic Bis(N,N-Diethylethylenediamine)-Copper(II)-Tetrafluoroborate. *J. Coord. Chem.* **1998**, *46*, 115−123.

(133) Fabbrizzi, L.; Micheloni, M.; Paoletti, P. Continuous and discontinuous thermochromism of copper(II) and nickel(II) complexes with N,N-diethylethylenediamine. *Inorg. Chem.* **1974**, *13*, 3019−3021.

(134) Grenthe, I.; Paoletti, P.; Sandstroem, M.; Glikberg, S. Thermochromism in copper(II) complexes. Structures of the red and blue-violet forms of bis(N,N-diethylethylenediamine)copper(II) perchlorate and the nonthermochromic violet bis(N-ethylethylenediamine)copper(II) perchlorate. *Inorg. Chem.* **1979**, *18*, 2687−2692.

(135) Thayer, J. *Organometallic Compounds and Living Organisms*; Elsevier Science: Amsterdam, 2012.

(136) Sines, I. T.; Schaak, R. E. Phase-Selective Chemical Extraction of Selenium and Sulfur from Nanoscale Metal Chalcogenides: A General Strategy for Synthesis, Purification, and Phase Targeting. *J. Am. Chem. Soc.* **2011**, *133*, 1294−1297.

(137) Lesnyak, V.; Brescia, R.; Messina, G. C.; Manna, L. Cu Vacancies Boost Cation Exchange Reactions in Copper Selenide Nanocrystals. *J. Am. Chem. Soc.* **2015**, *137*, 9315−9323.

(138) Ethayaraja, M.; Bandyopadhyaya, R. Model for Core−Shell Nanoparticle Formation by Ion-Exchange Mechanism. *Ind. Eng. Chem. Res.* **2008**, *47*, 5982−5985.

(139) Mehrer, H. *Diffusion in Solids: Fundamentals, Methods, Materials, Diffusion-Controlled Processes*; Springer: Berlin, 2007.

(140) Yalcin, A. O.; Fan, Z.; Goris, B.; Li, W.-F.; Koster, R. S.; Fang, C.-M.; van Blaaderen, A.; Casavola, M.; Tichelaar, F. D.; Bals, S.; et al. Atomic Resolution Monitoring of Cation Exchange in CdSe-PbSe Heteronanocrystals during Epitaxial Solid−Solid−Vapor Growth. *Nano Lett.* **2014**, *14*, 3661−3667.

(141) Bals, S.; Casavola, M.; van Huis, M. A.; Van Aert, S.; Batenburg, K. J.; Van Tendeloo, G.; Vanmaekelbergh, D. Three-Dimensional Atomic Imaging of Colloidal Core−Shell Nanocrystals. *Nano Lett.* **2011**, *11*, 3420−3424.

(142) Dorfs, D.; Härtling, T.; Miszta, K.; Bigall, N. C.; Kim, M. R.; Genovese, A.; Falqui, A.; Povia, M.; Manna, L. Reversible Tunability of the Near-Infrared Valence Band Plasmon Resonance in Cu$_{2−x}$Se Nanocrystals. *J. Am. Chem. Soc.* **2011**, *133*, 11175−11180.

(143) Luther, J. M.; Jain, P. K.; Ewers, T.; Alivisatos, A. P. Localized surface plasmon resonances arising from free carriers in doped quantum dots. *Nat. Mater.* **2011**, *10*, 361−366.

(144) Beberwyck, B. J.; Alivisatos, A. P. Ion Exchange Synthesis of III−V Nanocrystals. *J. Am. Chem. Soc.* **2012**, *134*, 19977−19980.

(145) Bothe, C.; Kornowski, A.; Tornatzky, H.; Schmidtke, C.; Lange, H.; Maultzsch, J.; Weller, H. Solid-State Chemistry on the Nanoscale: Ion Transport through Interstitial Sites or Vacancies? *Angew. Chem., Int. Ed.* **2015**, *54*, 14183−14186.

(146) White, S. L.; Smith, J. G.; Behl, M.; Jain, P. K. Co-operativity in a nanocrystalline solid-state transition. *Nat. Commun.* **2013**, *4*, 2933.

(147) Routzahn, A. L.; Jain, P. K. Luminescence Blinking of a Reacting Quantum Dot. *Nano Lett.* **2015**, *15*, 2504−2509.

(148) Ott, F. D.; Spiegel, L. L.; Norris, D. J.; Erwin, S. C. Microscopic Theory of Cation Exchange in CdSe Nanocrystals. *Phys. Rev. Lett.* **2014**, *113*, 156803.

(149) De Trizio, L.; Li, H.; Casu, A.; Genovese, A.; Sathya, A.; Messina, G. C.; Manna, L. Sn Cation Valency Dependence in Cation Exchange Reactions Involving Cu$_{2−x}$Se Nanocrystals. *J. Am. Chem. Soc.* **2014**, *136*, 16277−16284.

(150) Gupta, S.; Kershaw, S. V.; Susha, A. S.; Wong, T. L.; Higashimine, K.; Maenosono, S.; Rogach, A. L. Near-Infrared-Emitting Cd$_x$Hg$_{1−x}$Se Nanorods Fabricated by Ion Exchange in an Aqueous Medium. *ChemPhysChem* **2013**, *14*, 2853−2858.

(151) Xie, Y.; Bertoni, G.; Riedinger, A.; Sathya, A.; Prato, M.; Marras, S.; Tu, R.; Pellegrino, T.; Manna, L. Nanoscale Transformations in Covellite (CuS) Nanocrystals in the Presence of Divalent Metal Cations in a Mild Reducing Environment. *Chem. Mater.* **2015**, *27*, 7531−7537.

(152) Batsanov, S. S.; Batsanov, A. S. *Introduction to Structural Chemistry*; Springer: The Netherlands, 2012.

(153) Ning, J.; Xiao, G.; Wang, L.; Zou, B.; Liu, B.; Zou, G. Facile synthesis of magnetic metal (Mn, Fe, Co, and Ni) oxides nanocrystals via a cation-exchange reaction. *Nanoscale* **2011**, *3*, 741−745.

(154) Wang, Y.; Zhukovskyi, M.; Tongying, P.; Tian, Y.; Kuno, M. Synthesis of Ultrathin and Thickness-Controlled Cu$_{2−x}$Se Nanosheets via Cation Exchange. *J. Phys. Chem. Lett.* **2014**, *5*, 3608−3613.

(155) Li, X.; Chen, K.; Huang, L.; Lu, D.; Liang, J.; Han, H. Sensitive immunoassay for porcine pseudorabies antibody based on fluorescence signal amplification induced by cation exchange in CdSe nanocrystals. *Microchim. Acta* **2013**, *180*, 303−310.

(156) Zhang, J.; Gao, J.; Church, C. P.; Miller, E. M.; Luther, J. M.; Klimov, V. I.; Beard, M. C. PbSe Quantum Dot Solar Cells with More than 6% Efficiency Fabricated in Ambient Atmosphere. *Nano Lett.* **2014**, *14*, 6010−6015.

(157) Li, W.; Zamani, R.; Ibáñez, M.; Cadavid, D.; Shavel, A.; Morante, J. R.; Arbiol, J.; Cabot, A. Metal Ions To Control the Morphology of Semiconductor Nanoparticles: Copper Selenide Nanocubes. *J. Am. Chem. Soc.* **2013**, *135*, 4664−4667.

(158) Kovalenko, M. V.; Talapin, D. V.; Loi, M. A.; Cordella, F.; Hesser, G.; Bodnarchuk, M. I.; Heiss, W. Quasi-Seeded Growth of Ligand-Tailored PbSe Nanocrystals through Cation-Exchange-Mediated Nucleation. *Angew. Chem., Int. Ed.* **2008**, *47*, 3029−3033.

(159) Shao, H.; Wang, C.; Xu, S.; Wang, Z.; Yin, H.; Cui, Y. Fast Doping of Cu into ZnSe NCs by Hydrazine Promoted Cation Exchange in Aqueous Solution at Room Temperature. *J. Fluoresc.* **2015**, *25*, 305−310.

(160) Bouet, C.; Laufer, D.; Mahler, B.; Nadal, B.; Heuclin, H.; Pedetti, S.; Patriarche, G.; Dubertret, B. Synthesis of Zinc and Lead Chalcogenide Core and Core/Shell Nanoplatelets Using Sequential Cation Exchange Reactions. *Chem. Mater.* **2014**, *26*, 3002−3008.

(161) Zhang, D.; Wong, A. B.; Yu, Y.; Brittman, S.; Sun, J.; Fu, A.; Beberwyck, B.; Alivisatos, A. P.; Yang, P. Phase-Selective Cation-Exchange Chemistry in Sulfide Nanowire Systems. *J. Am. Chem. Soc.* **2014**, *136*, 17430−17433.

(162) Tan, C.-S.; Hsiao, C.-H.; Wang, S.-C.; Liu, P.-H.; Lu, M.-Y.; Huang, M. H.; Ouyang, H.; Chen, L.-J. Sequential Cation Exchange Generated Superlattice Nanowires Forming Multiple p−n Heterojunctions. *ACS Nano* **2014**, *8*, 9422−9426.

(163) Manzi, A.; Simon, T.; Sonnleitner, C.; Döblinger, M.; Wyrwich, R.; Stern, O.; Stolarczyk, J. K.; Feldmann, J. Light-induced cation exchange for copper sulfide based CO$_2$ reduction. *J. Am. Chem. Soc.* **2015**, *137*, 14007−14010.

(164) Jang, S. Y.; Song, Y. M.; Kim, H. S.; Cho, Y. J.; Seo, Y. S.; Jung, G. B.; Lee, C.-W.; Park, J.; Jung, M.; Kim, J.; et al. Three Synthetic Routes to Single-Crystalline PbS Nanowires with Controlled Growth Direction and Their Electrical Transport Properties. *ACS Nano* **2010**, *4*, 2391−2401.

(165) Wang, X.; Liu, X.; Zhu, D.; Swihart, M. T. Controllable conversion of plasmonic Cu$_{2-x}$S nanoparticles to Au$_2$S by cation exchange and electron beam induced transformation of Cu$_{2-x}$S-Au$_2$S core/shell nanostructures. *Nanoscale* **2014**, *6*, 8852−8857.

(166) Han, S.-K.; Gong, M.; Wang, Z.-M.; Gu, C.; Yu, S.-H. Colloidal Synthesis of Cu$_2$S$_x$Se$_{1−x}$ Hexagonal Nanoplates and Their Transformation to CdS$_x$Se$_{1−x}$ and ZnS$_x$Se$_{1−x}$ by the Cation-Exchange Reaction. *Part. Part. Syst. Charact.* **2013**, *30*, 1024−1029.

(167) Miszta, K.; Greullet, F.; Marras, S.; Prato, M.; Toma, A.; Arciniegas, M.; Manna, L.; Krahne, R. Nanocrystal Film Patterning by Inhibiting Cation Exchange via Electron-Beam or X-ray Lithography. *Nano Lett.* **2014**, *14*, 2116−2122.

(168) van der Stam, W.; Bladt, E.; Rabouw, F. T.; Bals, S.; de Mello Donega, C. Near-Infrared Emitting CuInSe$_2$/CuInS$_2$ Dot Core/Rod Shell Heteronanorods by Sequential Cation Exchange. *ACS Nano* **2015**, *9*, 11430−11438.

(169) Dong, C.; van Veggel, F. C. J. M. Cation Exchange in Lanthanide Fluoride Nanoparticles. *ACS Nano* **2009**, *3*, 123−130.

(170) Lei, L.; Chen, D.; Yu, Y.; Zhang, R.; Ling, H.; Xu, J.; Huang, F.; Wang, Y. Growth of hexagonal NaGdF$_4$ nanocrystals based on cubic

Ln³⁺: CaF₂ precursors and the multi-color upconversion emissions. *J. Alloys Compd.* **2014**, *591*, 370−376.

(171) Li, M.; Yu, X.-F.; Liang, S.; Peng, X.-N.; Yang, Z.-J.; Wang, Y.-L.; Wang, Q.-Q. Synthesis of Au−CdS Core−Shell Hetero-Nanorods with Efficient Exciton−Plasmon Interactions. *Adv. Funct. Mater.* **2011**, *21*, 1788−1794.

(172) Yin, Y.; Rioux, R. M.; Erdonmez, C. K.; Hughes, S.; Somorjai, G. A.; Alivisatos, A. P. Formation of Hollow Nanocrystals Through the Nanoscale Kirkendall Effect. *Science* **2004**, *304*, 711−714.

(173) Tian, L.; Yang, X.; Lu, P.; Williams, I. D.; Wang, C.; Ou, S.; Liang, C.; Wu, M. Hollow Single-Crystal Spinel Nanocubes: The Case of Zinc Cobalt Oxide Grown by a Unique Kirkendall Effect. *Inorg. Chem.* **2008**, *47*, 5522−5524.

(174) Sytnyk, M.; Kirchschlager, R.; Bodnarchuk, M. I.; Primetzhofer, D.; Kriegner, D.; Enser, H.; Stangl, J.; Bauer, P.; Voith, M.; Hassel, A. W.; et al. Tuning the Magnetic Properties of Metal Oxide Nanocrystal Heterostructures by Cation Exchange. *Nano Lett.* **2013**, *13*, 586−593.

(175) Chen, B.; Chang, S.; Li, D.; Chen, L.; Wang, Y.; Chen, T.; Zou, B.; Zhong, H.; Rogach, A. L. Template Synthesis of CuInS₂ Nanocrystals from In₂S₃ Nanoplates and Their Application as Counter Electrodes in Dye-Sensitized Solar Cells. *Chem. Mater.* **2015**, *27*, 5949−5956.

(176) Zhang, B.; Jung, Y.; Chung, H.-S.; Vugt, L. V.; Agarwal, R. Nanowire Transformation by Size-Dependent Cation Exchange Reactions. *Nano Lett.* **2010**, *10*, 149−155.

(177) Choi, D.; Pyo, J.-Y.; Kim, Y.; Jang, D.-J. Facile synthesis of composition-gradient Cd₁₋ₓZnₓS quantum dots by cation exchange for controlled optical properties. *J. Mater. Chem. C* **2015**, *3*, 3286−3293.

(178) Mao, B.; Chuang, C.-H.; Lu, F.; Sang, L.; Zhu, J.; Burda, C. Study of the Partial Ag-to-Zn Cation Exchange in AgInS₂/ZnS Nanocrystals. *J. Phys. Chem. C* **2013**, *117*, 648−656.

(179) Tang, X.; Ho, W. B. A.; Xue, J. M. Synthesis of Zn-Doped AgInS₂ Nanocrystals and Their Fluorescence Properties. *J. Phys. Chem. C* **2012**, *116*, 9769−9773.

(180) Wang, Y.-X.; Wei, M.; Fan, F.-J.; Zhuang, T.-T.; Wu, L.; Yu, S.-H.; Zhu, C.-F. Phase-Selective Synthesis of Cu₂ZnSnS₄ Nanocrystals through Cation Exchange for Photovoltaic Devices. *Chem. Mater.* **2014**, *26*, 5492−5498.

(181) Tang, B.; Yang, F.; Lin, Y.; Zhuo, L.; Ge, J.; Cao, L. Synthesis and Characterization of Wavelength-Tunable, Water-Soluble, and Near-Infrared-Emitting CdHgTe Nanorods. *Chem. Mater.* **2007**, *19*, 1212−1214.

(182) Wang, H.; Lou, S.; Tang, Z.; Xu, W.; Shang, H.; Shen, H.; Li, L. S. Thiolate-assisted cation exchange reaction for the synthesis of near-infrared photoluminescent HgₓCd₁₋ₓTe nanocrystals. *Dalton Trans.* **2012**, *41*, 12726−12732.

(183) Yang, L. W.; Li, Y.; Li, Y. C.; Li, J. J.; Hao, J. H.; Zhong, J. X.; Chu, P. K. Quasi-seeded growth, phase transformation, and size tuning of multifunctional hexagonal NaLnF₄ (Ln = Y, Gd, Yb) nanocrystalsvia in situ cation-exchange reaction. *J. Mater. Chem.* **2012**, *22*, 2254−2262.

(184) Dong, C.; Korinek, A.; Blasiak, B.; Tomanek, B.; van Veggel, F. C. J. M. Cation Exchange: A Facile Method To Make NaYF₄:Yb,Tm-NaGdF₄ Core−Shell Nanoparticles with a Thin, Tunable, and Uniform Shell. *Chem. Mater.* **2012**, *24*, 1297−1305.

(185) Abel, K. A.; FitzGerald, P. A.; Wang, T.-Y.; Regier, T. Z.; Raudsepp, M.; Ringer, S. P.; Warr, G. G.; van Veggel, F. C. J. M. Probing the Structure of Colloidal Core/Shell Quantum Dots Formed by Cation Exchange. *J. Phys. Chem. C* **2012**, *116*, 3968−3978.

(186) Abel, K. A.; Qiao, H.; Young, J. F.; van Veggel, F. C. J. M. Four-Fold Enhancement of the Activation Energy for Nonradiative Decay of Excitons in PbSe/CdSe Core/Shell versus PbSe Colloidal Quantum Dots. *J. Phys. Chem. Lett.* **2010**, *1*, 2334−2338.

(187) McDaniel, H.; Fuke, N.; Pietryga, J. M.; Klimov, V. I. Engineered CuInSexS₂₋ₓ Quantum Dots for Sensitized Solar Cells. *J. Phys. Chem. Lett.* **2013**, *4*, 355−361.

(188) Zhao, H.; Chaker, M.; Wu, N.; Ma, D. Towards controlled synthesis and better understanding of highly luminescent PbS/CdS core/shell quantum dots. *J. Mater. Chem.* **2011**, *21*, 8898−8904.

(189) Zhao, H.; Wang, D.; Zhang, T.; Chaker, M.; Ma, D. Two-step synthesis of high-quality water-soluble near-infrared emitting quantum dots via amphiphilic polymers. *Chem. Commun.* **2010**, *46*, 5301−5303.

(190) Park, J.; Kim, S.-W. CuInS₂/ZnS core/shell quantum dots by cation exchange and their blue-shifted photoluminescence. *J. Mater. Chem.* **2011**, *21*, 3745−3750.

(191) Shemesh, Y.; Macdonald, J. E.; Menagen, G.; Banin, U. Synthesis and Photocatalytic Properties of a Family of CdS-PdX Hybrid Nanoparticles. *Angew. Chem., Int. Ed.* **2011**, *50*, 1185−1189.

(192) Kriegel, I.; Wisnet, A.; Srimath Kandada, A. R.; Scotognella, F.; Tassone, F.; Scheu, C.; Zhang, H.; Govorov, A. O.; Rodriguez-Fernandez, J.; Feldmann, J. Cation exchange synthesis and optoelectronic properties of type II CdTe-Cu₂₋ₓTe nano-heterostructures. *J. Mater. Chem. C* **2014**, *2*, 3189−3198.

(193) Tang, L.; Gui, W.; Ding, K.; Chen, N.; Du, G. Ion exchanged YVO₄:Eu³⁺ nanocrystals and their strong luminescence enhanced by energy transfer of thenoyltrifluoroacetone ligands. *J. Alloys Compd.* **2014**, *590*, 277−282.

(194) Sun, X.; Huang, X.; Guo, J.; Zhu, W.; Ding, Y.; Niu, G.; Wang, A.; Kiesewetter, D. O.; Wang, Z. L.; Sun, S.; et al. Self-Illuminating ⁶⁴Cu-Doped CdSe/ZnS Nanocrystals for in Vivo Tumor Imaging. *J. Am. Chem. Soc.* **2014**, *136*, 1706−1709.

(195) Kalb, A.; Leute, V. The miscibility gap of the system CdSe-HgSe. *Phys. Status Solidi A* **1971**, *5*, K199−K201.

(196) Casu, A.; Genovese, A.; Manna, L.; Longo, P.; Buha, J.; Botton, G. A.; Lazar, S.; Kahaly, M. U.; Schwingenschloegl, U.; Prato, M.; et al. Cu₂Se and Cu Nanocrystals as Local Sources of Copper in Thermally Activated In Situ Cation Exchange. *ACS Nano* **2016**, DOI: 10.1021/acsnano.5b07219.

(197) Dalpian, G. M.; Chelikowsky, J. R. Self-Purification in Semiconductor Nanocrystals. *Phys. Rev. Lett.* **2006**, *96*, 226802.

(198) Demchenko, D. O.; Robinson, R. D.; Sadtler, B.; Erdonmez, C. K.; Alivisatos, A. P.; Wang, L.-W. Formation Mechanism and Properties of CdS-Ag₂S Nanorod Superlattices. *ACS Nano* **2008**, *2*, 627−636.

(199) Chen, X.; Lou, Y.; Samia, A. C.; Burda, C. Coherency Strain Effects on the Optical Response of Core/Shell Heteronanostructures. *Nano Lett.* **2003**, *3*, 799−803.

(200) Li, L.; Pandey, A.; Werder, D. J.; Khanal, B. P.; Pietryga, J. M.; Klimov, V. I. Efficient Synthesis of Highly Luminescent Copper Indium Sulfide-Based Core/Shell Nanocrystals with Surprisingly Long-Lived Emission. *J. Am. Chem. Soc.* **2011**, *133*, 1176−1179.

(201) Ostermann, J.; Merkl, J.-P.; Flessau, S.; Wolter, C.; Kornowksi, A.; Schmidtke, C.; Pietsch, A.; Kloust, H.; Feld, A.; Weller, H. Controlling the Physical and Biological Properties of Highly Fluorescent Aqueous Quantum Dots Using Block Copolymers of Different Size and Shape. *ACS Nano* **2013**, *7*, 9156−9167.

(202) Palazon, F.; Akkerman, Q. A.; Prato, M.; Manna, L. X-ray Lithography on Perovskite Nanocrystals Films: From Patterning with Anion-Exchange Reactions to Enhanced Stability in Air and Water. *ACS Nano* **2016**, *10*, 1224−1230.

(203) Powell, A. E.; Hodges, J. M.; Schaak, R. E. Preserving Both Anion and Cation Sublattice Features during a Nanocrystal Cation-Exchange Reaction: Synthesis of Metastable Wurtzite-Type CoS and MnS. *J. Am. Chem. Soc.* **2016**, *138*, 471−474.

(204) De Trizio, L.; De Donato, F.; Casu, A.; Genovese, A.; Falqui, A.; Povia, M.; Manna, L. Colloidal CdSe/Cu₃P/CdSe Nanocrystal Heterostructures and Their Evolution upon Thermal Annealing. *ACS Nano* **2013**, *7*, 3997−4005.